Analysis and Optimisation of Carcass Production for Flexible Pipes

Nielsen, Peter Søe

Publication date:
2014

Document Version
Publisher's PDF, also known as Version of record

Analysis and Optimisation of Carcass Production for Flexible Pipes

by

Peter Søe Nielsen

in partial fulfilment of the degree

Philosophiae Doctor

Department of Mechanical Engineering, Technical University of Denmark

National Oilwell Varco Denmark I/S

September 2014

To my late father

'Thank you for everything'

Preface

This thesis is submitted in partial fulfilment of the requirements for obtaining the PhD-degree at the Department of Mechanical Engineering (DTU-MEK) at the Technical University of Denmark (DTU). The project is part of the Industrial PhD programme in Denmark in which the PhD-student is employed in Industry and enrolled at University; Industry defines the problems and University defines the methods ensuring knowledge sharing between Industry and University. This specific project represents a collaboration between the Mechanical Engineering Department at the Technical University of Denmark and National Oilwell Varco Denmark I/S (NOV Flexibles). NOV Flexibles is a leading supplier of highly engineered flexible pipe systems.

The project is co-funded by Danish Ministry of Higher Education and Science and National Oilwell Varco Denmark I/S. The work has been carried out from July 2010 to September 2014 (1 year and 3 months leave of absence due to paternity leave and general leave of absence doing carcass related work for NOV Flexibles) under the supervision of Professor Niels Bay, PhD Martin Skjødt (between July 2010 and February 2011) and PhD Morten Storgaard Nielsen (between March 2011 and September 2014).

Oelstykke, September 2014

_____

Peter Søe Nielsen

Acknowledgements

First of all, I would like to thank Martin Skjødt, Erik Bendiksen and Niels J. Rishøj for suggesting and approving the PhD-project at NOV Flexibles and presenting me with the opportunity to work on this interesting project, which I have truly enjoyed. My sincere gratitude to my supervisors Professor Niels Bay, Martin Skjødt and Morten Storgaard Nielsen for the inspiration, support and discussions during the course of the project.

Furthermore I would like to thank my colleagues at NOV Flexibles for creating an inspirational and helpful atmosphere and I need to extend special thanks to the following colleagues who have helped with tasks and contributing discussions: Benny Christiansen, Peter Kjær, Casper Frimodt, Lasse Tang Koch, Torben Nielsen, Kristian Jørgensen, Martin Øst-Jacobsen, Steen Hjorth Hansen and Thomas Iversen Solfeldt.

I would also like to thank the staff at DTU-MEK, especially Peter Sanderhoff, Jakob Rasmussen, Rene Sobiecki and Lars P. Holmbæk for their laboratory assistance and for assistance during B.Sc.-projects in which I have been involved as supervisor. Also thanks to my fellow PhD students Ermanno Ceron, Chris Valentin Nielsen, Peter Christiansen, Alessandro Godi, Pavel Müller and Jais Andreas Breusch Angel to whom I owe a great working environment and consequently inspirational discussions.

I would furthermore like to thank project students Jacob T. Henckel, Benjamin A. K. Hartz and Casper A. Ormstrup for their contributions to simulative testing and weld investigations through their respective B.Sc.-projects.

Finally, a heartfelt gratitude to my family who has been supportive during the project, especially my girlfriend Kristina and our son Oliver whose support during the final stages of the project allowed me to focus my attention on the project.

Abstract

Un-bonded flexible pipes are used in the offshore oil and gas industry worldwide transporting hydrocarbons from seafloor to floating production vessels topside. Flexible pipes are advantageous over rigid pipelines in dynamic applications and during installation as they are delivered in full length on reels. Flexible pipes are constructed in a layer structure in which each layer adds specific properties to the pipe such as; collapse strength, fluid integrity, bursting strength, tensile strength etc. The inner-most layer of a flexible pipe is the carcass; a flexible interlocking stainless steel structure that provides mechanical and collapse strength for the flexible pipe. The manufacturing process of carcass is a combination of roll forming stainless steel strips and helical winding the profiles around a mandrel interlocking the profiles with themselves.

The focus of the present project is the analysis and optimisation of the carcass manufacturing process by means of a fundamental investigation in the fields of formability, failure modes / mechanisms, Finite Element Analysis (FEA), simulative testing and tribology.

A study of failure mechanisms in carcass production is performed by being present at the production floor when such incidents arise, the so-called 'Gemba' methodology. The outcome is a list of general failure mechanisms in the carcass process and it is noted that most issues are encountered in the winding stage.

Issues with carcass profile geometry is a recurring event and it was found that the degrees of freedom which the carcass profile experiences during interlock winding allow the profiles to minimise stresses and strains during winding by adjusting the profile geometry – the effect being more pronounced with decreasing mandrel size. This effect was effectively accounted for by changing the profile geometry in the roll forming stage.

LS-DYNA® is successfully used to construct simple winding models and a three-point-bend using shell elements. A convergence study is performed to ensure parameters for numerical stability. The simple winding models were in agreement with production measurements and they were successfully used in evaluation of weld relief-cut functionality. The three-point-bend FEA indicates possible problems with the shell elements when boundary conditions allow free-forming.

A simulative three-point-bend test is constructed to simulate profile tongue strains during winding. Preliminary testing shows promising results but problems in obtaining similar boundary conditions to the profile as in winding needs to be resolved. In the simulative test simple v-bent profiles shows comparable to roll formed profiles and seems to be a viable option for fully offline simulative testing of weld and weld relief-cut fracture.

Material characterisation of one austenitic and three duplex grade stainless steels is performed (EN 1.4404, EN 1.4162, EN 1.4462 and EN1.4410). Flow curves and anisotropy values are attained but problems with notched tensile specimens meant that only uni-axial tension FLC points were attained.

Analysis of weld fracture of duplex stainless steel EN 1.4162 is carried out determining strains with GOM ARAMIS automated strain measurement system, which shows that strain increases faster in the weld zone than the global strain of the parent material. Fracture in the weld zone occurs at an average global strain of 0.1 where the average fracture strain in the weld zone is 0.27. The reason is explained by lower hardness in the weld zone compared to the parent material.

Weld fracture can be suppressed with introduction of weld relief zones. However, production strain measurements and FEA analysis showed that cutting a relief zone creates high strains locally in the relief-cut itself – more than a factor two larger than the nominal highest strains elsewhere in the profile. Weld relief-cuts are optimised by moving the relief-cut next to the weld seam and only cutting 1 x strip thickness deep.

Simulative tribo-testing in the strip-reduction-test showed that biodegradable rapeseed oil is an acceptable lubricant for the carcass process. Testing of two lean duplex stainless steel surfaces showed that a EN 2E brushed surface had better lubricant entrapment capabilities than a EN 2B bright annealed surface.

Swarf was found to originate from either strip edge in contact with the forming tool or with another strip edge during interlocking or from pickup abrading the strip surface. An increase of tool curvature in contact with the strip edge is shown to have a positive effect on edge swarf.

Pickup was seen as an issue on the roll forming tools but it does not develop past a certain amount. It is, however, continuously formed and removed thus resulting in adhesive wear on the tools. The result, combined with cyclic contact loads, is tool failure by chipping.

Tribo-system performance was greatly improved by the use of an AlCrN tool coating. Unlike normal polished tools, where pickup on the tools is seen from less than 80km production, the coating enabled production of more than 650km EN 1.4162 stainless steel strip without any pickup forming or tool chipping.

Resume (dansk)

Fleksible rør bruges globalt i offshore olie of gas industri til at transportere kulbrinter op fra havbunden til flydende produktionsenheder på havoverfladen. Fleksible rør er fordelagtige frem for faste rørforbindelser i dynamiske applikationer og under installation, da rørene leveres i færdige længder på spoler. Fleksible rør er fremstillet i en lagdelt struktur, hvor hvert lag tilføjer specifikke egenskaber til rørets funktion såsom: kollaps styrke, fluid barriere, sprængningsstyrke, axiel styrke osv. Det inderste lag i et fleksibelt rør er carcassen, en fleksibel sammenlåst rustfast stål struktur, der giver det fleksible rør mekanisk styrke og modstand mod kollaps. Fremstillingsprocessen er en kombination af profilvalsning af rustfast stål og spiralformet vikling af det valsede profil omkring en dorn, hvor sammenlåsningen mellem profilerne foregår.

Nærværende projekt har haft fokus på analyse og optimering af carcass fremstillingsprocessen ved en fundamental undersøgelse af områderne formbarhed, fejl mekanismer, FE-analyse, simulative test og tribologi.

Et studie er udført af fejlmekanismer i carcass produktionen ved at være til stede ved produktionsgulvet, når de har optrådt, den såkaldte 'Gemba' metodologi. Resultatet er en liste af almene fejl mekanismer i carcass processen, og det er bemærket, at de fleste problemer opstår under vikleprocessen.

Carcass profil geometri er en tilbagevendende udfordring og det er konstateret, at carcass profilets frihedsgrader under viklingen / sammenlåsningen tillader, at profilet minimerer spændinger / tøjninger ved at ændre profilets geometri. Effekten er mere udpræget med aftagende dorn størrelser, et forhold der med succes er taget hensyn til, ved at ændre profilets geometri i profilvalsningen.

LS-DYNA® er med succes blevet brugt til at opbygge simple viklemodeller og et tre-punkts-buk, hvor skalelementer er anvendt. Et konvergensstudie er udført for at sikre parametre som giver numerisk stabilitet. De simple vikle modeller stemmer godt overens med produktionsmålinger, og de er succesfuldt brugt til evaluering af svejseaflastningsklip. Udfordringer med tre-punkts-buk FEA modellen indikerer, at der kan være problemer forbundet med skalelementerne, når randbetingelserne tillader fri formgivning.

Et simulativt tre-punkts-bukkeudstyr er konstrueret til at simulere profiltungens tøjninger under vikling. Foreløbige tests ser lovede ud, men udfordringer med tungens randbetingelser skal løses, så tøjningerne er sammenlignelige med carcass vikling. I den simulative test viste simple v-bukkede profiler sig at være sammenlignelige med profilvalsede profiler og synes anvendelige til offline simulativ testning af brud i svejsninger og svejseaflastningsklip.

Der er udført materialekarakterisering af et austenitisk- og tre duplex rustfaste stål (EN 1.4404, EN 1.4162, EN 1.4462 and EN1.4410). Værdier er opnået for arbejdskurver og materiale anisotropi. Problemer med en-akset trækprøvning med indklip betød, at FLC punkter kun er opnået for en-akset træk.

Svejsebrud med duplex rustfast EN 1.4162 er analyseret ved tøjningsmålinger med GOM ARAMIS automatiseret tøjningsmålingssystem under en-akset trækprøvning, hvor det er vist, at tøjningerne øges hurtigere i svejsezonen end de globale tøjninger for grundmaterialet. Der opstår brud i svejsezonen ved en gennemsnitlig global tøjning på 0.1, hvor den gennemsnitlige tøjning i svejsezonen er 0.27. Årsagen er forklaret ved lavere hårdhed i svejsezonen sammenlignet med grundmaterialet.

Brud i svejsningerne kan forhindres ved at introducere en svejseaflastningszone. Dog viser tøjninger fra produktion og FE-analyser at ved at klippe et aflastningsklip, genereres der store tøjninger lokalt i aflastningsklippet – mere end en faktor to større en de nominelle højeste tøjninger andre steder i profilet. Svejseaflastningsklippet er optimeret ved at flytte aflastningsklippet hen til svejsningen og kun klippe 1 x striptykkelse dybt.

Simulativ tribo-testning med strip-reduktions-testen viste at biologisk nedbrydelig rapsolie er et udemærket smøremiddel til carcass processen. Testning af to lean duplex rustfaste stål viste at en EN 2E børstet overflade er bedre til at indfange smøremiddel end en EN 2B blank glødet overflade.

Swarf er konstateret til at stamme fra enten båndets kant, som kommer i kontakt med værktøjerne eller en anden stripkant under sammenlåsningen, eller fra koldsvejsning af rustfast stål på værktøjets overflade, som river i båndets overflade. Ved at øge værktøjsrundinger, som kommer i kontakt med båndets kant, var det muligt at forebygge kant-swarf.

Koldsvejsning af det rustfaste stål på værktøjerne er et problem under profilvalsning, dog udvikler det sig ikke ud over et vist niveau. Det synes at koldsvejse og fjernes gentagen, hvilket resulterer i adhæsivt slid på værktøjerne. Det forhold, kombineret med cyklisk kontakt resulterer i værktøjssvigt på grund af flig dannelse.

Tribo-systemet blev i høj grad forbedret ved brug af en AlCrN belægning; i modsætning til normalt polerede værktøjer, hvor pickup kan ses på værktøjerne efter 80km produktion, så tillod belægningen produktion af mere end 650km EN 1.4162 rustfast stål bånd uden koldssvejsningsproblemer eller værktøjssvigt.

List of publications

Peer reviewed international conference papers

1. Peter Søe Nielsen, Morten Storgaard Nielsen, Niels Bay: *Tribological Study in Roll Forming of Lean Duplex Stainless Steel Sheets*, in: Proccedings of the 2012 International Deep-Drawing Research Group (IDDRG 2012), pp. 592-597, Mumbai, India

2. Peter Søe Nielsen, Morten Storgaard Nielsen, Niels Bay: *Size Effects in Winding Roll Formed Profiles: A Study of Carcass Production for Flexible Pipes in Offshore Industry*, in: Proceedings of the 15th Bi-annual International Sheet Metal Conference (SheMet13), pp. 117-124, Belfast, Northern Ireland

Submission pending final approval

3. Peter Søe Nielsen, Casper Alexander Ormstrup, Benjamin Arnold Krekeler Hartz, Morten Storgaard Nielsen, Niels Bay: *Simulative winding of roll formed profile in carcass production for flexible pipes*, submitted to: The 16th International Conference on Sheet Metal (SheMet15), hosted by: the Institute of Manufacturing Technology in Erlangen, Germany from March 16-18, 2015.

Planned submissions

4. Peter Søe Nielsen, Morten Storgaard Nielsen, Niels Bay: *Analysis and optimization of carcass production to flexible pipes for off-shore applications*, planned for 2015 CIRP Annals – Volume 1 – Papers

5. Peter Søe Nielsen, Morten Storgaard Nielsen, Niels Bay: *Galling Problems in Carcass Production to Flexible Pipes for Off-shore Applications*, to be submitted to J. Mater. Process. Technol.

Contents

Nomenclature

Symbols

A_1	Actual cross-sectional area [mm^2]
b	Width of tensile specimens / pre-strain in Swift's expression [-]
C_1	Strength coefficient in Hollomon's expression [MPa]
C_2	Strength coefficient in and Swift's expression [MPa]
e	Neutral plane position from strip centre line [mm]
k	Correction factor for neutral plane position in Chapter 4
k	Strength coefficient in LS-DYNA® [MPa]
M	Bending moment [Nm]
n	Strain hardening exponent in Hollomon's and Swift's expressions [-]
P_{max}	Maximum pitch [mm]
P_{min}	Minimum pitch [mm]
$P_{neutral}$	Neutral pitch [mm]
QL	Lip-half of the carcass profile
QT	Tongue-half of the carcass profile
R	Bending radius [mm]
R_α	Lankford coefficient / anisotropy coefficient [-]
t	Strip thickness [mm]
T	Tension [N]
t_0	Initial strip thickness [mm]
w	Strip width [mm]

α	Fish scaling angle [°]
ε	Logarithmic strain / true strain [-]
ε_1 / ε_l / ε_{major}	Longitudinal strain [-]
ε_2 / ε_w / ε_{minor}	Width strain [-]
ε_3 / ε_t	Thickness strain [-]
ε_{yp}	Elastic strain at yield point [-]
$\bar{\varepsilon}^p$	Equivalent plastic strain [-]
θ	Strip bending angle [°]
ρ	Radius of curvature at neutral plane [mm]
σ	True stress [MPa]
φ	Roll formed profile entry angle onto the mandrel [°]

Abbrevations

CAD	Computer Assisted Drawing
CAE	Computer Assisted Engineering
CC	Carcass
CFL	Courant-Friedrichs-Lewy
CMM	Coordinate Measuring Machine
DOE	Design of Experiments
EP	Extreme-Pressure
FEA	Finite Element Analysis
FLC	Forming Limit Curve
FLD	Forming Limit Diagram
HAZ	Heat Affected Zone
np	Neutral plane
PM	Powder-Metallurgical

RF	Roll Forming
SM	Steel manufacturer
SRT	Strip-Reduction-Test
TIG	Tungsten inert gas
UTS	Ultimate tensile strength [MPa]
WT	Winding tool

Chapter 1 Introduction

Flexible pipes are used in offshore oil and gas industry as well as chemical and water industry worldwide. Flexible pipes are delivered in full length and are advantageous over rigid pipelines during installation where rigid pipelines are welded on site, thus high precision is needed for good alignment between two pipe sections. Flexible pipes are also used in floating production units that due to wave cycles are in constant movement with respect to the well head or other connection points. A standard flexible pipe is an unbonded structure typically consisting of helically wound metallic armour wires or strips combined with concentric layers of polymers, textiles, fabric tapes and lubricants - see Figure 1-1. Unbonded flexible pipe systems must comply with API specification 17J [1].

Figure 1-1: Typical design of a flexible pipe (insulation and anti-wear layers are not shown) [2]

Explanation from inner- to outer layers:

1. **Carcass:** an interlocking structure that prevents collapse of the inner liner and provides mechanical protection against pigging tools and abrasive particles
2. **Inner liner:** an extruded polymer layer providing internal fluid integrity
3. **Pressure armour:** a number of structural layers consisting of helically wound steel wires and / or steel strips. The pressure armour layers provide resistance to radial loads from internal pressure

4. **Tensile armour:** a number of structural layers consisting of helically wound rectangular steel wires. The tensile armour layer provide resistance to axial tensile loads
5. **Outer sheath:** an extruded polymer layer. The function is to shield the pipe's structural elements from the outer environment and to offer mechanical protection

The innermost part of the flexible pipe is the carcass; an interlocking flexible structure. The carcass provides protection against collapse, due to water pressure, and mechanical crushing during production and installation of the pipe. The carcass is the critical component as regards to the flexible pipe's maximum installation depth and is also a main component regarding flexibility [3].

The topic of the present PhD project is carcass production for flexible pipe systems based on carcass production at NOV Flexibles.

Carcass manufacturing is a continuous two-stage production; the first stage is roll forming of stainless steel strips into an s-shaped carcass profile, Figure 1-2 (a), and the second stage winds the carcass profile onto a mandrel in a helix where the profile interlocks with itself as illustrated in Figure 1-2 (b). The roll forming and the winding stages are performed on the same machine in a setup, where the roll forming line rotates around the mandrel in order to obtain carcass lengths of several kilometres - mandrel diameter may vary from ø50mm to ø400mm. This imposes limitations to the number of roll forming tools due to machine size, which in turn has an effect on profile buckling and twisting. It also increases process loads because more bending is required in each step [4]. A more detailed description of the carcass production line is given in Chapter 2.

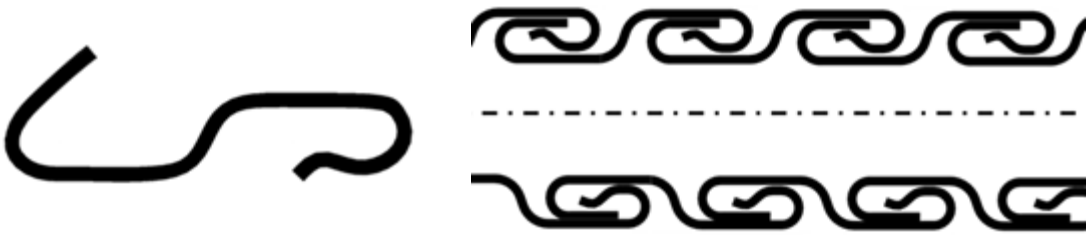

(a) (b)

Figure 1-2: (a) Roll formed profile cross-section for interlocking carcass production and (b) cross-section from the side of interlocked a carcass. Production direction is from left to right

1.1 Carcass functionality

Each carcass is designed to withstand a certain collapse pressure and satisfy the needs of flexibility (the main parameters for carcass functionality) for the specific conditions that the carcass will experience during production, installation and service life. Also the carcass must stay functional for the design life where corrosion resistance, wear and fatigue are determining factors. Carcass geometry is essential for satisfying these design parameters and the key geometrical factors are: pitch, displacement, wall thickness and ovality / diameter [3].

These parameters are assessed during production and require a window being cut into the carcass to enable measurements of profile geometry, wall thickness and visual inspection of the inside. A typical window is shown in Figure 1-3 where carcass profiles are welded together prior to cutting to keep the carcass from 'un-winding' due to stress release.

Figure 1-3: Typical measurement window being cut into carcass at production start and finish

1.1.1 Collapse strength

Carcass collapse in form of buckling of the carcass structure is generally governed by the following parameters: material yield strength, profile second moment of inertia, carcass ovality and pitch. As a result final carcass geometry is vital for collapse resistance [5, 6].

1.1.2 Flexibility

Figure 1-4 show the notation in a carcass profile. The optimal displacement for any given carcass profile is reached, when QT and QL are of equal length and the same goes for the tongue and lip respectively. If this 'symmetry' is not obtained then there is a loss of possible displacement. This particular problem is addressed in Chapter 3.

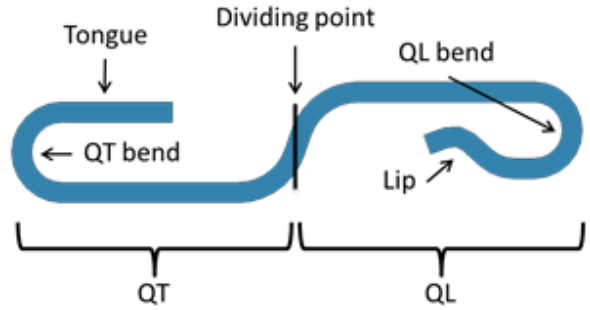

Figure 1-4: Illustration of a carcass profile with descriptions – the bends at dividing point are named s-bend

Carcass locking is a term used when the interlocking profiles reach their boundaries with regards to displacement, see Figure 1-5. In this figure both inner- and outer profile has reached their respective boundaries; locking is, however, also considered when either one of the inner- or outer profile has reached its boundary. During flexible pipe production, pipe installation and service life a carcass should not experience locking since this could damage the carcass.

Note from Figure 1-5 that carcass flexibility is determined by displacement and rotation between neighbouring profiles.

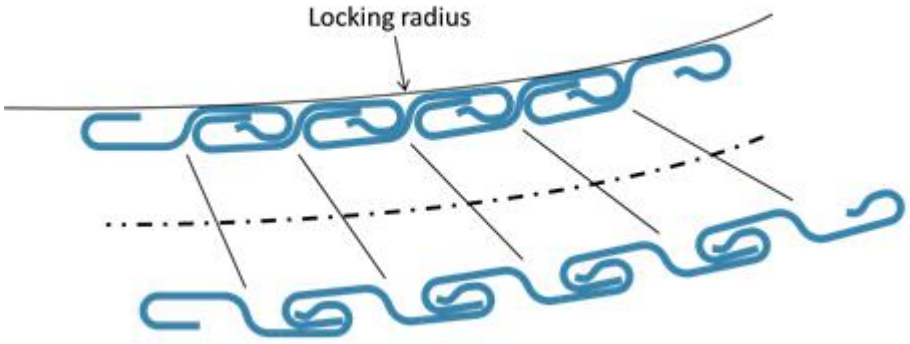

Figure 1-5: Illustration of a 2D cross-section of a carcass being bent to locking. The inner profile is fully compressed and the outer profile is fully extended. The angled lines between inner and outer profile are indicators that they are helically connected

1.1.3 Pitch

The carcass pitch is the distance between each helical 'thread' of the carcass profile and is equally important as regards collapse pressure and flexibility. Optimal displacement is ensured when an unbended carcass has a pitch in the neutral position meaning that the profile displacement is used fully. For every mm the pitch is off the neutral position the displacement will be similarly reduced. Figure 1-6 illustrates a carcass in three different situations: a) pitch is neutral; meaning that elongation and compression length are equal, b) pitch is at its minimum; meaning no further compression is possible and c) pitch is at its maximum; meaning no further elongation is possible. The carcass displacement is the full extent of movement (P_{max} - P_{min}). For cases b) and c) carcass is already locked before any bending is applied to the carcass.

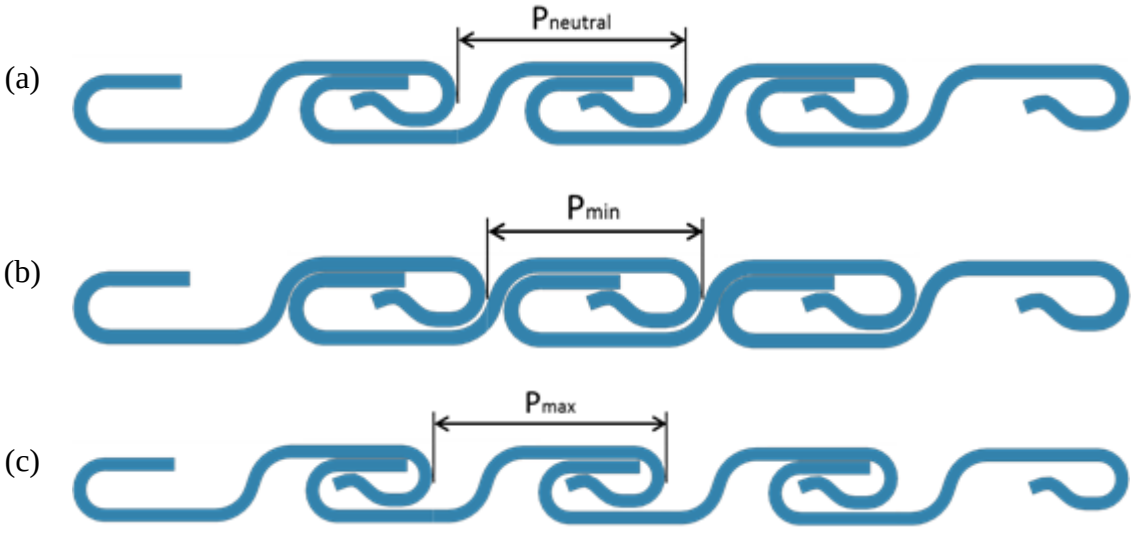

Figure 1-6: Pitch illustrations on 2D-cross sections of carcass. (a) carcass at neutral pitch, (b) carcass at minimum pitch and (c) carcass at maximum pitch

Collapse strength can be related to the amount of steel put in the carcass per meter. Thus a smaller pitch implies at stronger carcass with higher collapse strength and vice versa. Carcass designs are typically based on the pitch being in the neutral position.

1.2 Project description

The present project was proposed because of a desire to combine existing company process knowledge with scientific engineering methods to improve the fundamental understanding of the carcass process. The project is entitled "*Analysis and Optimisation of Carcass Production for Flexible Pipes*". The scientific topics covered by the project include; formability and failure modes in advanced sheet metal forming processes, Finite Element Analysis (FEA), simulative testing and tribology in stainless sheet forming processes.

1.2.1 Objective, goals and success criteria

The scientific objective of the project is through a fundamental investigation of the carcass manufacturing process to generate knowledge about failure modes and forming limits in complex stainless sheet metal forming processes. Understanding these failure modes and knowing the forming limits opens up for process optimisation to further ensure process stability, thus reducing production stops and expensive post-production processing of manufactured pipes. This knowledge will also enable development and optimization of the process and product itself.

An often discussed topic is geometrical issues in the final carcass profile such as profile geometry deviating from the desired one. This could be the possible axial displacement of the profile, which is a determining factor in carcass flexibility. Carcass pitch is also a significant parameter as it too is a determining factor in flexibility and collapse strength. These three geometrical parameters; profile, displacement and pitch should be viewed simultaneously, since they influence each other. An investigation of the geometrical issues in the carcass process as well as a subsequent analysis of the possibilities of avoiding these problems is desired.

Part of the project deliverables includes successful construction of Finite Element models and a simulative test. Both enable offline parametric studies of carcass process parameters, an important part of the systematic analysis of the process.

Welds between coils are required for continuous lengths of carcass, which sometimes cause problems with weld fracture, when using duplex stainless steels. The problem can, in part, be solved by stress relieving the welds. One goal is to understand the effect of stress relieving and optimise the relief zones as well as predicting, whether stress relieving is necessary by combining this effect with knowledge of carcass process formability.

Finally it is a goal to study swarf and galling in carcass production as this sometimes is a problem, and when it occurs, it is a costly affair to solve, since it usually has to be done post-production. At the onset of the project little was verified as regards the origin and cause of

swarf and galling, so improved understanding of these phenomena is an important goal. One natural course is to investigate the tribological system (tribo-system) and to optimise it.

The general success criterion is the successful completion of the aforementioned goals and through a systematic approach develop the knowledge of the carcass process and its failure modes as well as how to prevent these.

1.2.2 Value creation

Because the carcass is the innermost layer of a flexible pipe, optimizing the carcass affects all other layers in the pipe. For example; a thinner and lighter carcass with unaltered collapse strength will result in less demand on the pressure- and tensile armour layers and reduced amount of polymer used to shield the pipe. The consequence being a lighter pipe with reduced material costs, which is an important, competitive parameter.

In short, the value for the company created through this project can be described as; reduction of production costs and improvement of product quality. This is sought achieved through gathering knowledge from the existing process and product. Understanding the important process parameters in carcass production is the key to optimizing the carcass, for example by evaluating new materials against process requirements, which in turn can lead to a stronger and lighter carcass.

With the world's increasing energy needs there is still a high future demand for oil and gas, even with development of new green energy technologies [7]. Many new oil and gas fields are found on increasingly deeper waters, which demands product optimization in case of flexible pipes. An example is the Brazilian national oil company, Petrobas that consumes approximately half of the market for flexible pipes in the world. Petrobas is developing new oil fields off the coast of Brazil, the "Pre-salt development" [8]. Most of the oil is located in ultra-deep waters (+3,000m) and in order to reach these oil fields, a strong and light carcass is needed to withstand the high pressure they are subjected to at these water depths.

Another promising market is injection of super critical CO^2. This can be done either by injecting in a reservoir for storage or to pressurize existing wells where oil production then is combined with reducing atmospheric CO^2. These technical advances are only possible with fundamental knowledge about materials and process limits.

1.3 Methodology

Optimisation in the field of process technology is often an interdisciplinary task that implies a need to understand the chaotic system of individual influencing parameters, which make up an entire process line, before proper optimisation can be done. An expression that describes this approach is 'Gemba', a Japanese word used in many topics but the meaning is the same; place of value creation, factory floor etc. In quality management the term is used when problems occur; the engineers must go to the factory floor to gather all relevant infor-

mation from all sources otherwise valuable information might be lost. The basic meaning is; the need to understand before we can optimize [9].

Although being categorised as a roll forming process the carcass process is quite special and limited amount of is available about the process and the failure modes. It was therefore clear from the project start that staying close to the production floor and production personnel would generate valuable information. One could describe the work as a case-study of the carcass process, where the improved understanding leads to an ability to optimize. As such, understanding the failure modes and the chain of events that leads to those failure modes is very important in this work.

The work includes a combination of production tests, Finite Element Analysis (FEA) and simulative tests. Initially emphasis was placed on simulative tests and FE-modelling due to expectation of limited time on the production machinery. However, throughout the project it became possible to gain access to this, which implied that the significance of simulative testing and FE-modelling was reduced.

Chapter 2 Carcass process description

This chapter provide an in-depth step-by-step description of the carcass process from coiled strip to the finished carcass on the reel. The flow-chart in Figure 2-1 provides a visual representation of the carcass process. Investigating the metal forming process alone would probably yield interesting results but it is influenced by a number of preceding steps. Viewing the process as a whole is therefore vital to understanding the process and to reach a successful product.

It should be emphasised that the carcass production includes a chain of events that may lead to failure later in the production process and how optimising in one step could cause failure in a subsequent step. This is sought captured in the description of the known failure modes and mechanisms and their causes in Chapter 3.

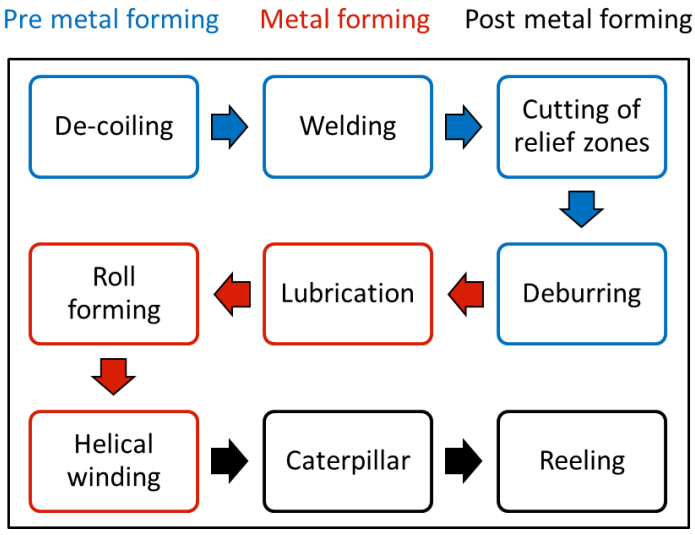

Figure 2-1: Flow-chart describing the step-by-step path of the carcass material through the carcass process

2.1 Pre metal forming

Pre metal forming describes a number of important coil / strip handling steps that are performed before the actual metal forming process. Since the process utilises the whole strip the strip edge is significant to the carcass process, and it is thus important to handle the edges during coil and strip handling with care.

2.1.1 De-coiling

The carcass materials are received as coils and the first step of the carcass process is to spool the material onto machine reels, known as pancakes. The coils are attached to a de-coiler and the material is transferred to the carcass machine. Sometimes the coils are delivered from the steel manufacturer with defects; these sections are cut out in this stage.

2.1.2 Welding

Between the de-coiler and the pancakes the coils are welded thus enabling continuous carcass production. Strips are auto-TIG welded without any welding consumables with shielding gas on both sides of the weld. Strip alignment is important as well as proper preparation of the strip ends that are welded together.

Duplex stainless steels are commonly used for carcass production due to their high strength, corrosion resistance and price, but welding is often critical as the mechanical properties in the weld zone are not as good as the parent material [10]. There is a tendency that weld fracture is more frequent on small thickness strips. This might be caused by the difficulty in inducing enough heat into the material to produce a good weld, as too much heat in a thin strip will result in burn-through. Also the cooling rate is faster for small strips due to the heat capacity of the fixture in contact with the strip in the welding zone.

2.1.3 Cutting of relief zones

Due to the reduced mechanical strength of duplex stainless steel welds a relief zone is sometimes prepared alongside the weld by cutting out material to the side that is wound onto the mandrel prior to the weld, see Figure 2-2. This ensures relief of the weld, which prevents fracture during helical winding. Positioning and design of the relief-cut is essential to its function and to ensure process stability; a closer investigation of the details of the relief-cut is performed in Chapter 8.

Figure 2-2: Weld and relief-cut on the left-hand-side of the weld

2.1.4 Deburring

While the strip is being coiled onto the machine a deburring of the strip edges is performed by edge-rolling. If the burr on the strip edge is too large it may interfere with the inter-

locking, explained in section 4.2.5, resulting in uneven closing of the profiles. This is likely a contributing factor during an experiment, where a section of strip that was not deburred caused the carcass to rotate in the production direction (explained in 4.2.1). Thus the edge-burr can influence the torque needed in the winding stage of the production. A well deburred edge will also reduce the risk of edge swarf in the process (explained in 4.3.13)

2.2 Metal forming

2.2.1 Lubrication

With the objective to prolong tool life and impede pickup formation on the tools lubrication of the strip is performed prior to entry to the roll forming line. Different types of lubricant can be used such as mineral oils, biodegradable vegetable oils and even emulsions. Inadequate lubrication will lead to galling – the series of events including pickup formation on the tools (cold welding of the stainless steel to the tool surfaces) and subsequent scoring of the carcass profile [11]. The carcass tribo-system is further investigated in Chapter 9.

2.2.2 Roll forming

The first stage of metal forming is ordinary roll forming where the sheet metal strip is continuously formed by multiple contoured rolls. Figure 2-3 shows a FEA of roll forming of a carcass profile with LS-DYNA®. Roll forming is a well-known metal forming process where steel stripes are continuously bent into various profile shapes – a very cost-effective way of producing profiles [4]. Fundamental deformation consists of longitudinal stretching, longitudinal bending, shear and transverse bending [12]. The transverse bending is what ensures the cross-sectional profile shape similar to v- and air bending of sheet metal [13].

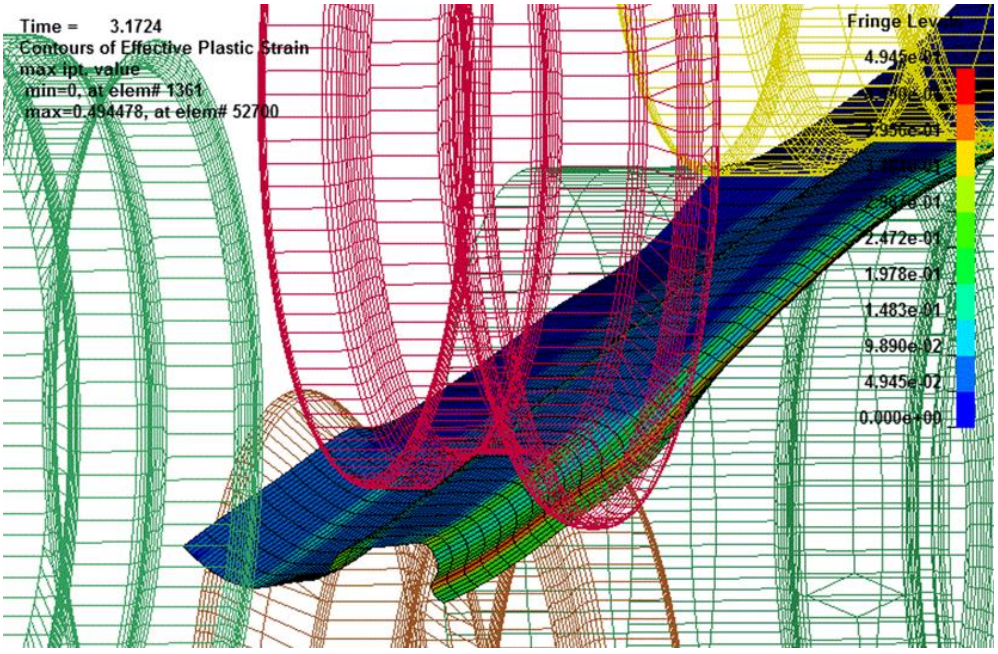

Figure 2-3: FE-model of roll forming – fringe contours are effective plastic strain

In the carcass roll forming line the metal strip is formed into the open s-shaped profile, Figure 1-2 (a), which is closed / interlocked, Figure 1-2 (b), in the helical winding process. A strip guide steers the strip correctly into the roll forming station no.1 positioning the strip edges correctly in the tools in order to ensure correct profile geometry. Depending on the machine size one can have from as little as 4 roll forming steps and up to 10-12 steps. The majority of this work is focused on 4 and 6 step machines. Compared to standard roll forming the number of forming steps is low and does cause severe plastic deformation, which is not viable, since it leads to failure modes such as skewness of the profile [4]. But in carcass production the roll formed profile is subsequently helical winded, wherefore any skewness in the profile is not seen in the final product as the residual stresses are released.

From the roll forming line there are two general approaches to feed the profile into the helical winding process: a loop feed (Figure 2-4) and direct feed (Figure 2-5). These two strategies require two different machine control strategies as regards to the amount of roll formed profile being fed into the helical winding and the resultant pre-stressing of the profile.

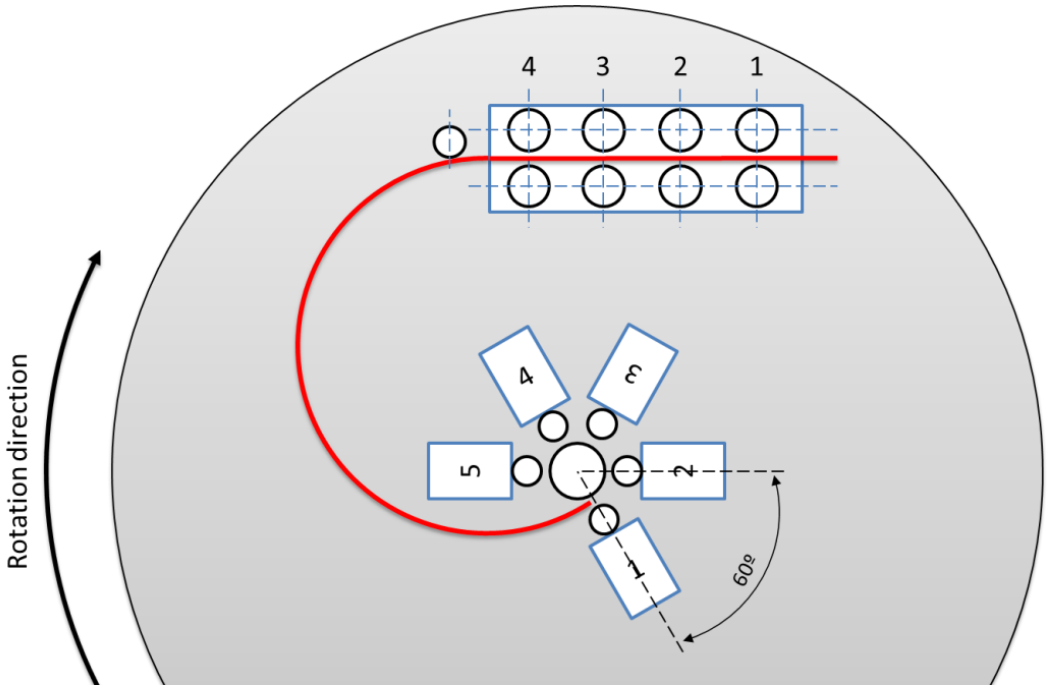

Figure 2-4: Schematic front-view of a loop type carcass machine where the red line exemplifies the profile path

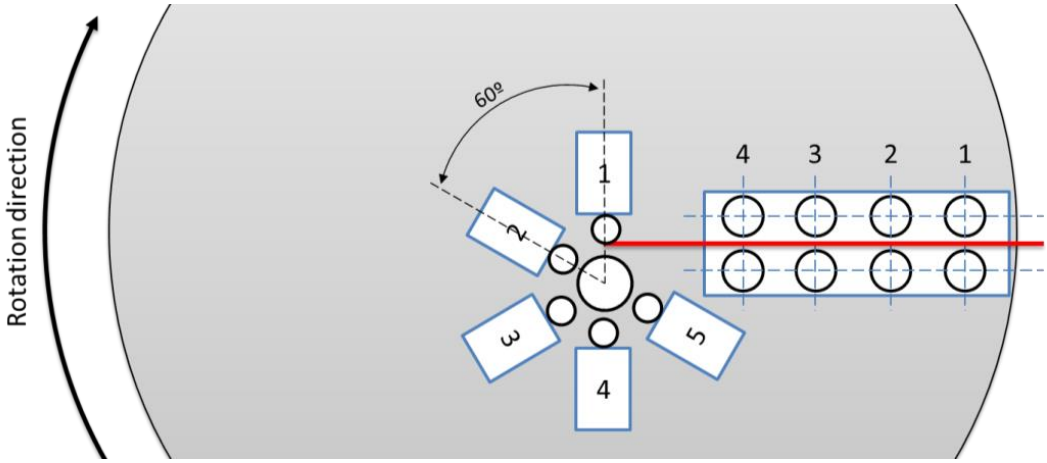

Figure 2-5: Schematic front-view of a direct feed carcass machine where the red line exemplifies the profile path

The loop type feed utilises a dancer position control that ensures a 'buffer' of roll formed profile in the loop before the winding process. In this way the roll forming and winding processes are separated by the buffer zone, and the winding process is free to 'take' the required profile per revolution. Another effect is that this leaves the profile some degrees of freedom that can be utilised in order to ease interlocking by allowing sufficient gap between the profiles for the interlocking to be successful. No significant axial pre-stress of the profile before the winding process occur because of the buffer zone.

Direct feed into the winding process allows pre-stressing of the carcass profile before winding because of the stable connection between the roll forming line and winding process through the carcass profile. Without the buffer zone the feeding rate from the roll forming line to the winding needs to be determined rather accurate in order to minimize the wear on the roll forming tools, otherwise the profile will be pulled through the roll forming line. Also the degrees of freedom of the profile is lower because of the rigid connection, owed to the short distance, between roll forming and winding. Twisting of the profile is more difficult albeit not impossible.

2.2.3 Helical winding

The most challenging stage of the carcass process is the helical winding because of the degrees of freedom that the profile has during winding and due to the failure modes specific for helical winding. Much more details on the winding process will be given in Chapter 3 and Chapter 4, e.g. the geometrical effects and failure modes during winding are discussed.

The roll formed profile is wound onto a mandrel by a set of winding tools (WTs) that, depending on carcass diameter, may vary in number and size. Figure 2-6 shows winding tools and the incoming roll formed profile by a front-view of a loop type machine. As the roll formed profile enters the winding stage it will be guided under winding tool no.1 (WT1) where interlock with the previous profile is initiated. The main interlock and bending defor-

mation takes place between WT1 and WT2 as these two tools along with the mandrel in the centre form a three-point bending, in which the profile is formed to the desired bore diameter. The winding tools are positioned on the mandrel, so that the profile runs a helical path thus ensuring the helical winding, which sets the carcass profile pitch. The winding tools also define the wall thickness of the carcass by their distance to the mandrel.

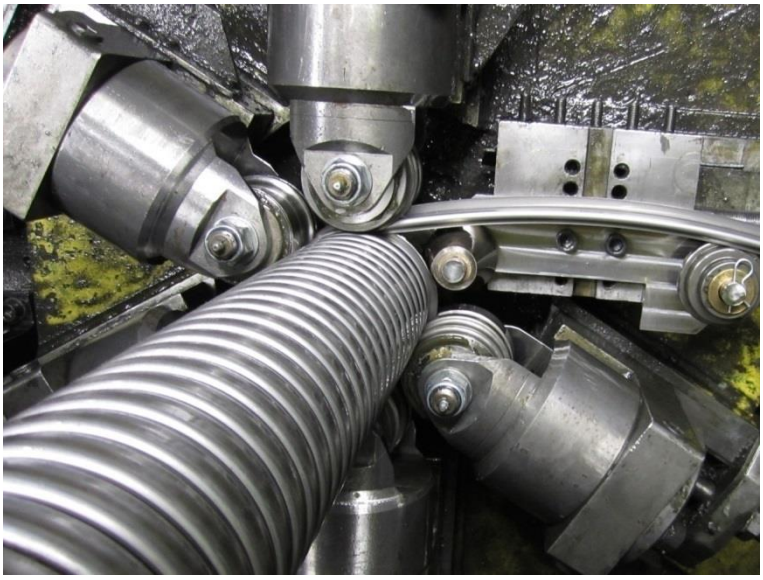

Figure 2-6: Front-view of helical winding on a loop type carcass machine

The interlocking between two profiles is depicted in Figure 2-7 and illustrated in Figure 2-8. During the first part of rotation around the mandrel the tongue is held open, whilst the lip / QL is being interlocked with the tongue from the previous rotation. The interlocking is occurring from the situation in Figure 2-8 (a) to (b). The upright position of the tongue induces high strains during the first part of rotation around the mandrel before it is interlocked. This raises quality demands to the strip edge as a local notch could initiate necking and fracture.

Figure 2-7: View of the interlock. There must be sufficient gap between the two legs of the profile to achieve a stable interlock – the gap is good in the shown picture

Occasionally, issues regarding the interlocking are noticed by the presence of “gunshots”, i.e. loud cracking sounds coming from the winding stage and often causing tongue buckling. The cracking sounds indicate discontinuous winding and are caused by stress release, when the tongue or lip folds into place.

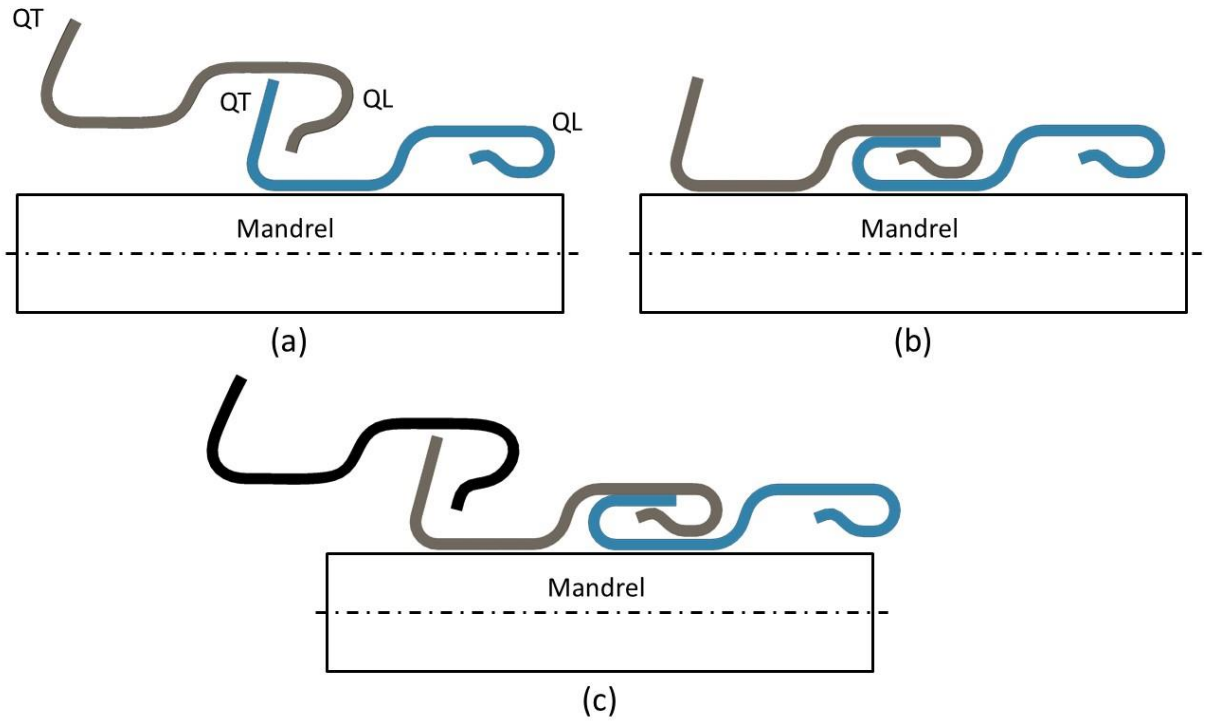

Figure 2-8: Illustration of winding: (a) two profiles just before WT1, (b) QL is interlocked with QT of the previous profile and (c) after one rotation QL is now being interlocked with the next profile

2.3 Post metal forming

2.3.1 Caterpillar

Without constraining of the finished carcass, the helical winding would simply result in rotation of the carcass. It is furthermore, required to remove the carcass off the mandrel, whilst setting the correct carcass pitch. During the removal operation from the mandrel the finished carcass is constrained by a so-called caterpillar, a device with rubber padded belts that hold on to the carcass a fixed distance away from the mandrel / winding tools, see Figure 2-9. The caterpillar speed is of significant influence to the carcass pitch.

One could argue that the caterpillar is part of the metal forming process because winding is not possible without it, and it can have an effect on the winding process. But for the sake of simplicity and the fact that the caterpillar is just an influencing factor, it will be described as a post metal forming operation.

Figure 2-9: Caterpillar that constrains the carcass from rotating and transports the carcass from mandrel to the reel

2.3.2 Reeling

The final stage of the carcass process is reeling it up on large reels that are used to store and transport the carcass. Depending on the size of the carcass there is space for several km of carcass on a single reel, see Figure 2-10.

Figure 2-10: Reel with carcass. The radius of the reel flange is approximately 4m

Chapter 3 Geometrical effects in carcass production

As described in the introduction the carcass profile geometry, especially the dividing point position, is important to the carcass flexibility; a shift in profile dividing point will cause reduced flexibility and alter carcass neutral pitch. Optimum is equal length of QL and QR (see Figure 1-4) and that also goes for the length of lip and tongue. Experiences from carcass production show that staying within production tolerances becomes increasingly difficult, when producing smaller sized carcass' compared to their larger counterparts – especially if the same tool set is being used for the whole range.

This chapter investigates the parameters causing geometry change during winding and expands on the paper [14]. Understanding these effects will allow the tool designer to account for any geometrical change during winding. The analysis is based on production tests, where profiles are analysed before and after winding, as well as visual identification of profile deformation through all winding tools.

3.1 Production test

An in-depth investigation of the geometric effect, where several profile and mandrel sizes are included, is not feasible because of time-consuming carcass machine setup. For that reason the production tests are performed with a single profile of 1.0mm strip thickness, which is wound on three mandrel sizes presented in Table 3-1. The forming tools are the same for tests A and B, whereas geometrical restrictions in the machine demands a slightly different tool setup for test C, where every second forming tool around the mandrel was replaced with smaller cylindrical guide tools to ensure that the carcass would not localise bending between the remaining WTs, see Table 3-2. The strip material is EN 1.4162 lean duplex stainless steel, and the tests were performed on a 4-step loop type carcass machine.

Table 3-1: Production test mandrel sizes and test order

Test	Test order	Mandrel [mm]
A	3	Ø203.2 (8")
B	1	Ø101.6 (4")
C	2	Ø63.5 (2.5")

Table 3-2: Winding tools mounted for the production test

Winding tool	2.5” carcass	4” carcass	8” carcass
1	WT1	WT1	WT1
2	Cylindrical tool	WT2	WT2
3	WT3	WT3	WT3
4	Cylindrical tool	WT4	WT4
5	WT5	WT5	WT5

3.1.1 Profile evaluation

The evaluation of profile geometry is done by cutting out a piece of the finished carcass profile and scanning it into 2D CAD software, where it is digitised thus facilitating measurements and comparisons. Figure 3-1 (a) shows a scanned, finished profile cross-section and (b) show the digitised version of the scanned profile along with the roll formed profile together with a drawing of the winding tool. Dividing point movement is evident from this comparison between the roll formed and finished profile. The dividing point position and total width of the roll formed profile is as expected. The profile width does not change after winding, but QL has decreased and QT has increased in length thus causing the dividing point movement.

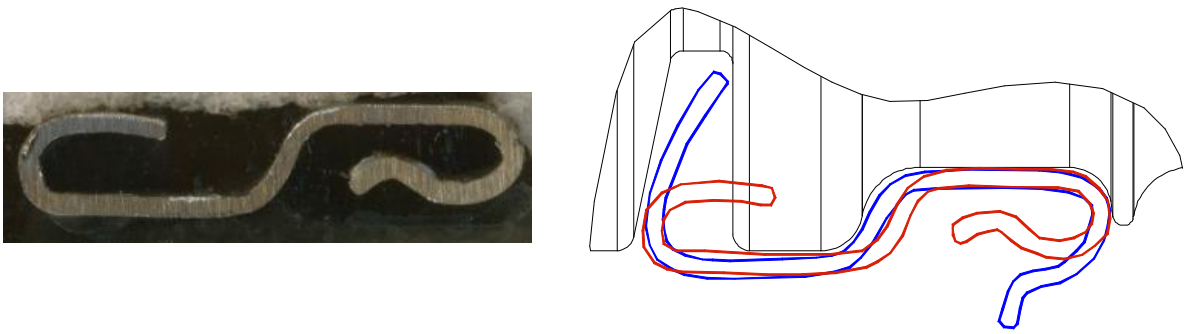

(a) (b)

Figure 3-1: (a) Scanned cross-section of a carcass profile. (b) Carcass profile before winding (blue, open profile) and after winding (red, closed profile) where movement of profile dividing point is evident

3.1.2 Mandrel size effect

Profile comparisons before and after winding in tests A, B and C are shown in Figure 3-2 (a). The result shows a change in profile geometry after winding. The QT-length is increased by a reduction of tongue length through un-bending of the original QT-bend causing the tongue to get shorter from test A to B and from B to C. Material movements also take place, which changes QL, where the lip moves closer to the profile centre due to bending of the QL-bend causing a reduction in the QL-length.

Figure 3-2 (b) shows how material movement and profile dividing point location is affected by mandrel size, as illustrated by the dimensional change of QL and QT. For tests A and B,

good correlation is obtained between reduction of QL and increase in QT indicating unchanged profile width. However, test C shows an increase in profile width as QT is increased more than QL is reduced. The difference is too large to be caused by measurement error and suggests that the mandrel size in test C has passed the limit, where dimension changes of QL and QT are equal in magnitude. Winding tool measurements confirm that there is sufficient space to allow the profile to widen from the roll formed geometry.

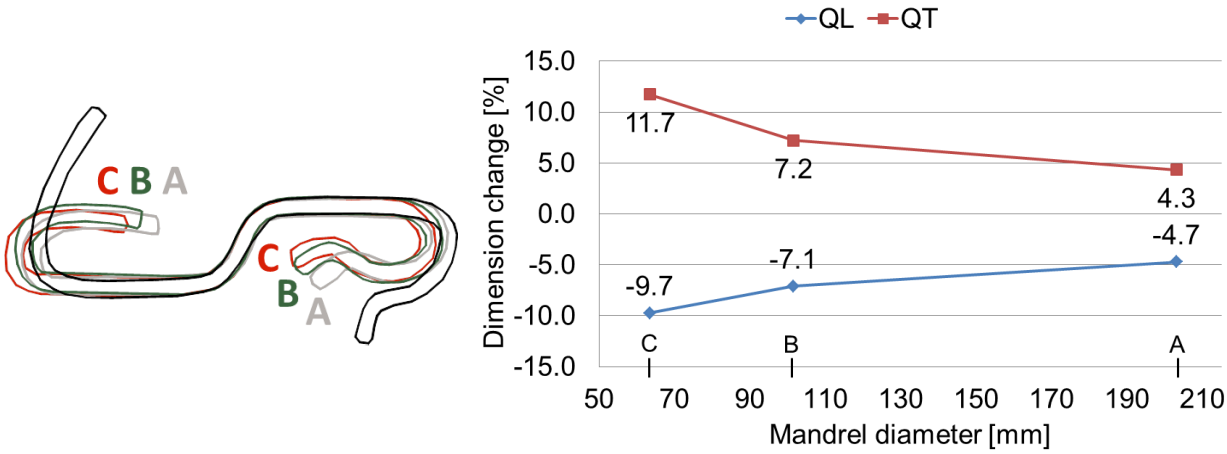

(a) (b)

Figure 3-2: (a) shows the profiles before and after winding for test A, B and C with the profiles centred on the dividing point. (b) Mandrel size influence on dividing point movement in percent from the roll formed carcass profile

The mandrel size effect on the profile dividing point location seems non-linear, which indicates that the main effect is found in factors that vary non-linearly with mandrel size. One such factor is the pitch angle i.e. the angle, at which the profile is bent to reach the helical pitch. This angle changes with mandrel size, since the pitch is fixed for the specific profile. Figure 3-3 shows the profile pitch angles in the production test. An increased profile pitch angle is likely to affect the profile stress state and deformation between WT1 and WT2 corresponding to an increase and a decrease in QT and QL respectively (positive longitudinal stress / strain on QT and negative longitudinal stress / strain on QL).

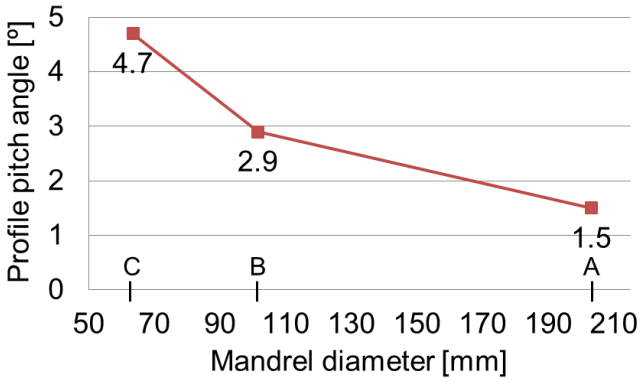

Figure 3-3: Calculated pitch angle according to mandrel size and profile pitch

On loop type carcass machines the loop radius might affect the entry onto the mandrel. The profile entry angle affects the strain path as illustrated in Figure 3-4; (a) tangential entry and (b) oblique entry at an angle φ onto the mandrel. A tangential entry allows the profile to bend smoothly on the mandrel immediately after exiting WT1, whereas an oblique entry requires a reverse bending before entering WT1. This change in strain path and stresses is likely to have a significant effect on profile deformation behaviour. The effect was unfortunately not noticed until after the production tests were concluded, which is why data was not acquired regarding profile entry for the three tests.

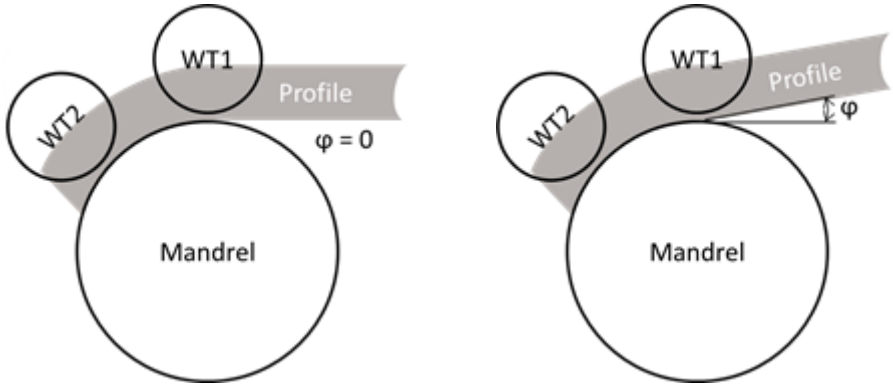

(a) (b)

Figure 3-4: (a) tangential profile entry and (b) oblique entry onto the mandrel where the profile bends in the reverse direction to the winding path before being shaped around the mandrel

3.1.3 Winding deformation

Analysis of the carcasses after the winding stage showed that the dividing point movement takes place between WT1 and WT2, with no further development before the interlocking, see Figure 3-5 (a). This is an interesting observation, since QL is decreasing and QT is increasing simultaneously outside the tools, which implies that the effect is not directly caused by the contoured tools but rather by the deformation around the mandrel.

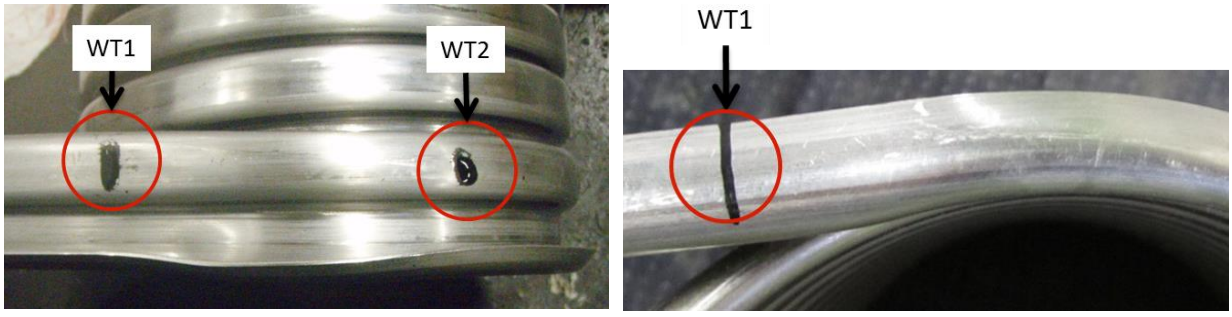

(a) (b)

Figure 3-5: (a) Main deformation during interlock winding take place between WT1 and WT2. Tongue is reduced in height between WT1 and WT2 resulting in broader QT

Figure 3-5 (b) shows that the tongue height over the mandrel is reduced between WT1 and WT2 from an unbending motion of the QT-bend. The material motion during winding is best

explained by introduction of a neutral plane during winding, see Figure 3-6. The figure illustrates the profile during interlocking. It is noticed that the winding tool is only able to influence the tongue angle and the total profile width - indicating the degrees of freedom the profile experience during winding. During the roll forming stage male and female tools ensure accurate geometry, whereas the winding stage, because of the profile interlocking, is a partially free forming process, where winding tools and mandrel control carcass diameter, wall thickness, pitch and profile width, while the profile geometry is otherwise determined by profile stresses. At the profile neutral plane strains and stresses are zero during winding, which implies that the tongue experiences tensile strains and the lip compressive. Smaller mandrel sizes result in larger strains in these parts of the profile. Reduction of these process stresses and strains occur by moving the material closer to the profile neutral plane, which is possible due to the degrees of freedom available during winding - as observed in Figure 3-2 (a).

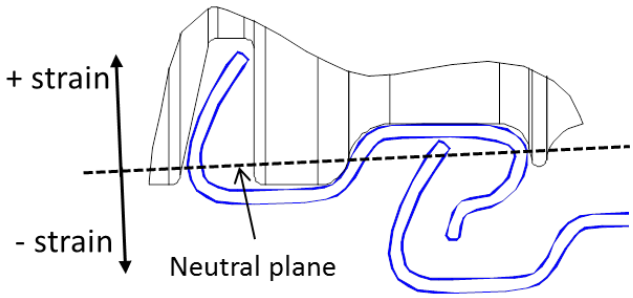

Figure 3-6: Illustration of carcass profile in the interlock with an assumed global neutral plane for the profile and positive and negative strain directions

Deformation will seek to minimize the tongue stresses and strains by lowering the tongue height approaching the neutral plane. This causes an increase in the QT length. The easiest would be to close the tongue by lowering of the angle but the winding tools keep the tongue upright causing the tongue height to reduce instead. As regards the lip minimisation of winding stresses is possible by closing the lip-section and moving the lip closer to the neutral plane. The explanation why QL is reduced in length can be explained by strain hardening during the roll forming stage in the QL-bend, which will cause the ‘free-form’ bending to have rotational centre in the flat part of QL, where it intersects with QL-bend. It is likewise assumed that strain hardening in the QT-bend resists the unbending motion of the tongue. Even though strain hardening prior to winding is the same for all three tests, it cannot be concluded that the effect is negligible, since the strain gradient through the profile varies with mandrel size.

3.1.4 Accounting for dividing point movement by trial and error approach

Profile geometry and path in the winding stage is seen to have an effect on the final carcass profile geometry and the degrees of freedom during winding suggests that attempts to control the profile geometry should be done in the roll forming stage.

Accounting for dividing point movement is achieved by adjusting QL- and QT-bend positions in the roll formed profile, using the results obtained from test B in repeated tests. Figure 3-7 displays the result, where QL and QT are shown in percent of the total width before and after winding. An increase and decrease of five percent of QL and QT respectively produces a profile that after winding has a dividing point located at the profile centre. Thus, a trial and error approach, where profile geometry is adjusted in the roll forming stage, makes it possible to achieve the desired target for dividing point location.

Applying tools, which are adjustable by shims, will allow quick adjustments to the roll formed profile during setup, so that the desired profile is obtained after winding.

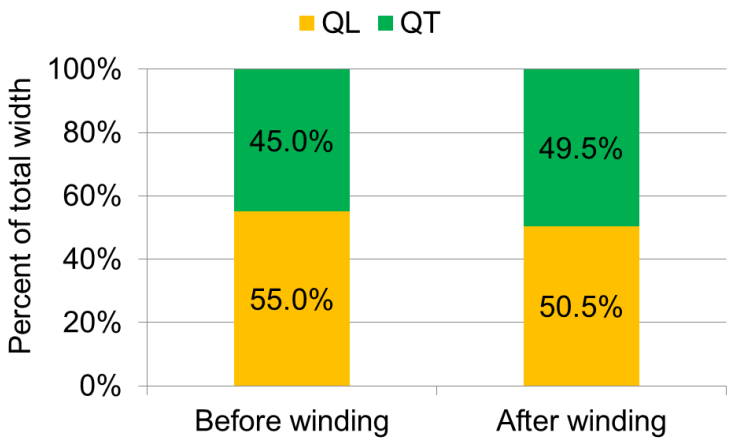

Figure 3-7: Position of profile dividing point before and after winding for the adjusted test B. Dividing point location at profile centre is achieved by accounting for the winding movement in the roll forming stage

3.2 Results and discussion

Due to the 'free forming' during winding, profile strains determined by mandrel size, are influencing profile dividing point position. A smaller mandrel leads to higher strains and thus increased movement of the dividing point. As the profile is wound onto the mandrel the material furthest away from the profile neutral point will experience the highest strains. In the present case this is the tongue- and the lip-sections. The winding stage allows the profile sections to move closer to the neutral point thus reducing the maximum strains, which in turn affects the width of QL and QT and thereby the position of the profile dividing point. Mandrel size related factors such as profile pitch angle and entry angle are expected to affect dividing point movement - also through increased profile strains.

During the course of this project observations have been made, which suggest that small changes in winding tool positions can have a significant effect on final carcass geometry and it seems very likely that the superimposed stress from the profile path influences the deformation that takes place during interlock winding. As a result tool design should account for

winding deformation as well as the profile path into the winding tool. It would be interesting to perform tests that vary the pitch angle, at which the profile is being fed into WT1.

Because profile stresses during winding are influencing the geometry, the direct feed type carcass machines are likely to increase the geometry / dividing point effect as reducing profile feed to the winding stage will induce higher stresses in the profile than a loop type machine. This effect was not methodically investigated in this project, but there are indications that 'starving' the winding stage of the RF profile (by increasing the back tension) does have a negative impact on profile geometry.

It is likely that forming a more closed profile shape in the roll forming stage will minimize or even remove many of the issues that arise during the winding stage in the present production regarding dividing point movement and poorly defined bends. However, it is a challenge to ensure interlocking between the profiles, of only a slightly opened geometry, which can be difficult to control during winding.

It was attempted to investigate the winding geometry effects with FEA but without proper interlocking deformation the obtained results were not satisfactory and are therefore not included in the thesis. However, a validated FE-model would prove useful in parametric studies on the influencing parameters on the profile geometry during winding. As the present results suggest, however, the model would be quite sensitive to the boundary conditions set by the user and with the sensitivity in tool settings on the machine it could be difficult to achieve a suitable model.

The production tests showed that carcass tool design starts with the final profile, and the designer must work backwards through the process thus accounting for the individual process steps, which in turn indicates that the profile completed from the roll forming stage might be quite different from the desired final geometry. A more thorough investigation into these geometry effects is suggested as future work, since this project only has uncovered the effect and that it is manageable by trial and error but the specific factors and their effects are not accounted for and therefore left unanswered.

Chapter 4 Failure mechanisms in carcass production

In this chapter the typical failure mechanisms in carcass production will be examined together with a discussion on how to resolve them, when they occur and even account for them prior to production. The failure mechanisms relating to the main themes of this project will be presented but not discussed in detail, since in-depth investigations are presented in subsequent chapters.

4.1 Categorisation procedure

The majority of this work was carried out on the factory floor by being available for issues regarding product quality. This is in line with the Gemba methodology and allows verification of the hypotheses made and enabling interviews with personnel at the factory floor – where most process knowledge regarding failure modes is available. Based on observations the failure mechanisms are categorised into the following failure modes: *Process failure* and *design deviation*.

Figure 4-1 and Figure 4-2 provide a schematic representation of the failure modes in roll forming and winding - as evident; most problems occur in the winding stage.

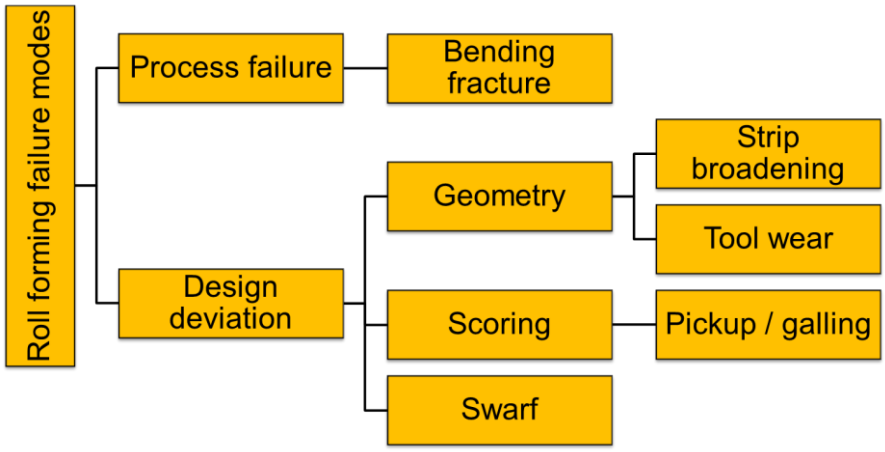

Figure 4-1: Failure mechanisms in roll forming

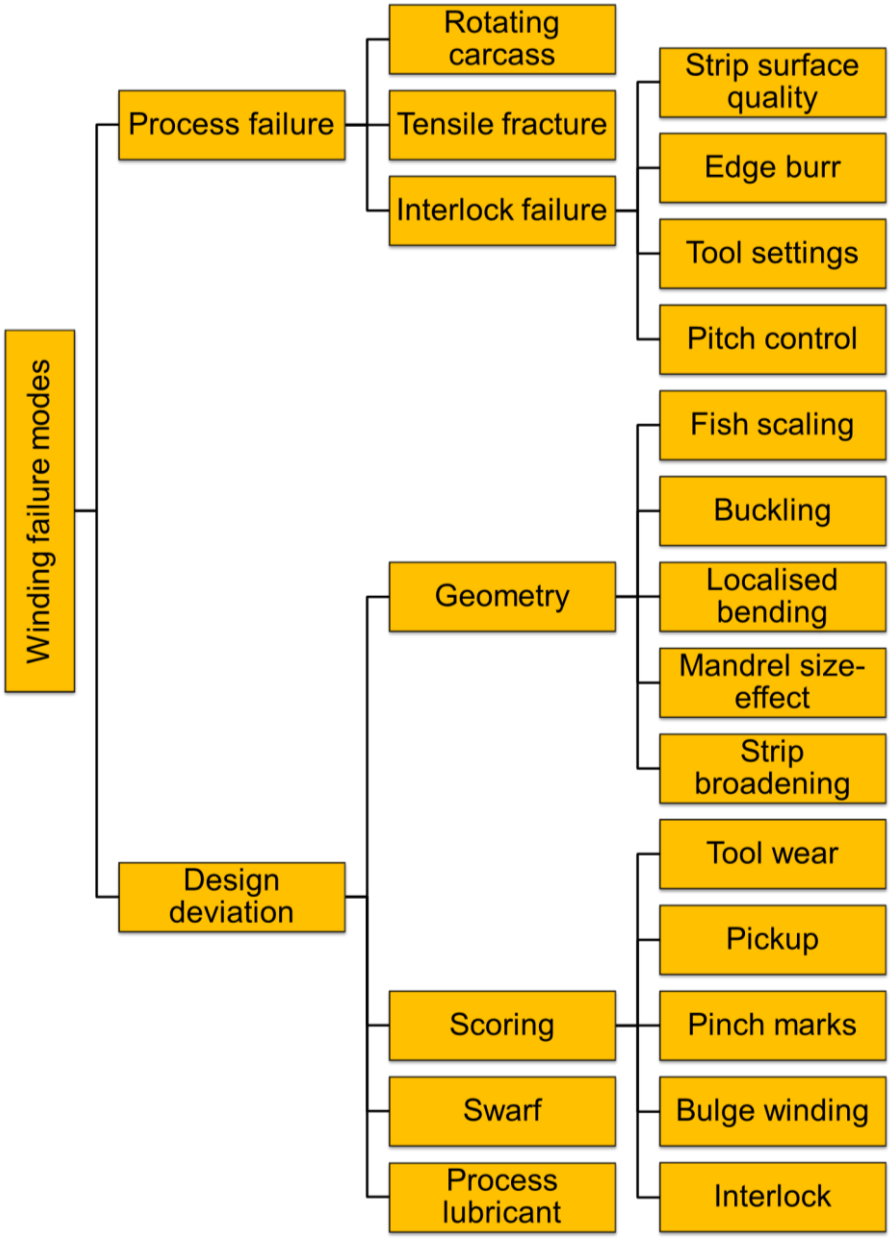

Figure 4-2: Failure mechanisms in winding

4.2 Process failure

4.2.1 Rotating carcass

Rotating carcass may appear during winding either in the same direction or opposite to the winding direction.

If the caterpillar does not prevent the carcass from rotating during production the whole carcass will rotate slightly with the machine rotation on its way to the reel in this way pre-stressing the carcass, see Figure 4-3 (a). This is a failure mechanism that arises because torque is transferred to the carcass on the reel such that it is pre-stressed. When being fed into the extruder line, the carcass will rotate backwards as it leaves the reel again, which causes re-

peated bending of the carcass, so that it is no longer straight but curls like a pig's tail – the failure mechanism called pig-tailing shown in Figure 4-3 (b). Solutions include to ensure sufficient friction between the carcass and the caterpillar or to reduce the torque needed to wind the profile.

(a) (b)

Figure 4-3: (a) Carcass rotating with machine direction shown by the angle of the blue line and (b) carcass hinting pig-tailing on its way onto the reel

In rare occasions carcass rotates opposite to the winding direction. The mandrel rotates slowly opposite to the machine rotation and when the torque needed to bend the profile around the mandrel is low and friction conditions between carcass and mandrel are high enough, carcass will follow mandrel rotation. Instead of pig-tailing a diameter increase is the result and buckling of carcass between winding centre and caterpillar occurs, see Figure 4-4. In that specific case the solution was to lower the pre-load of the WTs on the profile / mandrel, which lowered friction between mandrel and profile thereby avoiding carcass rotation.

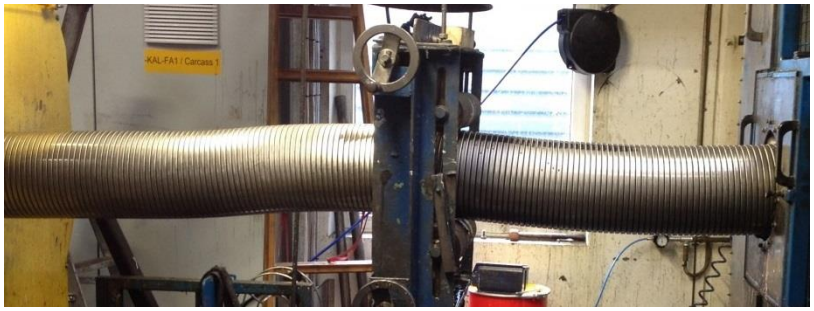

Figure 4-4: Carcass buckling due to rotation opposite machine direction which increases the carcass length

4.2.2 Bending fracture

Bending fracture is a failure mechanism occurring in the roll forming stage but it is not a formability issue. Problems with fracture in roll forming are rare and are related to material properties not satisfying the raw material specifications. Since bending tests, of the sheet strip towards itself are sufficient to verify, whether a specific material batch is viable for carcass roll forming. When fracture occur during roll forming it is on the outside of QT- and QL-bends (Figure 1-4) that experience plain strain bending as illustrated by Figure 4-5.

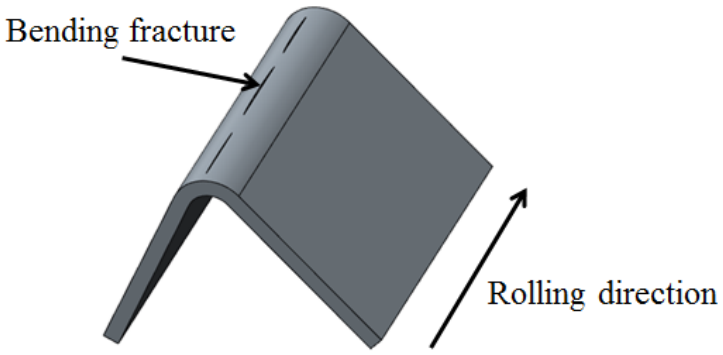

Figure 4-5: Fracture in bends in roll forming stage

4.2.3 Tensile fracture

Tensile fracture is a common failure mechanism because of the sheer number of welds that are produced for each pipe and the difficulty in attaining the required properties in the weld and heat affected zone (HAZ). The tensile strains appearing in the tongue during winding are significant, and the most common fracture location in carcass production is in the HAZ. The failure mechanism is necking followed by fracture. The mechanism is further treated in Chapter 8.

Figure 4-6: Weld fracture during winding

Fracture at the tongue edge outside welds could be due to lack of formability in the basic material but it is more likely combined with damage to the strip edge, like a notch causing strain localisation. When possible the process will try to localise bending during winding like explained in paragraph 4.3.4. It will be shown in Chapter 8 that the strains in the tongue during winding are well below the material forming limit.

The weld between coils ensures production of continuous carcass lengths but these welds are sometimes critical since the formability of the weld is significantly reduced compared to the parent material. Fracture next to the weld seam is seen in Figure 4-6. Optimizing weld procedures and heat treatment of the weld can improve weld ductility [10]. Otherwise introducing weld relief zones will alter the strain distribution around the weld to prevent fracture.

However, weld relief-cuts themselves are prone to fracture. If weld reliefs are cut too deep the strip will fracture here instead in the HAZ. Therefore a precise definition of the weld relief-cut is needed for each strip size. In short: correct positioning and design of the relief-cut is imperative to obtain necessary weld relief as well as to avoid fracture in the relief-cut. This is further treated in paragraph 8.3.

4.2.4 Interlock failure: strip surface quality

Since the interlocking occurs between two stainless steel profiles in contact deforming each other, basically working as tools, tribology is an important factor regarding smooth interlocking procedure. Therefore strip surface quality is an influential factor in this stage of the process. Figure 4-7 shows two strip surfaces; (a) normal surface which gave no problems during production and (b) a strip surface with oxide residuals that caused interlocking failure. Gunshots were overheard preceding failure.

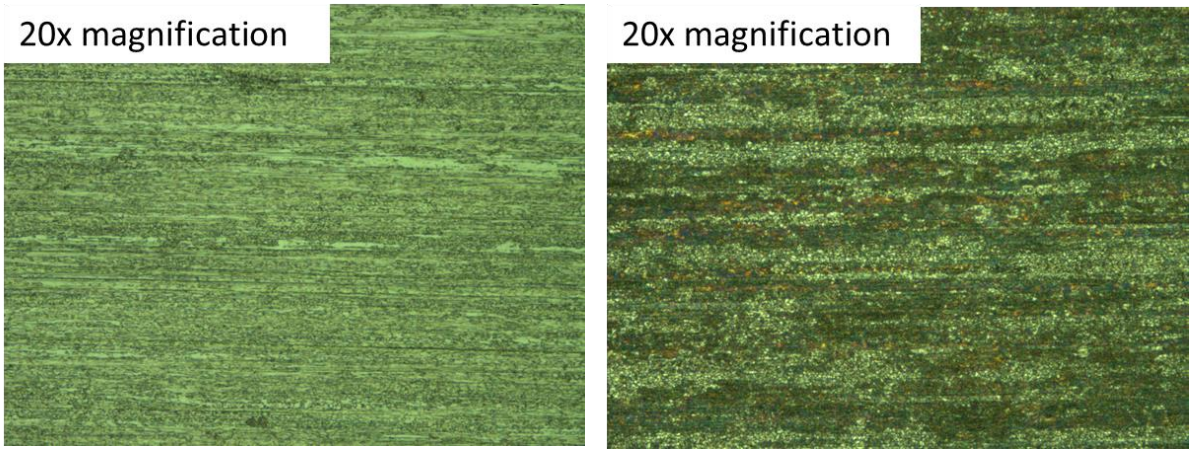

(a) (b)

Figure 4-7: (a) normal strip surface, 20x magnification and (b) strip surface with oxide residuals, 20x magnification

4.2.5 Interlocking failure: edge burr

Interlocking failure in form of edge burr can be both a process failure and an environmental factor on the production floor. A large burr on either of the strip edges can cause ‘gunshots’, which can be very loud and in severe cases also lead to buckling of the tongue. A large burr is also known to increase winding torque, causing carcass to rotate in the caterpillar, as described in 4.2.1. The solution is a better edge quality or burr removal prior to loading the material onto the machine.

4.2.6 Interlocking failure: tool settings

Proper tool settings are important for a stable interlocking. The winding tools must be properly setup with angles matching the carcass pitch, and the roll formed profile must be guided on its way to WT1. With the roll forming tools it is a balance of closing the profile but not too much as this could create problems in the winding operation. In any case of interlocking failure it is important to check the tool settings. Especially with an open profile issues appear with the profile not deforming as desired as illustrated in Figure 4-8:

1. Interlock contact force is pressing on the almost vertical lip-section
2. The leg of the lip collapses and rotate opposite of normal closing rotation
3. Rotation of the leg of the lip force a translation the profile opposite production direction causing interlock failure and in some cases the tongue is sheared off because it is forced under the WTs

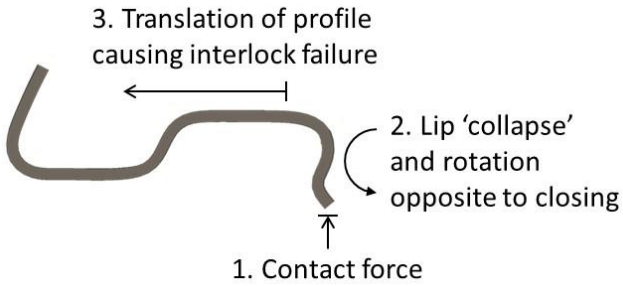

Figure 4-8: Interlocking failure because of an almost vertical leg of the lip

4.2.7 Interlocking failure: pitch control

The caterpillar is normally set to a pitch that matches the required carcass pitch, so that the caterpillar just transports the carcass from winding stage to the reel. However, in some cases the caterpillar can be used to adjust the carcass pitch to a lower value simply by reducing the transport speed. Obviously this sends a backwards force towards the winding tools which impedes the carcass from being pushed off the mandrel. If the force is too large the winding tools will fail in pushing the carcass off the mandrel causing them to cut the carcass and interlocking fails. Using the caterpillar as a pitch control in the winding phase should be limited and if used, the pitch reduction should be minor.

4.3 Design deviation

4.3.1 Geometry: tool wear

Tool wear is not a major problem in production but occasionally tool wear leads to tool fracture by chipping, especially in the roll forming tools that form the lip, so that the lip does not obtain the desired shape. This part of the profile includes a small bend and, the tools

experience rather high alternating stresses and adhesive wear, which is the cause of fracture. This is investigated in Chapter 9.

4.3.2 Geometry: fish scaling

The fish scaling failure is named after the defective carcass profile shape defined by the angle α, see Figure 4-9. Fish scaling is un-wanted because of the excessive stresses that the carcass will exert on the inner liner.

Figure 4-9: Illustration of fish scaling where the angle α indicates the severity of fish scaling

The occurrence of fish scaling if often the result of poor tool design that fails to account for the deformation during winding, which indicates that the roll formed profile does not have a proper geometry. In some cases fish scaling is the result of improper setup of the winding tools.

The best solution is to account for the whole deformation path in the tooling design thus leaving little risk due to tool setup.

4.3.3 Geometry: buckling

Buckling is an effect limited to the tongue, which occurs during winding, either before or after interlocking, which severely limits profile displacement. Tongue buckling before interlocking occurs during the first part of profile revolution prior to interlocking. It is caused by non-intended tool contact of the tongue end and the ensuing strain path, see Figure 4-10. Point B will elongate (plastic) as it moves under the WT, along a longer path than point A, whereas point A does not change its length (elastic). This causes a strain gradient that leads to buckling in a zone around the tongue edge – point B. The problem arises when tool contact with the tongue edge appears before interlocking due to a tongue angle from the roll forming stage, which is not suitable. It could furthermore be an indicator of the failure mode described in 4.2.6, where the profile is being forced backwards under the WTs, and the tongue starts deforming against the WTs.

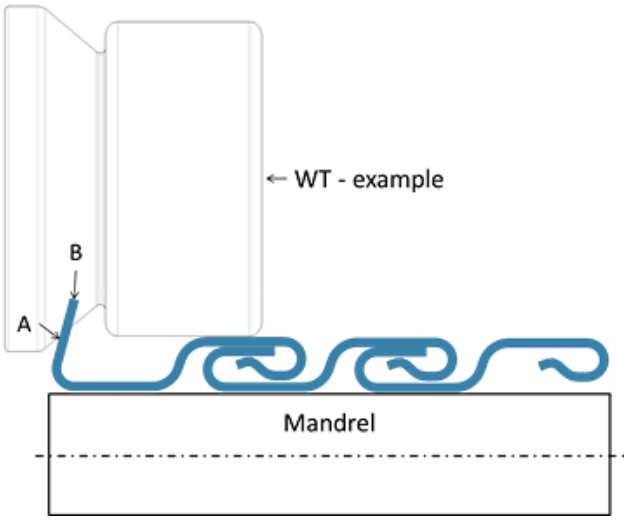

Figure 4-10: 2D example of a tool contact situation that would cause tongue buckling before interlock – the profile is already wound onto the mandrel. A cross section is shown just before entering the WT. Point B travels a longer distance under the WT than point A causing compressive strains around point B

Tongue buckling after interlock appears in the final profile and is often difficult to discover without cutting out a piece of carcass for visual inspection, see Figure 4-11. In some severe cases buckling has an effect on the tool-profile contact showing an irregular contact pattern on the outer surface of carcass. The strain path the tongue experiences start with elongation and ends with compression as the profiles are interlocked, which in turn makes the tongue vulnerable to buckling.

Figure 4-11: Tongue buckling after interlock

However, the main contributing factor seems to be the deformation length over which the interlocking is achieved as tongue buckling is often seen, when producing small carcass diameters with relatively large profile sizes; short interlock length due to the short radial distance between WT1 and WT2 on small radii mandrels. Furthermore, tongue buckling can be solved by interlocking the profiles over a longer length; achievable through lifting the winding tool away from the mandrel thus generating a longer ‘ramp’ for the interlocking. Those two observations strongly indicate that interlocking deformation length is an important factor regarding tongue buckling.

The simple winding FEA is able to show buckling, when the tongue is closed too rapidly, see Figure 4-12. The analysis show a large longitudinal stress gradient through the strip thickness indicating tensile stresses and compressive stresses on the outer- and inner strip surfaces respectively, where tongue closing deformation initiates – at point A. It seems likely that when this deformation is too severe, the tongue obtains a curvature that is not straightened out before the tongue passes the closing WT at point B, where the tongue must rest at its final height over the mandrel causing the tongue buckling. The phenomena is not investigated in depth, but in future work it is planned to identify the strip sizes and deformation paths that lead to tongue buckling. Within the tool design a minimisation of the strain path of the strip edges surely will help avoiding this failure. So far, however, similar strain paths have shown that thicker profiles show higher buckling resistance, as to be expected.

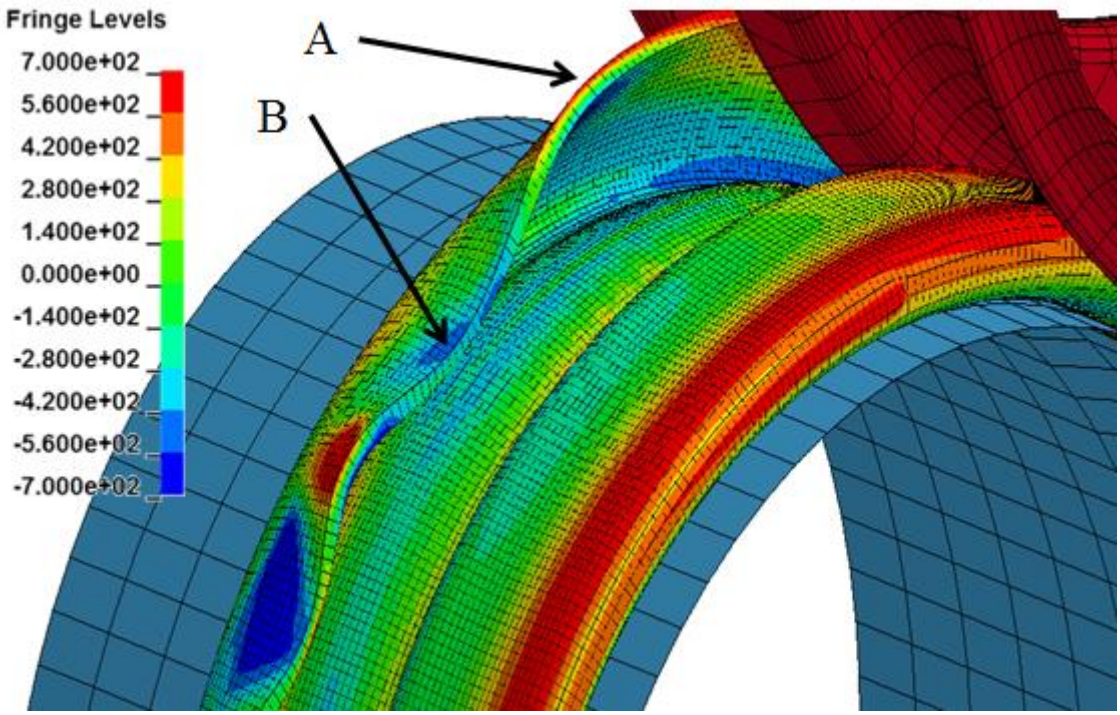

Figure 4-12: Tongue buckling indicated by FEA simple winding model (1.1mm profile on a 4" mandrel) – the tool closing the tongue is hidden in this view. Fringe colours are longitudinal stresses and they show a stress gradient from strip outer to inner surface at point A where tongue closing initiates and point B indicates where the tongue is passing under the closing WT

Tongue buckling is sometimes seen together with gunshots. During stress build-up (each gunshot is caused by a sudden release of stresses in the tongue) it is likely that the tongue edge experiences further plastic straining than it would under normal, "smooth" winding conditions. Furthermore, during each shot a shock wave is sent through the material, which possibly induce large local compressive stresses. Smooth winding is an important issue toward minimizing risk of tongue buckling.

4.3.4 Geometry: localised bending

Localised bending can arise as a result of the above mentioned buckling of the tongue. When WT1 is lifted away from the mandrel to ensure a longer deformation path the boundary conditions on the profile change and it is more free to deform. The effect is the same as a three-point-bend, where the bending moment is largest at the centre tool (in case of carcass winding the centre tool is the mandrel), see Figure 4-13. This failure repeats itself with regular intervals as depicted in Figure 4-14.

The solution is to restrict profile degrees of freedom by keeping the profile in contact with the mandrel and preventing localised the bending between WT1 and WT2.

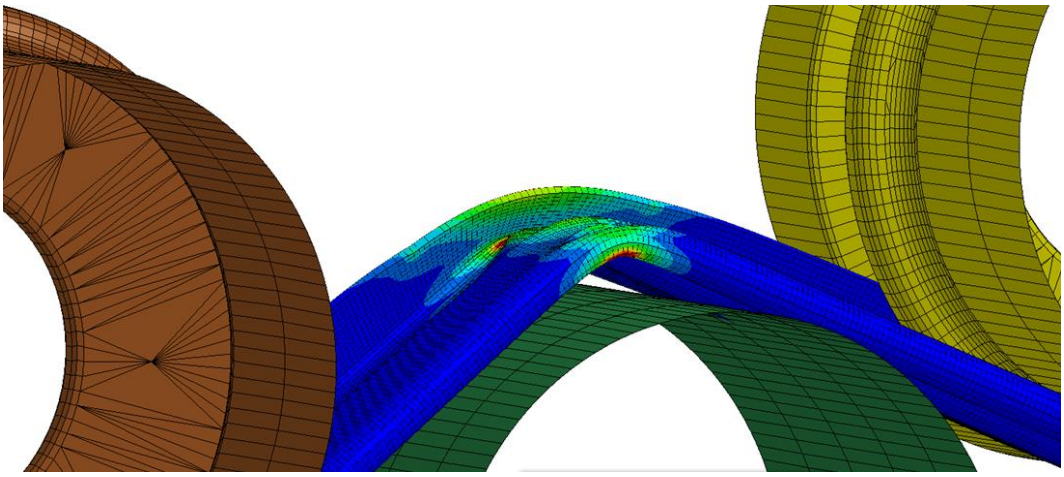

Figure 4-13: Localised bending illustrated by three-point-bending in FEA where constraints tying the profile to the mandrel has been removed

(a) (b)

Figure 4-14: Experiment moving the WTs away from the mandrel allowing the profile to buckle during winding. (a) Inside look of the buckled profile and (b) ‘waviness’ of the WT contact with the profile indicating bend localisation

4.3.5 Geometry: mandrel size-effect

The carcass profile experiences large local tensile and compressive stresses, when it is being wound onto the mandrel, and a way to minimize these stresses is to move material towards the profile neutral plane (tongue- and lip-sections are experiencing the highest strains). Because of the degrees of freedom that the profile has during winding (explained in section 2.2.3) this is actually possible and the tongue- and lip-sections will move towards the profile neutral plane. The amount of movement depends on the stress level in the profile. Figure 4-15 show this effect as a change in dividing point position from before to after winding – an effect further described in Chapter 3.

Tool design must account for the mandrel size, since investigations have shown that mandrel size greatly influences final carcass geometry. Because the carcass process is a combined roll forming and winding the winding tool design depend on the roll forming tool design, which implies that adjustments in the profile geometry often have to be done in the roll forming stage to account for the winding stage deformation.

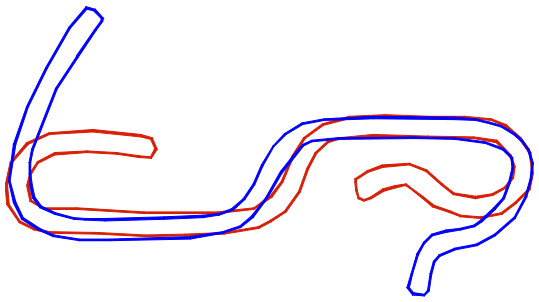

Figure 4-15: Carcass profile before winding (blue, open profile) and after winding (red, closed profile) where movement of profile dividing point is evident

4.3.6 Geometry: strip broadening

In bending processes the term neutral plane, point or axis is used to explain positions in the work piece, where stresses and strains are zero and thus unaffected by deformation. Figure 4-16 illustrates the variables in bending theory, where t is strip thickness, w is strip width, R is the bending radius, ρ is the radius of curvature at the neutral plane and θ is the bending angle [13]. In simplified theory an ideal plastic material subjected to a pure bending moment the neutral plane (np) is assumed to be located at the centre of the strip (np = t / 2) as depicted in Figure 4-17 (a). However in reality the neutral plane is usually moved towards the centre of curvature explained by bending with super-imposed tension; Figure 4-17 (a) + (b) results in the strain distribution shown in (c) where e is the distance from np to the strip centre. This shift in np-position will cause elongation of the strip at the bend [15, 16].

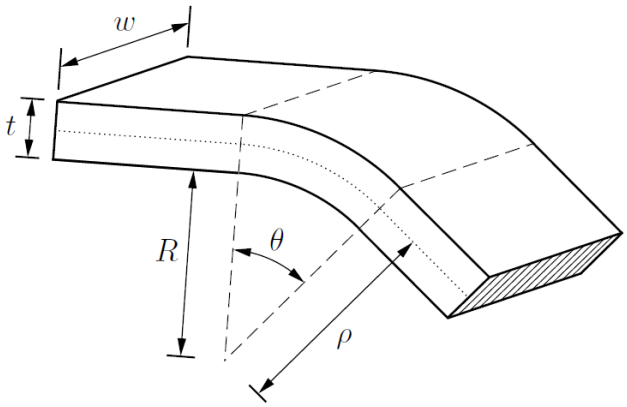

Figure 4-16: Variables in sheet bending

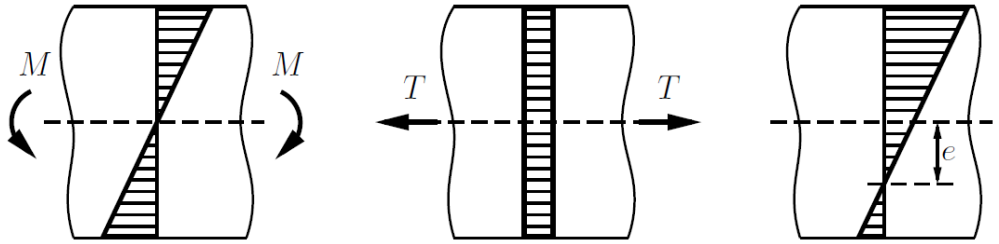

(a) (b) (c)

Figure 4-17: Bending strains in: (a) pure bending where np is at strip centre, (b) pure tensile strain and (c) bending with super-imposed tension moving the np away from strip centre toward the centre of curvature

In sheet metal bending theory an estimate of the np-position can be made based on DIN 6935, where the final length of a bended sheet metal is calculated with the neutral point position placed according to eq. (4-1) [17]:

$$\rho = R + \left(\frac{t_0}{2} \cdot k\right), \tag{4-1}$$

where *k* is:

$$k = 0.65 + \frac{1}{2} \cdot \log\frac{R}{t} \quad for \quad \frac{R}{t} \leq 5$$
$$k = 1 \quad for \quad \frac{R}{t} > 5 \tag{4-2}$$

Another solution is given in [18], where the neutral plane position is empirically determined as a factor 0.4 of the sheet thickness:

$$\rho = R + (0.4 \cdot t_0) \tag{4-3}$$

In carcass roll forming the position of the neutral plane in each bend will move away from the strip's geometrical centre causing slight material thinning at the bend and broadening of the profile strip length. Figure 4-18 illustrates the effect where the blue profile is the target profile but the actual end-points of the tongue and lip is shown as the yellow segments; the resulting failure mechanism will be loss of displacement and a reduced maximum and neutral pitch.

Figure 4-18: The effect of strip broadening; blue profile is the desired geometry and the yellow indicate the actual profile if strip broadening is not accounted for

Figure 4-19 shows the average strip broadening for four strip thicknesses along with the standard deviation of the measurements. The measurements are based on profile scans (of finished carcass) and CAD measurements of these with the assumption that original strip width is nominal. The result is an average strip broadening of about 2.3%, which will cause a reduction of the displacement flexibility of around 35%. The variation in the measurements could be a result of:

- Measurement uncertainty; scanning and measuring profile centre line in CAD software
- Tolerances; initial strip width most likely deviates from the nominal width and between each production
- Tool setup; varying mandrel size as well as different settings of roll forming and winding tools are known to affect deformation path and are likely also affecting strip broadening

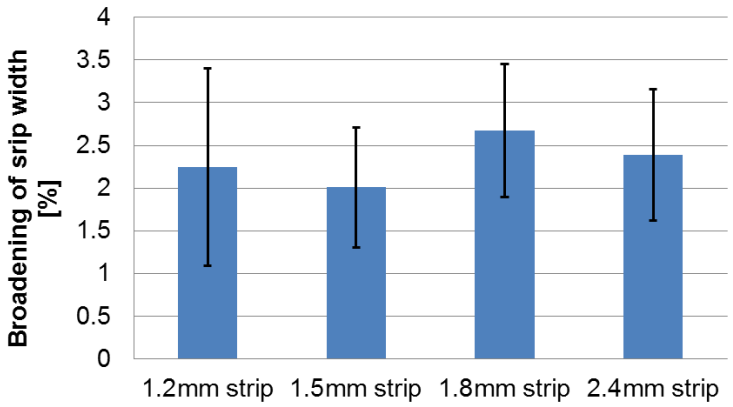

Figure 4-19: Strip width broadening measured on the final profile in percent

The above result is compared with bending theory to see which provide the best estimate for carcass production. The elongation for each bend is calculated from bending angle and radii from the theoretical final profile with the assumption that each bend is completed in one step.

Table 4-1 show the result based on eq. (4-1) and eq. (4-3). Both theories are close to the measurements and could be used for an initial estimate of strip broadening.

The solution to strip broadening is straightforward; reduce initial strip width to account for strip broadening.

Table 4-1: Strip broadening calculations based on theory and the theoretical final carcass profile - the factor k is explained above

Theory	Broadening [%]
eq. (4-1): np position = $\frac{t_0}{2} \cdot k$ [17]	3.0
eq. (4-3): np position = $0.4 \cdot t_0$ [18]	2.2

4.3.7 Scoring: tool wear

Tool wear can cause chipping of the roll forming tools that form the lip or one of the features of the winding tools that helps setting the pitch. Fractured tools will cause scoring of the profile for every revolution the tool takes. It is therefore important to look for periodical marks on carcass, as they indicate tool problems.

4.3.8 Scoring: pickup

Pickup / cold-welded stainless steel formed on critical tool surfaces will act like an abrading surface when in contact with the stainless steel thus scoring the strip surface - sometimes creating galling swarf as explained in paragraph 4.3.13 and Chapter 9.

4.3.9 Scoring: pinch marks

Pinch marks derive from the winding tools and are marks found on the profile s-section, near the dividing point, as seen in Figure 4-20. Normally these marks originate from two situations:

1. Winding tool angle does not correspond to carcass pitch
2. Caterpillar pitch is too low, which forces the carcass profile against the winding tools

In some cases pinch marks might be discovered by a bulge winding failure mechanism described below in paragraph 4.3.10. This issue can be resolved by carcass machine settings or a change in tool design.

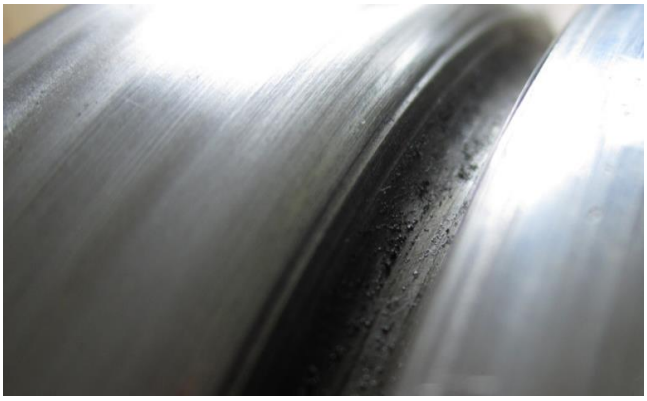

Figure 4-20: Pinch mark from winding tool on carcass profile

4.3.10 Scoring: bulge winding

Bulge winding can occur during winding, when conditions such as a large radial distance between the winding tools allow the wound profile to bulge between WT5 and WT1 as illustrated in Figure 4-21. The condition of the profile is similar to Figure 2-8 (b), where the tongue is still open, ready for interlocking, and the lip is interlocked with the previous profile. The bulged profile has a larger radius than the rest of the carcass wherefore it is reduced in radius by WT1. Geometry dictates that a relative motion must occur between the two interlocked profiles and galling initiates with the result shown in Figure 4-22. The image show signs of material ploughing into the tongue surface and investigations of the opposite surface in contact, QL, show signs of missing material 'ripped' out of the surface.

An experiment was attempted to apply a better lubricant added just prior to winding. This slightly diminished galling but did not remove scoring completely. The solution is to ensure that a bulge between winding tools does not occur either by adding supporting rolls or increasing back tension in the roll formed profile. During the experiment it was also noted that bulge winding can cause irregular pitch due to varying movement of the interlocked profiles as the bulge moves under WT1.

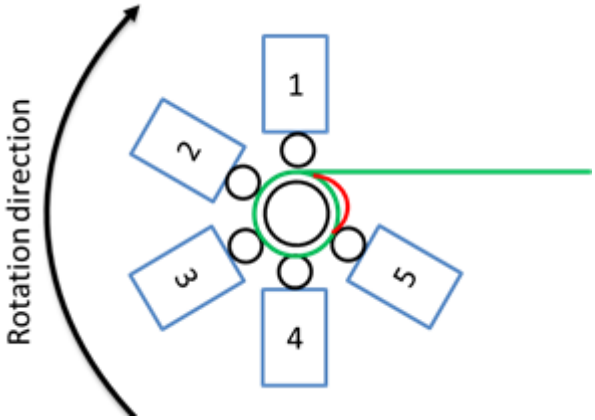

Figure 4-21: Illustration of bulge winding where the red line represents the profile bulging between WT5 and WT1. The green line indicate normal carcass profile position

Figure 4-22: Severe scoring of the tongue as a result of bulge winding - only observable by cutting a window into the carcass.

4.3.11 Scoring: interlock

During interlocking severe contact conditions can cause scoring of the tongue and surface of QL. High strength in the tongue leads to severe scoring of the tongue edge and QL-surface initially in contact during interlocking as seen in Figure 4-23 (a) and (b). The problem is too large tongue angle, Figure 4-23 (c), causing high contact pressures between tongue and QL-surface and the fact that a higher load must be applied before the tongue starts bending to produce the carcass interlocking. This can cause interlock deformation to be abrupt instead of smooth. This is seen as the jagged marks in Figure 4-23 (a), which indicates irregular interlocking and causes gunshots in this particular production. Tongue buckling may arise in this localised contact because the deformation is abrupt instead of smooth and constant.

The problem is solved by creating a more smooth interlocking by lowering tongue angle or allowing the interlocking to take place over a longer distance.

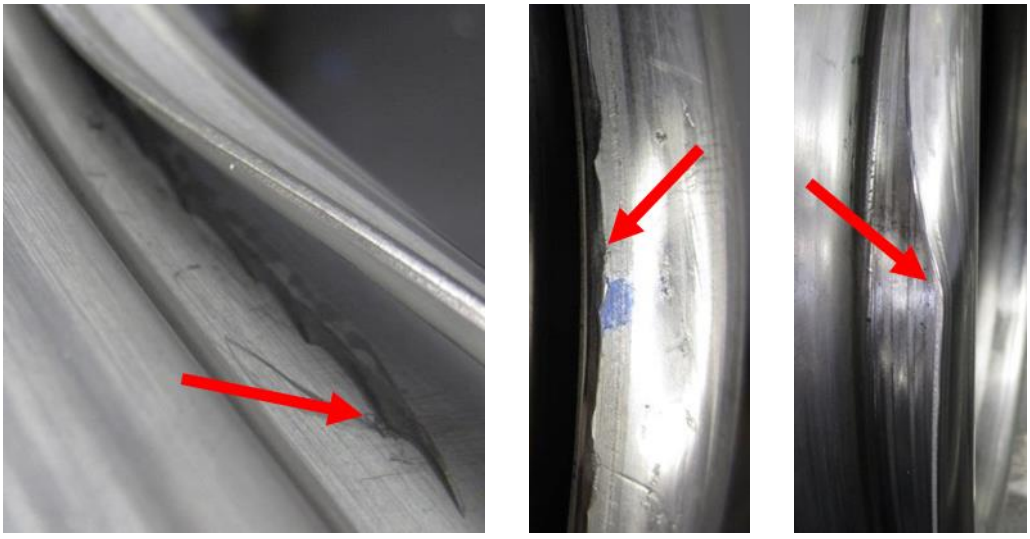

(a) (b) (c)

Figure 4-23: Scoring during interlocking; (a) on QL surface, (b) folded edge at tongue and (c) non-smooth interlocking of tongue

4.3.12 Process lubricant

The use of lubricant in the carcass process is necessary to reduce wear, process temperatures and to maintain a smooth interlocking. Problems appear due to excessive amount of lubricant that is trapped inside the carcass after production, since a continuous production of a closed pipe limits the possibilities of subsequent cleaning, which would be costly.

Excess lubricant creates two problems in later stages of production:

- Extruder issues: in the extrusion process too much lubricant can cause the process to fail, especially if it contains water that will expand at elevated temperatures
- Polymerised lubricant: the elevated temperatures during pipe production and the large stainless steel surface in the carcass accelerate oxidation of the lubricant, which turn into thick rubber-like substance that could plug valves during use of the pipe. To remove the residuals the pipe is cleaned by pigging [19], often several times, which is a costly procedure

The solution to both problems is to keep lubricant use in carcass production at a minimum and only lubricate, where it is needed.

4.3.13 Swarf

Swarf is also a topic covered in more detail in Chapter 9. Therefore the following just provides a short description of the failure modes connected to swarf. Swarf is found to stem from the following three modes of failure:

- Strip edge: when the strip edge comes into heavy loaded contact with tools, or even with the profile itself during interlocking, a burr may be created and removed or just removed from the strip edge thus generating swarf, see Figure 4-24 and Figure 4-25. This effect is present in roll forming, profile path to winding, winding and in the interlocking stages
- Galling: Tool pickup can lead to scoring of the strip surface that creates so-called galling swarf; a type of swarf that is significantly finer in appearance compared to edge swarf. This type of swarf is only generated in the roll forming stage, where pickup is formed on tool edges in contact with the profile. It is not a significant factor in itself, but it will leave residues in the machine causing excessive wear on mechanical parts
- Scoring: in severe cases, where the tools are scoring the profile, such as pinch marking described in paragraph 4.3.9, severe plastic deformation of the profile surface may create a burr or swarf. This type of swarf is therefore not a failure mechanism in itself but rather an indication that something else is wrong

Figure 4-24: Edge swarf being dislodged in roll forming

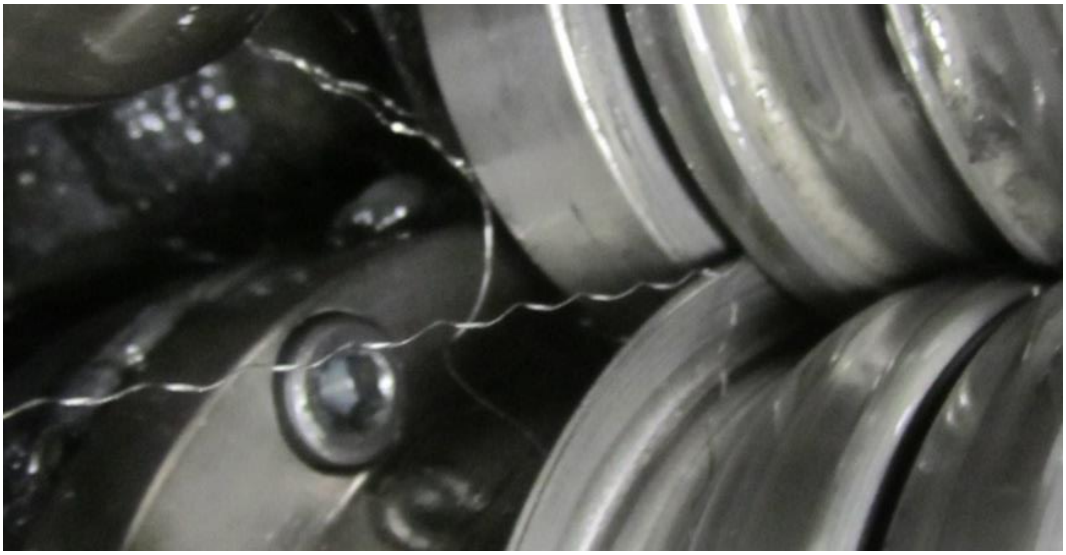

Figure 4-25: Edge swarf from tongue edge during winding

Chapter 5 Material characterisation

Process engineering involves the use of material characterisation because understanding of material behaviour and forming limitations is essential for process and product optimisation. This often involves testing and a need to know about the different tests and analysis methods that are available for material characterisation. This chapter studies literature on various methods and techniques for sheet metal testing and forming limit determination as well as characterising four different grades of stainless steel sheets used in carcass production; one austenitic grade and three duplex grades. The characterisation includes determination of flow curves, anisotropy and forming limit curves. Strain measurements for forming limit determination are performed with GOM ARAMIS automated 3D strain measurement system.

5.1 Flow curve expressions

Uni-axial tensile testing is the most widely used material test, often carried out in universal testing machines where load and displacement are acquired during the test. This simple setup allows fast testing and test specimen fabrication is normally also simple. ASTM A370-11 describes how to perform the tensile test and how specimen geometry should be prepared. Using this standard ensures similarities between tests thus allowing cross test comparisons. Often the results are shown as engineering stresses and strains, which are useful regarding definition of yield stress, ultimate tensile strength and fracture point. But for flow curves used in finite element analysis (FEA) and analytical methods true stresses and strains are required. True stress is calculated by eq. (5-1) where A_1 is the actual cross-sectional area of the tensile specimen and true, or logarithmic, strain is calculated by eq. (5-2).

$$\sigma = \frac{F[N]}{A_1[mm^2]} \tag{5-1}$$

$$\varepsilon = \ln\left(\frac{l_1}{l_0}\right) \tag{5-2}$$

A general flow curve often looks like the graph depicted in Figure 5-1. The flow curve can be obtained by tensile testing and when such a curve is available a mathematical expression of the flow curve is often used to describe the stress / strain behaviour.

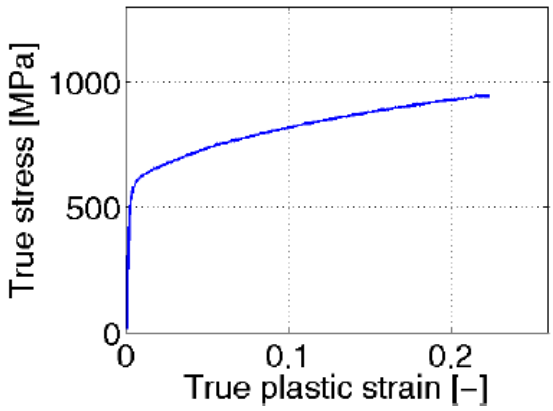

Figure 5-1: True stress strain flow curve obtained by tensile testing of stainless steel strip

There are quite a few flow curve expressions to choose from and the selection of a proper one depends on the material flow behaviour [20]. Two frequently used expressions are; Hollomon in eq. (5-3) and Swift in eq. (5-4), which both take strain hardening into account. Figure 5-2 shows the difference between the two and it is evident that Swift's expression is better suited than Hollomon's for pure plastic flow curves, which demand the flow stress being zero at ε = 0.

$$\sigma = C_1 \cdot \varepsilon^n \tag{5-3}$$

$$\sigma = C_2 \cdot (b + \varepsilon)^n \tag{5-4}$$

One should keep in mind that flow curve expressions are approximations, which may not be accurate for all strain levels, and they should not be used for strains outside the tested region. Furthermore they are not valid for strains above diffuse instability – indicated by the ultimate tensile strength (UTS) [21].

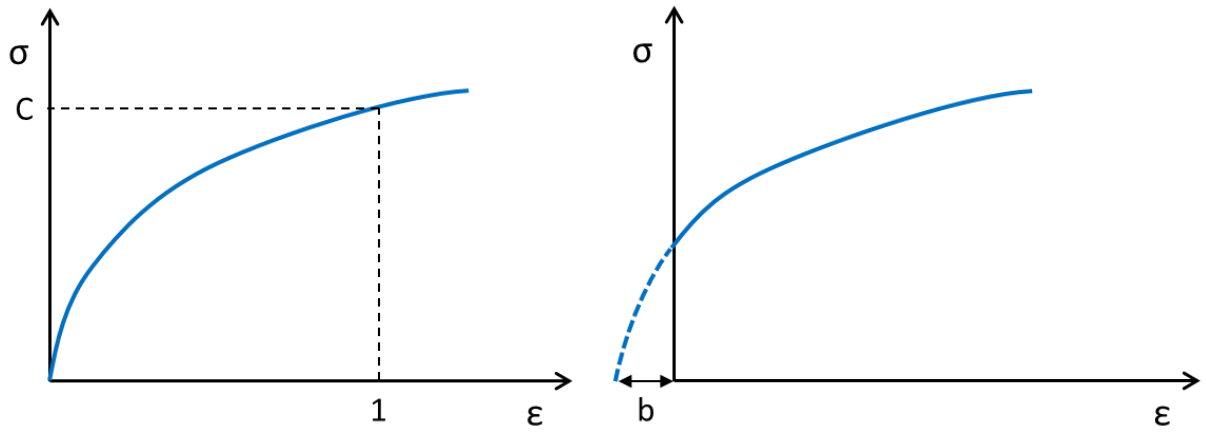

(a) (b)

Figure 5-2: a) flow curve from Hollomon's expression and b) from Swift's expression [20]

Some FEA software can utilise piece-wise linear material flow curves. This permits the use of actual test data by dividing the flow curve into linear sections, as depicted in Figure 5-3.

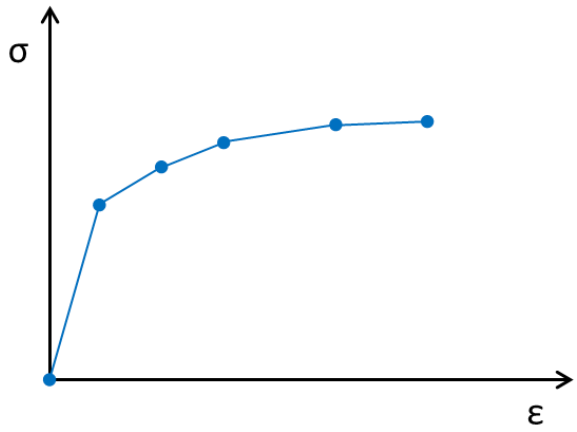

Figure 5-3: Illustration of a piece-wise linear material flow curve

5.2 Anisotropy of sheet metals

Sheet metal anisotropy is a measure of the difference in mechanical properties, which the sheet metal exhibits in different directions. It is due to the preceding process where plane strain conditions make the grains elongate in the longitudinal direction with an insignificant change in the transversal direction. This generates a preferred crystallographic orientation, which causes anisotropy. Sheet metal anisotropy can be estimated by uni-axial tensile testing and is described by the anisotropy coefficient R_α, also known as the Lankford coefficient. By convention the R-values are usually determined at 20% elongation and a material with an R-value equal to 1 is isotropic [22]. Figure 5-4 illustrates specimen direction measured from the rolling direction.

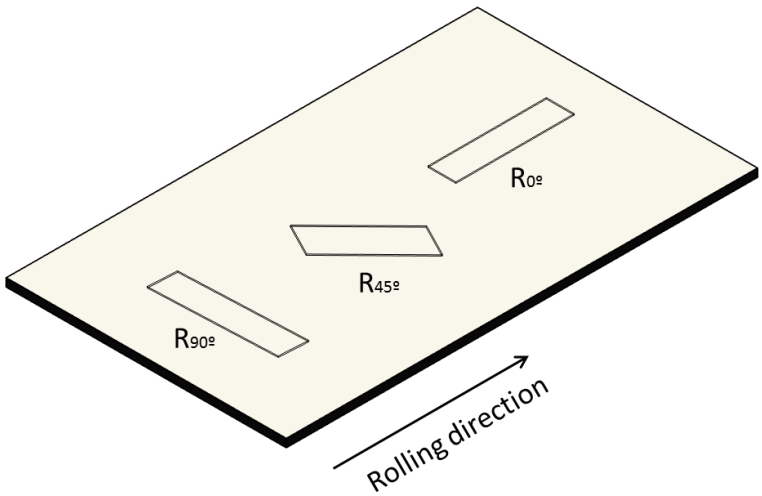

Figure 5-4: Illustration of specimen directions for anisotropy coefficients of 0º, 45º and 90º

The Lankford parameter or anisotropy coefficient in the direction α, where α is the angle between test direction and is given by the ratio between width strain ε_w and thickness strain ε_t:

$$R_\alpha = \frac{\varepsilon_w}{\varepsilon_t} \tag{5-5}$$

It is sometimes difficult to measure thickness strains with sufficient precision. Volume constancy, however, dictate that thickness strains can be calculated from longitudinal and width strains, due to volume constancy thus eq. (5-5) becomes:

$$R_\alpha = -\frac{\varepsilon_w}{\varepsilon_l + \varepsilon_w}, \tag{5-6}$$

where ε_l is the longitudinal strain.

The normal anisotropy is the average anisotropy value based on the anisotropy coefficient along the three directions 0º, 45º and 90º respectively:

$$\bar{R} = \frac{R_{00} + 2 \cdot R_{45} + R_{90}}{4} \tag{5-7}$$

Planar anisotropy is a measure of the anisotropy variation in the plane of the sheet:

$$\Delta R = \frac{R_{00} - 2 \cdot R_{45} + R_{90}}{2} \tag{5-8}$$

5.3 Forming limit diagrams

Forming limit diagrams (FLDs) are used to determine sheet metal formability plotting the in-plane major and minor strain combinations that leads to necking [22, 23, 16]. A FLD is shown in Figure 5-5 where the blue line is the forming limit curve (FLC) indicating the limit strains regarding onset of necking - in this figure for a not specified material.

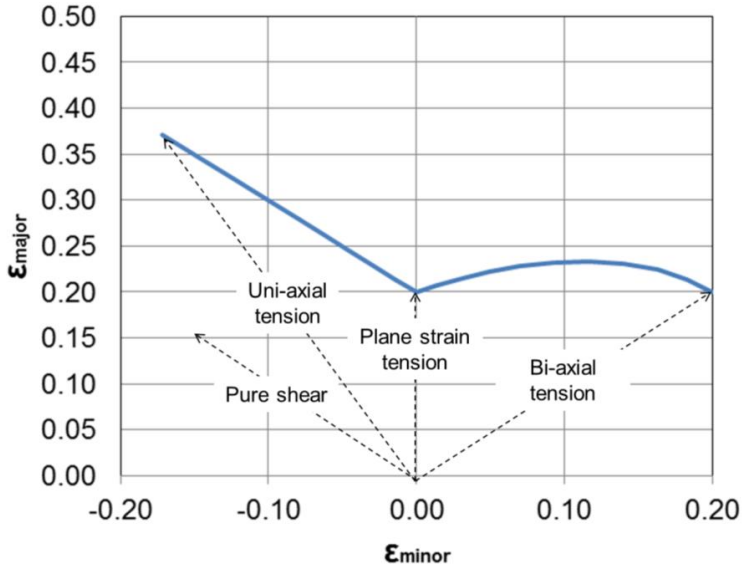

Figure 5-5: Example of a FLD where the different strain path directions are presented

FLCs are only valid for linear strain paths, wherefore limit strains in multistage forming operations must be evaluated differently. Müchenborn & Sonne developed a calculation rule for strain path dependence by calculating the remaining formability in a two-stage deformation by means of the effective strain, eq. (5-9). Limit strains for the second-stage deformation can be calculated when the FLC for the first stage (linear strain paths) is known [24].

$$\varepsilon_e = \sqrt{\frac{4}{3}(\varepsilon_1^2 + \varepsilon_2^2 + \varepsilon_1 \cdot \varepsilon_2)} \tag{5-9}$$

The procedure is visualised by Figure 5-6 and Figure 5-7. Figure 5-6 show the first forming stage to be uni-axial tension stopping at point A. From point A, the effective strain is calculated and assumed constant thus the effective strain ellipse is calculated (yellow curve). From the strain ellipse the remaining formability is indicated by drawing straight lines from origo to the blue FLC – the length from the effective strain ellipse to the blue FLC is the remaining formability after tensile deformation to point A, indicated by the dotted lines in Figure 5-6. In Figure 5-7 the dotted lines are parallel shifted to start in point A and the ensuing red curve is the forming limit for the second stage deformation.

Some parts of the carcass profile actually do experience non-linear strain paths such as the QL-, QT- and s-bends that are subjected to plane strain bending during the roll forming stage and uni-axial tension and / or compression during the winding stage. But because necking and fracture occur at the tongue edge normal FLDs are viable for formability assessment in carcass production because the tongue experiences uni-axial tension in both the roll forming and the winding stage.

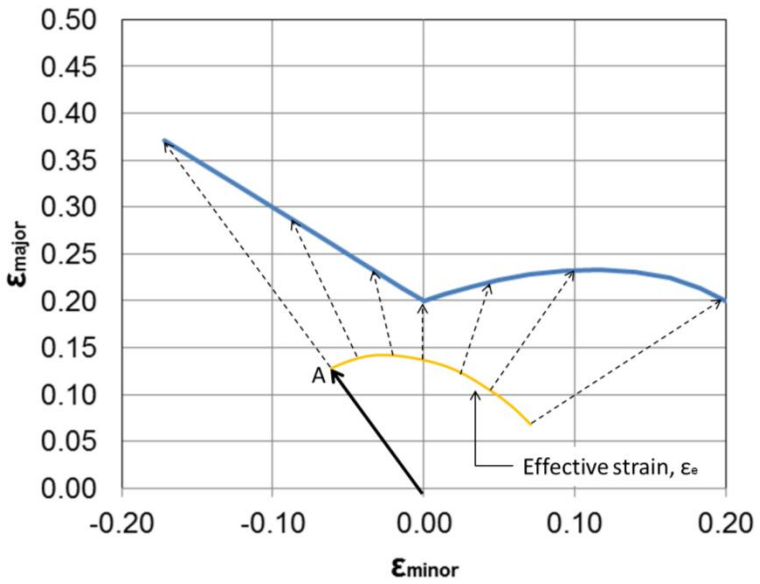

Figure 5-6: Illustration of Müschenborn & Sonne's calculation rule for strain path dependence. The blue curve is the FLC for linear strain paths, point A is the uni-axial tension point

for the first stage deformation and the dotted lines indicate remaining formability in the second stage deformation

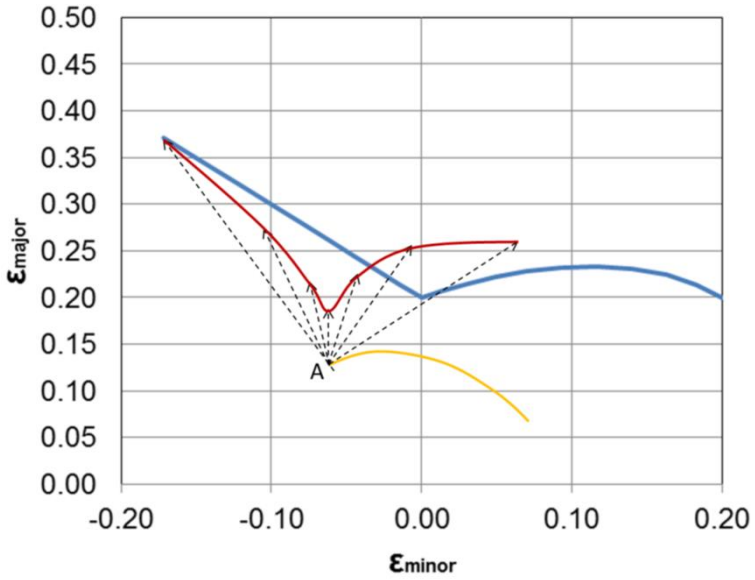

Figure 5-7: Illustration of Müschenborn & Sonne's calculation rule for strain path dependence. The dotted lines from Figure 5-6 are parallel shifted to point A and their endpoints indicate the limit strains for the second stage deformation marked by the red curve

5.3.1 Influencing factors on the FLC

Studies have shown that various factors influence the FLC some of which are discussed in [22, 23, 16, 25, 26]. The relevant factors for the present investigation are presented below. The test method is a factor because of differences in strain path, strain gradient, curvature and type of necking [23]. Therefore the selected test for determining the FLC should reflect the conditions in the process that is being evaluated. Figure 5-8 show the difference in FLC between 5 test methods [22].

Mechanical properties such as normal anisotropy '$\bar{R}$' and strain hardening exponent 'n' influences strain path. For simple tensile tests an increase in '$\bar{R}$' will shift the FLC to the right and result in lower limit strains ε_{major}. Higher 'n' indicates more strain hardening, thus the material can reach higher limit strains by delay of necking [22]. These effects are also noticed from the experimental results in section 5.6.6.

It is generally known that increasing sheet thickness will improve formability, and literature states that this is due to larger necking zone and different strain path [22, 26]. Kleemola et al [26] concludes that if the effects of strain path and strain gradient are taken into account, then limit strains are independent on sheet thickness or curvature.

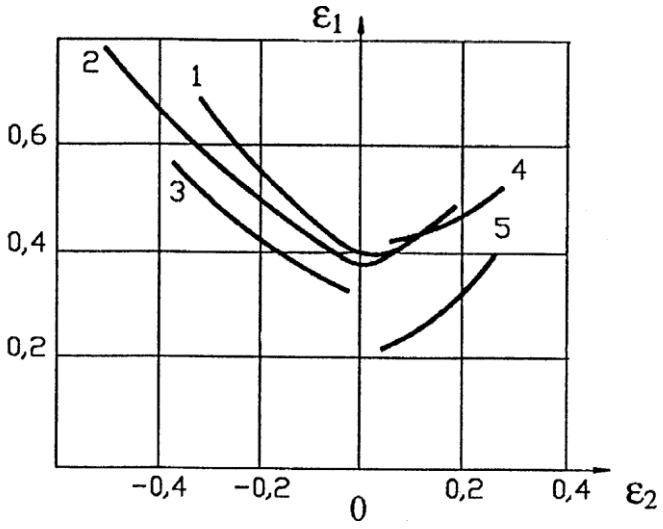

Figure 5-8: FLC's based on different testing methods: (1) Hasek, (2) Nakazima, (3) uni-axial tension, (4) Keeler, (5) hydraulic bulge test [22]

The grid size for strain measurements influences the measurement resolution and in combination with strain gradients around necking / fracture it is affecting the limit strain measurements. A smaller grid size improves resolution and thus the measurement of the limit strains [22, 26].

The FLC is strain rate sensitive, and the behaviour can be explained by a different mechanical response of the different materials, when strain rate is altered. There is no specific correlation between change in strain rate and formability as it is material dependent [22].

Because of these influencing factors and the general uncertainty regarding the use of FLDs, the introduction of a forming limit band, as suggested by [27], is beneficial as it give a statistical range, where limit strains are probable.

5.3.2 Theoretical models for the FLC

Several theoretical models and software have been developed for calculation of limit strains, many of which are discussed in [22]. The early models for calculating limit strains were developed by Hill and Swift, which estimated localised and diffuse necking strains respectively assuming homogeneous sheet metals and Hollomon's flow curve expression (eq. (5-3)). Both models indicate necking strains in plane strain condition equal to the strain hardening coefficient 'n' [22, 16].

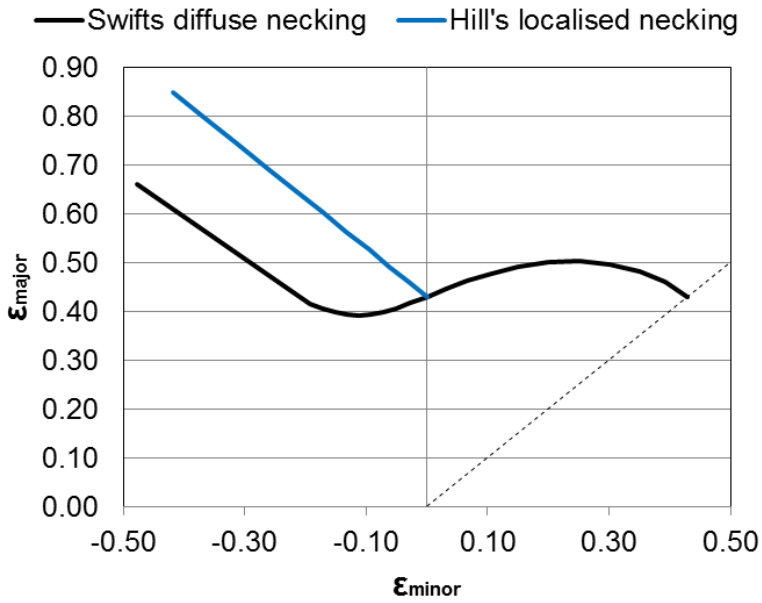

Figure 5-9: FLC prediction by Hill and Swift based on Hollomon's material model: n = 0.43. Note that the limit strain in plane strain condition is equal to strain hardening coefficient 'n'

5.4 Strain measurement techniques

There are several methods for measuring strains and they all somehow depend on applying a grid of a known size to the un-deformed workpiece and measuring the change in grid / pattern size following deformation. The grid shapes are often either circular or square and their size varies depending on the object that needs to be measured. Even stochastic patterns can be applied in case of automated strain measurement systems that utilises digital image correlation. The following describes common strain measurements methods, some of which are used in this project for material characterisation.

There are several methods to choose from regarding grid application and selection. Which to choose depends on the environment and process that is studied as well as the required resolution and quality of the grid. To get an idea of the expected resolution from each method a comparison is made by measuring the undeformed grids with an optical Coordinate Measuring Machine (CMM), DeMeet-220 from Shut Geometrical Metrology. The results are shown in Figure 5-10.

The included reference grid is from an ASAME table model and is one of the calibration artefacts that are used for calibrating the system. It is noted that the reference and laser marked grid have similar precision thus verifying that laser marking is a very precise grid manufacturing method. The quality of the serigraphy grid is slightly lower, while the rubber stamped grid is the poorest method of the three - although the precision is still within ± 2%. Though precision is likely to change with the user that applies the grids as rubber stamping and serigraphy depends on the precision of the operator, this is also true for electro-chemical etching, which, however, is not investigated in the present work.

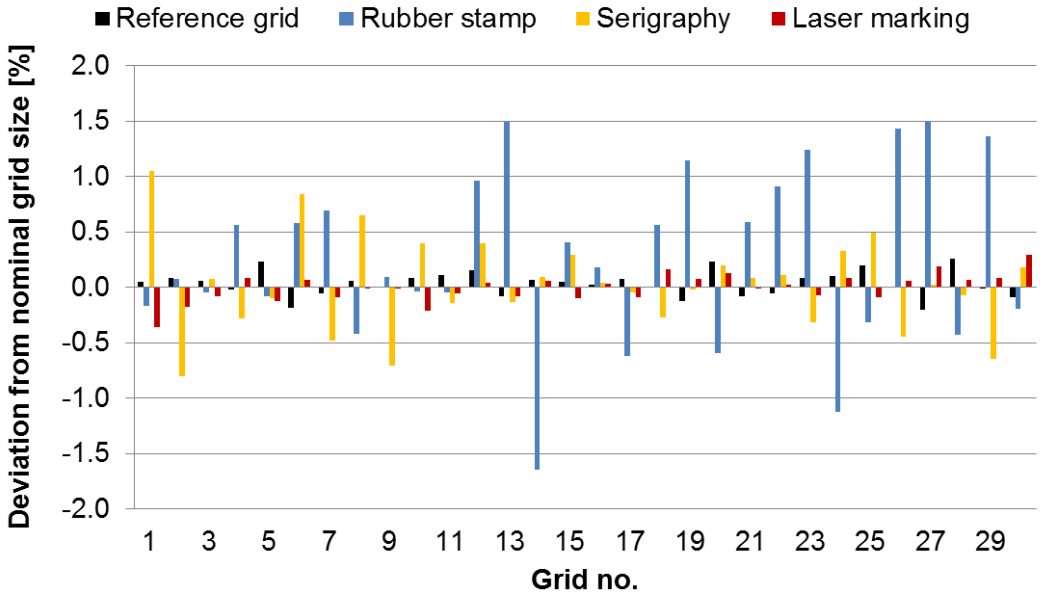

Figure 5-10: Comparison of 30 undeformed grids in an optical CMM, by percent deviation from the nominal grid size. All of them are 5mm square grids except for the laser marked 3mm square grid.

5.4.1 Rubber stamp + printing ink

Printing with a rubber stamp is a simple and quick method of applying a measureable grid by means of printing ink and a dedicated rubber stamp. However, this method should only be used for applications, where grid resolution and quality is of less importance since great care must be taken when stamping in order to have uniform lines in the grid, see Figure 5-11. Also the ink is easily removed, thus usage in oily environments and in sliding contact with tools is not feasible.

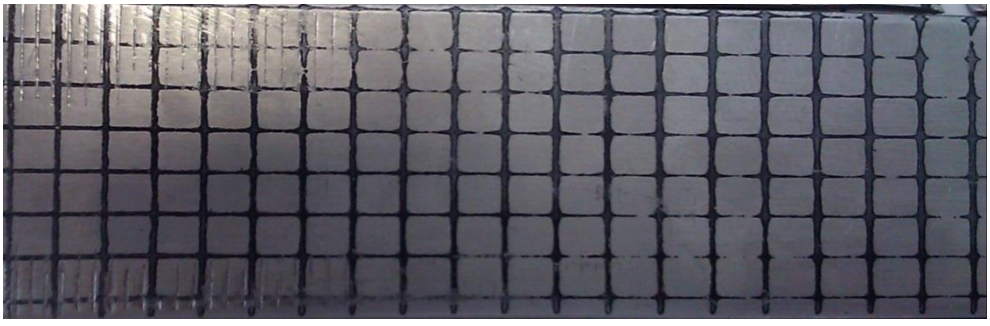

Figure 5-11: 3x3mm grid produced by rubber stamp. The lines in the grid have varying thicknesses which is partly because of the applied pressure during stamping and due to the amount of ink

5.4.2 Serigraphy

Serigraphy, also known as silk screen printing, is a printing method where the ink is transferred onto the metal sheet through a stencil, which defines the grid [28]. Though a fairly

good quality and reproducible grid is obtainable there is still an issue with smearing of the grid due to oil and sliding tool contact.

5.4.3 Laser marking

Laser marking is a destructive method, where the marked surface layer is affected by rapid heating and cooling to create the desired grid. The grid size and shape is created in the laser control software. Because of the 'damage' to the strip surface it is likely that laser marking has an effect on fracture and forming limits and as such it should not be used for forming limit determination – at least not until it is confirmed that the effect is insignificant. The quality and reproducibility of the grid is excellent, see Figure 5-12. The laser marked grid is resistant towards oil and only severe, sliding tool contact will cause damage to the grid.

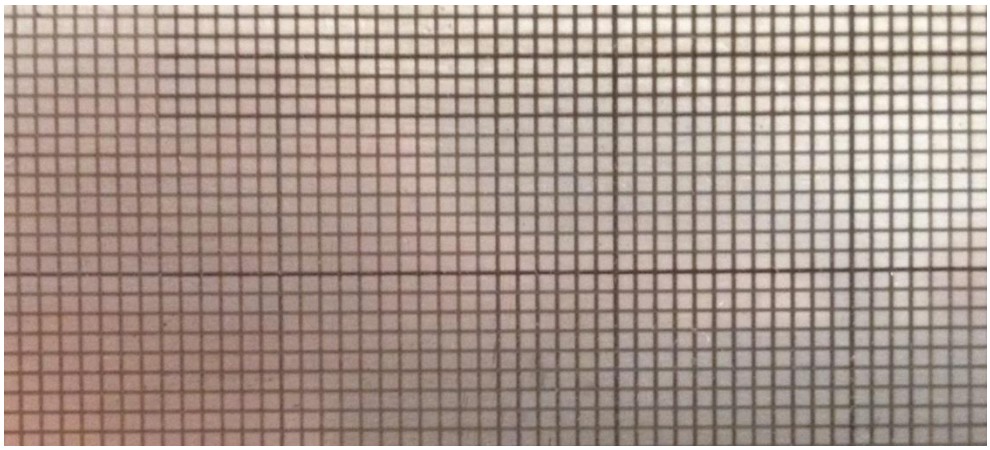

Figure 5-12: 1x1mm laser marked grid on a stainless steel sheet

5.4.4 Electro-chemical etching

This is a widely used method for engraving metal surfaces and therefore also for grid manufacture. Standard equipment is commercially available along with stencils of varying size and shapes. This technique is fast and reliable and can be compared to the laser grid precision as the grid is robust and resistant towards oil and only severe tool contact will cause damage to the grid. For industrial process applications this is the best grid technique as it is possible to manufacture a good quality and robust grid at the production machinery without needing to weld pre-prepared grid samples onto the sheet metal coil in production.

5.4.5 Speckle pattern

Speckle pattern is not a viable method for manual measurements, but some automated strain measurement systems, such as the GOM ARAMIS system, can measure strains from a speckle pattern through digital image correlation. If a black speckled pattern is desired then the procedure is to paint the specimen samples white then applying a black, stochastic speckle pattern with a spray can, see Figure 5-13. It is a bit of an art to apply the stochastic patterns as the measurement resolution partly depends on the quality of the pattern. It can take some time

to perfect the technique, but then it is a fast method to generate a pattern for strain measurements, and when a good pattern is applied, it possible to attain high resolution. The method is very good for controlled lab investigations but rather difficult to use in industrial processes because of the lack of robustness of the speckle pattern.

One drawback in case of very high strain the speckle pattern might distort to an extent that the digital image correlation software will have problems identifying the pattern.

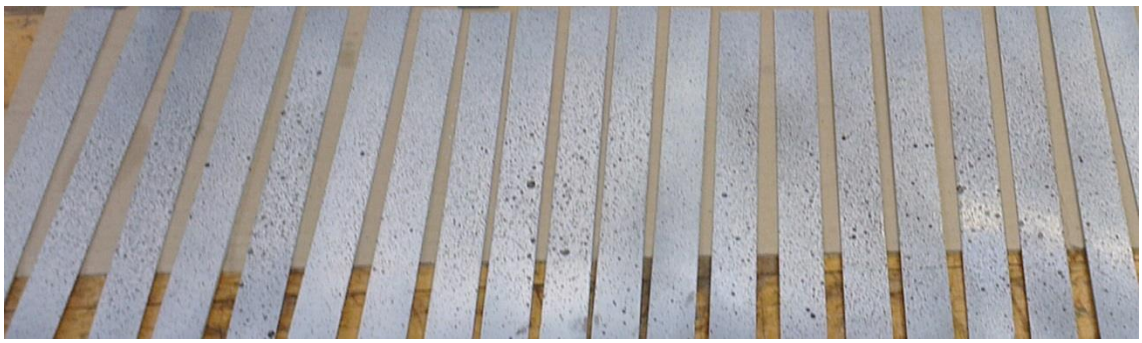

Figure 5-13: Tensile specimens with black on white speckle pattern for ARAMIS strain measurement

5.5 Grid measurement

Manual strain measurements are often time consuming but for small batches it is a fast and reliable method. As mentioned before some automated strain measuring systems are also available such as; ARAMIS from the German manufacturer GOM [29] and ASAME target model from South Korean manufacturer WebVision 21C Co. Ltd [30]. Those systems require setup time and calibration, so they are best suited for large quantity strain measurements.

5.5.1 Manual strain measurement

Equipment needed is rulers, callipers or other measurement devices that suits the purpose and the resolution needed from the results. Also the use of a stereo microscope makes it easier to perform the measurements. In this work the manual measurements are carried out using flexible, transparent rulers that are calibrated using the aforementioned optical CMM. Figure 5-14 shows one of these flexible rulers on top of a square grid. One of the advantages of the flexible rulers is that they follow the specimen curvature, which makes a proper measurement of curved surfaces possible. The use of a stereo microscopes makes it easier to perform the measurements as the jumps between the rulers' measurement lines is quite small ~ 0.01mm.

In case of measurement on plane surfaces such as the strains from the Marciniak test or tensile strains, it is possible to use photos before and after and measure pixels between grids in a photo editing software. The requirement is that the picture be taken perpendicular to the surface at the exact same position and distance.

Manual strain measurements can be time consuming and are rather tedious but preferable for small investigations and quick evaluation.

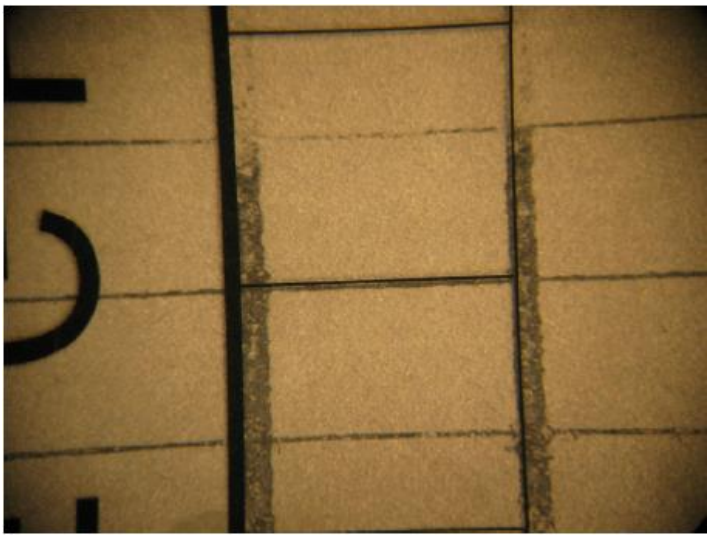

Figure 5-14: View through a microscope of a plastic ruler atop a stamped square grid [31]

5.5.2 Automated strain measurement

Automated strain measurement systems rely on digital image correlation to calculate the strains [29]. Because of this good lightning on the specimens and calibration of the systems are essential for precise measurements. Also facet size (the 'grid' defined in ARAMIS) and speckle pattern must be chosen for optimum sample resolution, which can be obtained by trial and error until a satisfying pattern is obtained. The technique require operator skills, but with training it is easy to generate satisfying speckle patterns.

An advantage of automated measurements is that the system is able to determine fracture strains and thus useful for FLD generation, something that is normally quite time consuming using manual measurement methods. Automated systems record several images during testing, which implies that an actual strain path can be recorded, something that can be relevant for FLD evaluation.

A typical approach for automated strain measurements, using ARAMIS, is as follows:

1. Identify measuring volume – size of specimen
2. Position cameras at correct distances to each other and the specimen according to the measuring volume
3. Calibrate the system using the proper calibration artefact (again this depends on the measuring volume)
4. Set a proper frame rate / acquisition rate according to the strain rate
5. Acquire pictures
6. Perform image correlation and strain calculation (automated)

Figure 5-15 shows the ARAMIS setup used for the tensile testing described in later sections. It is a 3D setup with two 4M cameras pointing towards the specimen from two different angles. The light source provides constant light exposure since any change in lighting conditions could result in a change in system settings and in worst case require re-calibration of the system.

The ARAMIS software has the capability to calculate FLDs based on the last image before fracture occurs, indicating the fracture strain. When several strain paths are available ARAMIS can build the FLC in accordance to ISO 12004-2:2008 [32]. Figure 5-16 show how ARAMIS calculate necking strains for a tensile sample just before fracture.

Figure 5-15: ARAMIS 4M system setup: light source, cameras, data acquisition box and computer

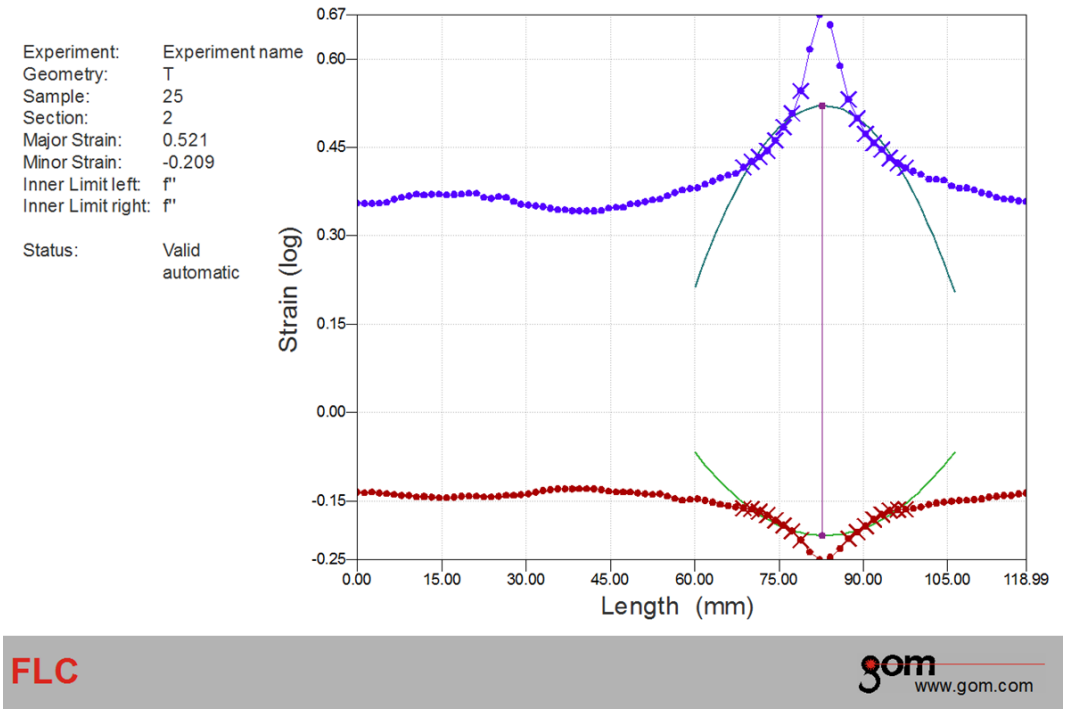

Figure 5-16: Calculation of necking strains in ARAMIS

5.6 Materials testing

Four stainless steels have been selected for characterisation with varying thicknesses. For an overview of the test campaign on stress-strain curves and FLDs, see Figure 5-17. The four materials with varying thicknesses and repetitions result in a total of 216 tensile tests providing flow curves and FLD's. The test plan is fully randomised in order to eliminate the effects of unknown or uncontrolled nuisance factors [33].

	EN 1.4404			EN 1.4162			EN 1.4462	EN 1.4410	
	t = 0,6mm	t = 1,5mm	t = 2,5mm	t = 0,6mm	t = 1,5mm	t = 2,5mm	t = 0,68mm	t = 0,8mm	t = 1,5mm
Tensile (0º)	3	3	3	3	3	3	3	3	3
Tensile (45º)	3	3	3	3	3	3	3	3	3
Tensile (90º)	3	3	3	3	3	3	3	3	3
Tensile b (0º)	3	3	3	3	3	3	3	3	3
Tensile b/2 (0º)	3	3	3	3	3	3	3	3	3
Tensile b/3 (0º)	3	3	3	3	3	3	3	3	3
Tensile b/4 (0º)	3	3	3	3	3	3	3	3	3
Tensile b/8 (0º)	3	3	3	3	3	3	3	3	3

Figure 5-17: The four stainless steel materials and their thicknesses. The number in each cell '3' indicates the number of repetitions and the column on the left specify the specific tensile specimen

5.6.1 Tensile test equipment

The tensile test equipment depicted in Figure 5-18 is used in the Amsler press located at DTU-MEK. The Amsler is a hydraulic press, where press speed is obtained by opening and closing hydraulic valves. Testing speed is relatively slow: 0.1 – 0.15 mm/s thus the strain rates are rather low. The equipment is based on an IDDRG recommendation for measuring material anisotropy and enables load, strip width and elongation measurements during uniform elongation [34]. The equipment utilises a 20mm wide strip with a length of minimum 200mm and thicknesses up to 2.5mm.

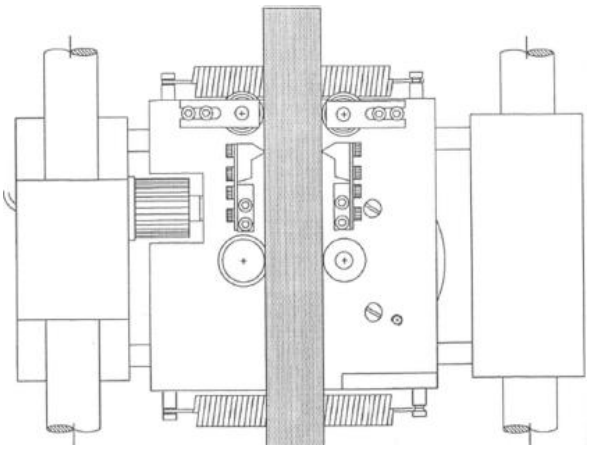

Figure 5-18: Tensile testing equipment at DTU-MEK section for Manufacturing Engineering. The material specimen is the grey rectangle in the centre [34]

5.6.2 Specimen preparation

All the tensile specimens are cut from metal sheets in three directions with respect to the rolling direction (0º, 45º and 90º) and they are milled on the edges resulting in a more uniform edge removing defects from previous cutting operations. Slight plastic deformation is likely on the milled edge but it is not believed to influence the results. Strip width and thickness is measured for all specimens prior to testing.

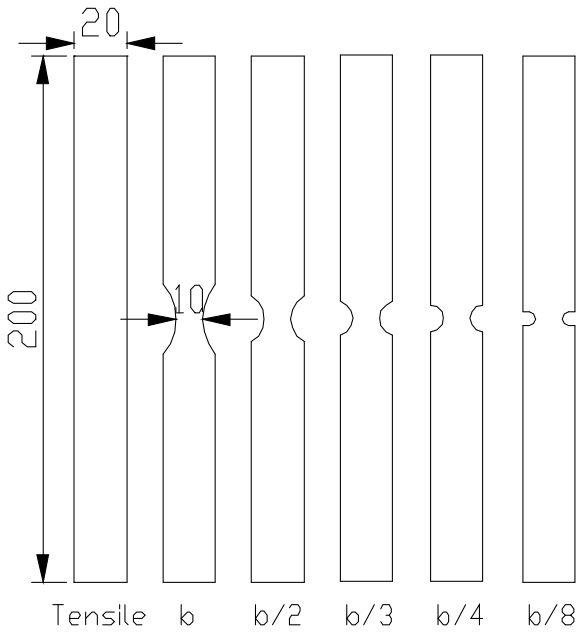

Figure 5-19: Tensile specimens for determining stress-strain curves and forming limits. Specimen b has a notch radius r20 mm and is the reference specimen meaning that specimen b/2 has a notch radius 1/2 of b, b/3 has a notch radius 1/3 of b etc.

Tensile tests with notched specimens are used to obtain the left-hand-side of the FLD ($\varepsilon_{minor} < 0$), which is the simplest method of testing. In order to achieve necking strains for 6 different strain paths, 1 un-notched and 5 notched specimen geometries were applied according to [22], with the dimensions shown in Figure 5-19. This should provide 6 points on the left-hand-side of the FLD. All of the notched specimens have a centre width of 10 mm, and only the notch radius is varied. From left to right the specimens will, in theory, provide points on the FLC ranging from uni-axial tension to plane strain.

5.6.3 Strain measurement for FLDs

An ARAMIS 4M system is used for automated FLD calculation, which implies that all specimens are prepared with a stochastic speckle pattern using spray paint. In order to obtain good contrast the specimens are first painted matt white and subsequently a black paint is applied by gently pressing the spray paint nozzle, such that it “ejects” out paint droplets, which forms a black speckle pattern on the specimens. It was attempted to create completely similar colour tones on the specimens but it was difficult and some specimens did show

'holes' in the strain measurement grids, where ARAMIS could not recognise the pattern. The general focus was to create speckles that would allow sufficient resolution for strain measurements – especially for the notched specimens, where the measurement area is confined to the notched region.

5.6.4 Flow curve data analysis

The data from the un-notched specimens were analysed to determine stress-strain curves and anisotropy. A Python script was created to save time in the data analysis, since many individual files needed to be treated. This allowed fast analysis as well as direct output of the material data from each test – a couple of minutes per test compared to 10-15 minutes when manually importing and calculating in Excel. An example of the GUI is shown in Figure 5-20, whereas the Python script is attached in appendix A. The script is constructed to read the specific data files that are acquired from the LabVIEW program developed for the test.

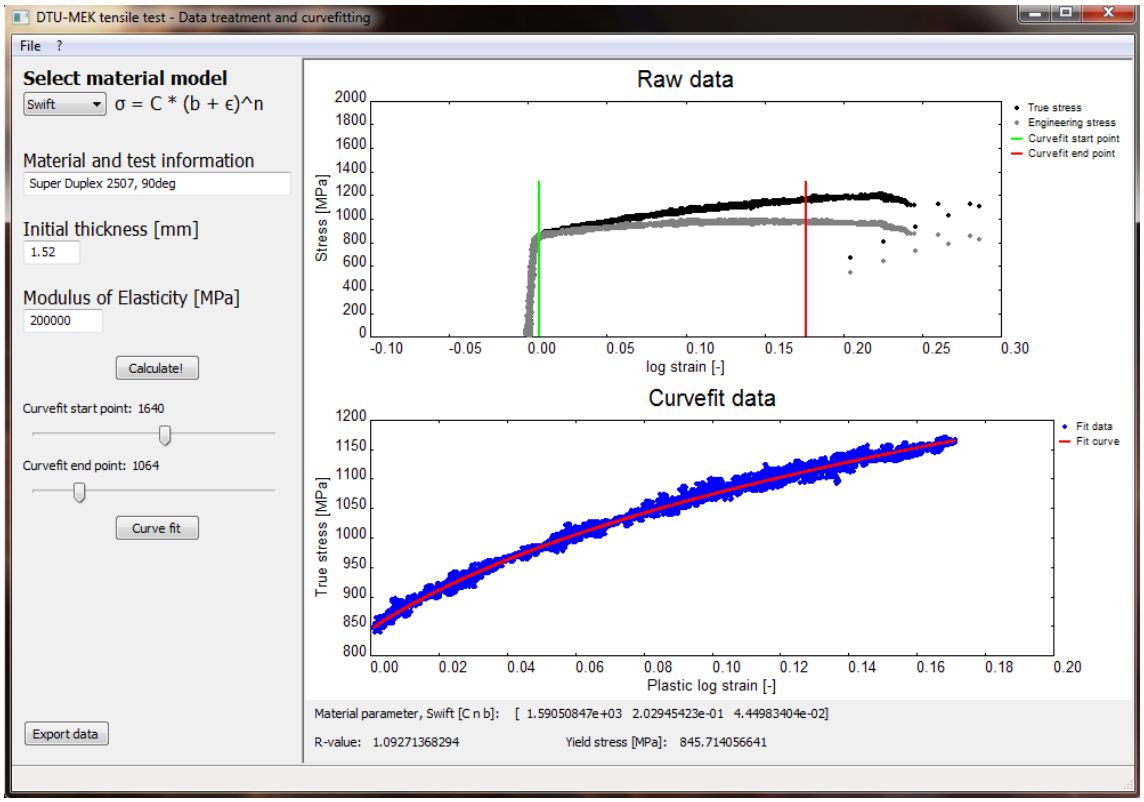

Figure 5-20: Python script GUI for tensile test data analysis

The modulus of elasticity defined in the Raw Material Specification, 200 GPa for all four materials, is used to subtract the elastic strain from the flow curves. This will result in a minor error since the modulus of elasticity is defined rather than measured. True stress and strain is calculated from the acquired test data and the elastic part of the flow curve is removed, so that only plastic stress-strain relationship is described by the flow curves – the reason being that the data is going to be used as input to a FEA. The test data are curve fitted to Swift's flow

curve expression, eq. (5-4). Three repetitions of each test are performed to increase validity and in this investigation the deviations between the repetitions were small, which can be seen in appendix B, where the flow curve data are collected. The results of flow curve analysis are presented in the following sections and average flow curves for the four materials are shown in Figure 5-21.

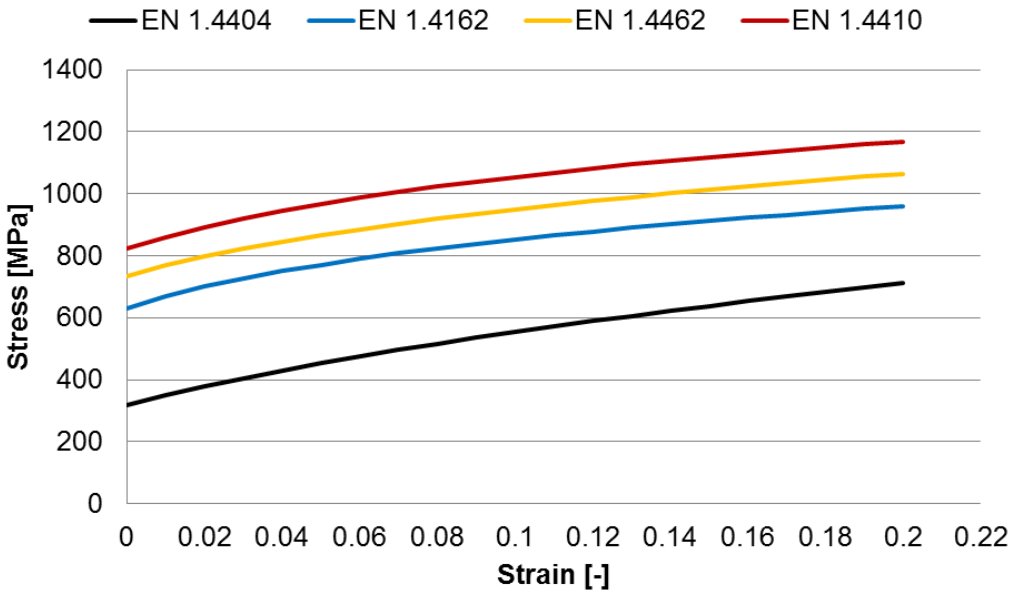

Figure 5-21: Plastic flow curves averaged across the different thicknesses along the rolling direction (0º)

Austenitic EN 1.4404

Table 5-1: EN 1.4404 material data for 0º, 45º and 90º with regards to rolling direction and three sheet thicknesses

0º					
t [mm]	σ_y *[MPa]*	*C [MPa]*	*n [-]*	*b [-]*	R_{00} *[-]*
0.6	286	1,366	0.444	0.028	0.83
1.5	303	1,328	0.426	0.030	0.82
2.5	316	1,331	0.429	0.036	0.79
45º					
0.6	288	1,459	0.529	0.049	1.98
1.5	303	1,417	0.497	0.051	1.43
2.5	316	1,358	0.474	0.053	1.56
90º					
0.6	302	1,457	0.497	0.042	2.17
1.5	311	1,393	0.509	0.059	1.94
2.5	353	1,377	0.481	0.064	1.85

Normal and planar anisotropy:

$$\bar{R}_{0.6mm} = 1.74; \quad \bar{R}_{1.5mm} = 1.41; \quad \bar{R}_{2.5mm} = 1.44$$

$$\Delta R_{0.6mm} = -0.48; \quad \Delta R_{1.5mm} = -0.05; \quad \Delta R_{2.5mm} = -0.24$$

Lean Duplex EN 1.4162

Table 5-2: EN 1.4162 material data for 0º, 45º and 90º with regards to rolling direction and three sheet thicknesses

0º					
t [mm]	σ_y *[MPa]*	*C [MPa]*	*n [-]*	*b [-]*	R_{00} *[-]*
0.6	655	1,421	0.230	0.035	0.89
1.5	606	1,322	0.227	0.032	0.77
2.5	579	1,270	0.211	0.028	0.53
45º					
0.6	648	1,349	0.205	0.032	1.13
1.5	603	1,276	0.214	0.033	1.12
2.5	584	1,221	0.199	0.030	1.12
90º					
0.6	631	1,322	0.201	0.031	1.21
1.5	608	1,295	0.200	0.026	1.09
2.5	625	1,244	0.179	0.024	0.81

Normal and planar anisotropy:

$$\bar{R}_{0.6mm} = 1.09; \quad \bar{R}_{1.5mm} = 1.03; \quad \bar{R}_{2.5mm} = 0.90$$

$$\Delta R_{0.6mm} = -0.08; \quad \Delta R_{1.5mm} = -0.19; \quad \Delta R_{2.5mm} = -0.45$$

Duplex EN 1.4462

Table 5-3: EN 1.4462 material data for 0º, 45º and 90º with regards to rolling direction

0º					
t [mm]	σ_y *[MPa]*	*C [MPa]*	*n [-]*	*b [-]*	R_{00} *[-]*
0.7mm	697	1,484	0.222	0.039	0.48
45º					
0.7mm	661	1,419	0.235	0.049	1.67
90º					
0.7mm	762	1,443	0.201	0.048	0.70

Normal and planar anisotropy:

$$\bar{R}_{0.7mm} = 1.13$$

$$\Delta R_{0.7mm} = -1.08$$

Super Duplex EN 1.4410

Table 5-4: EN 1.4162 material data for 0º, 45º and 90º with regards to rolling direction and two sheet thicknesses

0º					
t [mm]	σ_y *[MPa]*	*C [MPa]*	*n [-]*	*b [-]*	R_{00} *[-]*
0.8mm	806	1,562	0.190	0.032	0.58
1.5mm	760	1,556	0.202	0.032	0.56
45º					
0.8mm	819	1,505	0.183	0.037	1.17
1.5mm	771	1,476	0.194	0.038	1.25
90º					
0.8mm	865	1,545	0.173	0.038	1.16
1.5mm	845	1,548	0.185	0.040	1.13

Normal and planar anisotropy:

$$\bar{R}_{0.8mm} = 1.02; \quad \bar{R}_{1.5mm} = 1.05$$

$$\Delta R_{0.8mm} = -0.3; \quad \Delta R_{1.5mm} = -0.41$$

5.6.5 Forming limit diagrams

It was noted during testing that the notched specimens fractured shortly after onset of deformation and from the subsequent analysis it is also clear that they did not perform as expected. Figure 5-22 show the FLD results for EN 1.4162 along with a two point FLD from the steel manufacturer (SM). The points for uni-axial tension (tensile specimen in Figure 5-19) seem reasonable and show the effect of material anisotropy of the different strip thicknesses. However, all of the points towards plane strain show much lower limit strains than expected. The global strains were compared between the tensile test equipment and ARAMIS during uniform elongation and the two measurement methods correspond well.

It is likely that the result is influenced by the specimen size:

- the measurement area is rather small and it is possible that the necking strains only cover a marginal area that is not measureable by ARAMIS due to speckle pattern size and a large strain gradient towards the fracture

- the small area between the notches of each specimen might cause the material to fracture early due to material defects, possibly also affected by the milled surface

Further testing is necessary in order to fully understand the results but for the present investigation only the uni-axial points are usable for the FLD.

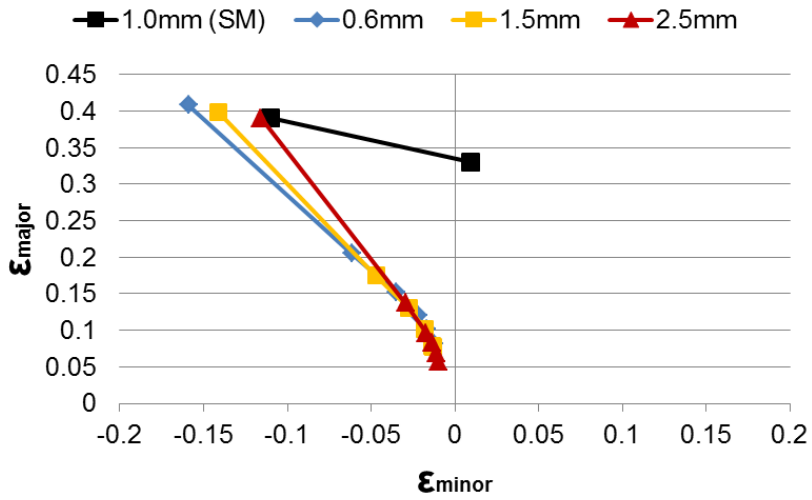

Figure 5-22: FLD for EN 1.4162. The curve marked (SM) is a two point curve from the steel manufacturer. The three other curves are the results from the tensile specimens where the notched specimens deviate from expected values, and the (SM) curve

5.6.6 Uni-axial forming limit results

The uni-axial forming limit points for all four materials and thicknesses are shown in appendix C. For a quick overview of the results Figure 5-23 show the average ε_{major} and ε_{minor} for the four tested materials. The austenitic EN 1.4404 has the highest formability with an ε_{major} around 0.53 followed by the Lean Duplex EN 1.4162 with an ε_{major} around 0.4. Both the Duplex EN 1.4462 and EN 1.4410 have an ε_{major} around 0.32 but with different ε_{minor} due to the difference in anisotropy.

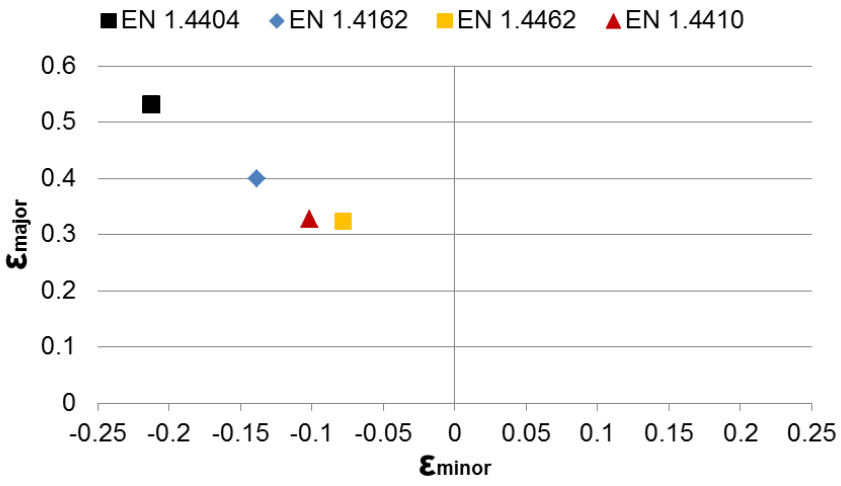

Figure 5-23: Average uni-axial tension FLC points for the tested materials

5.7 Results and discussion

Flow curves, normal- and planar anisotropy have been successfully determined for four selected stainless steel sheets with different thicknesses. A randomised test plan with three repetitions for each specimen was created, and testing was carried out on tensile testing equipment available at DTU-MEK. To support the data analysis, which would have been time consuming considering 81 single files, a Python script was successfully made for fast data analysis.

The austenitic stainless steel has more than twice the strain hardening exponent around 0.45 as the duplex steels around 0.2, which are still relatively ductile. An interesting observation made on the duplex steels is that the strain hardening exponent is almost the same for all three grades. The difference in the duplex steels is the different yielding point, whereas the flow curve shapes are similar because of similar strain hardening exponent. Anisotropy calculations show the same trend where the three duplex steels have very similar values $\bar{R}$ close to 1, whereas the austenitic has a higher anisotropy $\bar{R}$ significantly above 1.

The GOM ARAMIS 4M system was used to measure necking strains during tensile testing. Problems with local strain measurements of the notched specimens lead to the determination of only the uni-axial tension points on the FLDs. It is believed that the specimen size, 10mm width in the notch, is causing early fracture of the specimens. EN 1.4404 had the highest limit strain followed by EN 1.4162, EN4462 and EN 1.4410. It was considered to construct experimental / theoretical two-point FLCs by utilising plane strain necking point from theory (paragraph 5.3.2). But actually, only the uni-axial points are necessary for estimation of limit strains in the carcass process, which is further clarified in Chapter 8.

Chapter 6 Finite Element Analysis

From the project start there was a desire to develop a complete FE-model of the carcass process in order to carry out parametric studies of tool design and machine setup for a first optimization without the need of expensive and time consuming production tests. However, with added knowledge of the complexity of the process especially the interlock mechanisms, which are challenging to simulate correctly, focus shifted towards simplified models that focus on specific investigations such as studies on weld fracture in Chapter 8.

6.1 Choice of software

For some time FEA of roll forming has been reported in literature with objectives to analyse factors such as: springback, longitudinal strains and general failure mechanisms in the roll forming process such as buckling and flaring [4]. From scientific publications it is clear that roll forming can be successfully simulated using general purpose software with both implicit and explicit solvers. It is noted that MSC.MARC implicit seems to be the most utilised general purpose software for roll forming, see for example Lindgren [35], Görtan et al [36] and Larrañaga et al [37]. But LS-DYNA® explicit, e.g. Sheu [38] and Paralikas et al [39], and ABAQUS implicit/explicit, e.g. Tehrani et al [40] and Daniel et al [41], are also being used for roll forming simulations.

In the present work, dedicated roll forming Computer-Aided Engineering (CAE) software such as SHAPE-RF [42] and Copra® RF [43] was not considered because of the different elements in carcass production, where a general purpose code would allow investigations beyond roll forming. This project has not made actively use of Copra® RF, but during the later stages a benchmark test was performed, which showed very promising results with regards to tool design and geometrical effects during winding. Furthermore it was noticed that dedicated software like Copra® RF facilitate faster pre-processing and tool design changes than typical CAD to FEA interfaces.

The software choice depends on which type of solver is considered necessary for stability and successful simulation without convergence problems. It is generally known that implicit solvers demand longer simulation times as well as being more challenging as regards convergence. They are, however, more likely to produce reliable results, because they are only unconditionally stable [44]. This is the problem with explicit solvers because they are conditionally stable. If the time step is too large, the result might deviate considerably from the ‘true’ one. However, explicit solvers gives less convergence problems and with mass-scaling it is possible to speed up simulation time. Consequently an explicit solver is generally faster than an implicit solver [44, 45].

The FEA performed in the project were done with LS-DYNA® licensed by DYNAmore Nordic. From the literature study of FEA results with different commercial software the selection of software program was based on affordability and capability:

- General purpose software with capabilities that lie beyond roll forming
- Explicit solver for time optimisation and overcoming convergence issues (because of the complexity of the non-linear interlock conditions in the carcass process there was an expectation of convergence problems by using an implicit solver)

The following paragraphs describes the parameters used to construct the models and the convergence study performed that would allow a numerical stable solution. Also the thoughts and assumptions behind each model are described.

6.2 Model parameters

The fixed parameters, i.e. material models, element formulation and contact conditions, are documented in this paragraph. Roll forming and winding models constructed in 3D explicit mode and a few investigations of tool-workpiece contact were performed in 2D implicit mode.

6.2.1 Material models

The material models and parameters defined for tools and workpiece are listed in Table 6-1. The tools are considered rigid, which is an appropriate assumption since the sheet is softer and the height of the strip is quite small compared to the tool dimensions. Rigid elements are bypassed in elements processing so they do not cost extra simulation time [46], thus allowing a finer mesh to be allocated to the tools. Another advantage with rigid tools is that the rotational centre is located at the centre of mass and is therefore defined for proper rotation of the rolls. The material information for the rigid material must be entered for contact definition with the strip. The information is used to determine sliding interface parameters and the inertial properties for the specific rigid parts [46].

Table 6-1: Material models and parameters for tools and workpiece

Parameter	Tools	Workpiece
Material model	020_Rigid	018_Power_Law_Plasticity
Modulus of elasticity, E [MPa]	200,000	200,000
Poisson's ratio, ν	0.3	0.3
Density, ρ [tonne/mm³]	7.8e-9	7.8e-9
Strength coefficient, K [MPa]	-	*Swift parameter* 'C_2'
Strain hardening exponent, n	-	*Swift parameter* 'n'
Yield strength [MPa]	-	*Calculated from Swift parameter* 'b'

The workpiece material is defined as a LS-DYNA material model 18: Power Law Isotropic Plasticity. This is an elastoplastic material model with isotropic hardening following the equation:

$$\sigma = k \cdot \left(\varepsilon_{yp} + \bar{\varepsilon}^{p}\right)^{n} \quad (6\text{-}1)$$

The material constants k and n are the strength coefficient and the strain hardening exponent respectively. ε_{yp} is the elastic strain at yield, which is calculated from the yield stress, and $\bar{\varepsilon}^{p}$ is the effective plastic strain [46]. As noticed from the material model strain rate effects are not considered in the present investigation.

6.2.2 Element formulation

The tools and workpiece are defined as shell elements with the parameters listed in Table 6-2 below. One issue with shell elements is the assumption of plane stress conditions, which must be met as shell elements cannot exhibit through thickness stresses - this is investigated in paragraph 6.8.

Table 6-2: Section settings for tools and workpiece

Parameter	Tools	Workpiece
Element formulation, 3D explicit	Type 2 (Belytschko-Tsay)	Type 16 (Fully Integrated)
Element formulation, 2D implicit	Type 13 (Plane strain)	Type 13 (Plane strain)
Integration points	2	7
Thickness [mm]	1.0	'*Strip size*'

Note that the integration points for the tools are unimportant since stresses will not be calculated for them, so they are set to the standard value of two. Two integration points are sufficient for linear elastic materials, but for non-linear elastoplastic materials four to five integration points are suggested [47]. The convergence study in 6.6.3 indicates that 7 integration points is sufficient for model stability.

6.2.3 Contact formulation

The contact formulation for 3D explicit simulation is a penalty type: FORMING_ONE_WAY_SURFACE_TO_SURFACE in which contact between two parts, slave and master, is defined, and a contact definition is set between the workpiece and tools. The workpiece is set as the slave and the only parameters set in the contact definition are:

- Coefficient of friction (FS) = 0.15
- Viscous damping coefficient (VDC) = 20.0
- Shell thickness (SHLTHK) = Eq.1: shell thickness is considered but rigid bodies are excluded

- Penalty stiffness value option (PENOPT) = Eq.4: use slave node value, area or mass weighted

Contact for 2D implicit simulation is 2D_AUTOMATIC_SURFACE_TO_SURFACE with the same above mentioned settings.

6.2.4 Mass scaling

Due to stability issues explicit time integration involves a critical time step that should not be exceeded in the numerical process [48]. However, satisfying the critical time step does not necessarily assure stability of the numerical model. The critical time step is determined by the CFL condition, after Courant, Friedrichs and Lewy [46], stated in eq. (6-2) below:

$$\Delta t_{cr} \leq \frac{L}{c}, \tag{6-2}$$

where c is:

$$c = \sqrt{\frac{E}{\rho(1-\nu^2)}} \tag{6-3}$$

L is the length of the smallest element and c is the speed of sound through the material defined by: the modulus of elasticity E, poissons ratio ν and the density ρ – eq. (6-3). The CFL condition determines the time it takes for a sound wave to travel across an element, which implies that the time step is controlled by the smallest element and the defined material [48]. If a very fine mesh is applied in a model the corresponding time step would be very small leading to extended calculation times and a high resolution of the results, which might not be needed. Therefore, for optimization purposes, the mesh size should correspond to the desired resolution of the results.

A way of increasing the time step without compromising with mesh size is to use mass scaling. The time step can efficiently be increased by mass scaling, where the material's density is artificially increased, consequently increasing the critical time step. There are several important issues to be aware of when utilizing mass scaling. One issue is the inertia effects that might escalate and influence the results due to the large mass added to the model [49]. Another issue is instability in the contact conditions, which can lead to penetration of parts in a model. Too aggressive mass scaling could also cause drift of the numerical calculations by lowering the total amount of iterations in the model consequently decreasing simulation resolution. Convergence study regarding mass scaling is therefore of importance in order to ensure that the selected time step is within the range of numerical convergence, but it is equally important to determine optimum for optimization as regards to total calculation time.

LS-DYNA calculates the initial, critical time step (DTINIT) and as a safeguard a default value of 90% of this critical time step (TSSFAC) is used as the actual time step. The critical time step will change during metal forming simulations as deformation of the initial mesh will cause a change of L in eq. (6-2). Hence the simulation time might increase considerably with highly distorted/deformed mesh. By utilising mass scaling the time step is determined at the start of the simulation, such that the change in element size is accounted for with mass increase instead of reducing the time step. Logically the effect is that mass scaling is not consistent throughout the calculations, only the time step is.

6.2.5 Selective mass scaling

The mass scaling described above is known as conventional mass scaling. Using conventional mass scaling the addition of mass introduces artificial inertia effects that might affect the global solution [47]. With the present roll forming models these inertia effects can be seen by increased high frequency vibrations in the strip.

The method of selective mass scaling is to decrease the highest Eigen frequencies of the system, while not affecting the lower Eigen frequency domain. This is done by modifying the element mass matrix in a manner that least affects the low frequencies [47, 49]. As a result selective mass scaling can be utilized in less rapid processes, where most of the kinetic energy is located in the lower frequency domain of the system. Although selective mass scaling is more CPU intensive compared to conventional mass scaling, because the mass matrix is no longer diagonal, the advantage is higher levels of mass scaling without inertia effects affecting the solution [49].

6.3 Roll forming model

The tools are imported as CAD surface models via the IGES import function in LS-PREPOST. Unimportant surfaces, such as the tool sides, are deleted from the model thus only the surfaces in contact with the workpiece are being meshed, see Figure 6-1. The tools are meshed one-by-one with the Tmesh function and they are set to rotate, so that friction between tools and the strip / profile drives the deformation. Each tool's rotational speed is kept constant at 4 π/s, which, based on tool diameter, roughly corresponds to a strip speed of 1100 mm/s. A high tool speed can be set because neither temperature nor strain rate effects are present in the model, thus the only risk of running faster is increased kinetic energy and simulation stability. Axle distances and tool diameters are fit to the specific carcass machine that is being modelled.

The strip is constructed in LS-PREPOST with nominal width and thickness and a length that cover at least two rolls forming stations at a time. The strip leading and trailing edges are locked in transverse direction to ensure correct transverse positioning in the roll gaps. Additionally the backend of the strip is restricted in all rotations and translations except longitudinal translation and rotation through the forming stations. Because of the initially small surface

in contact, when the S-section is being formed, friction cannot by itself pull the strip into the roll gap. An initial velocity of the incoming strip edge is applied corresponding to the translation defined by the tools' rotational speed. A "death-time" is set for this boundary condition equal to the time, when the incoming strip edge has reached the centre of the first roll gap. From this point on friction between the tools and the strip will control the workpiece movement.

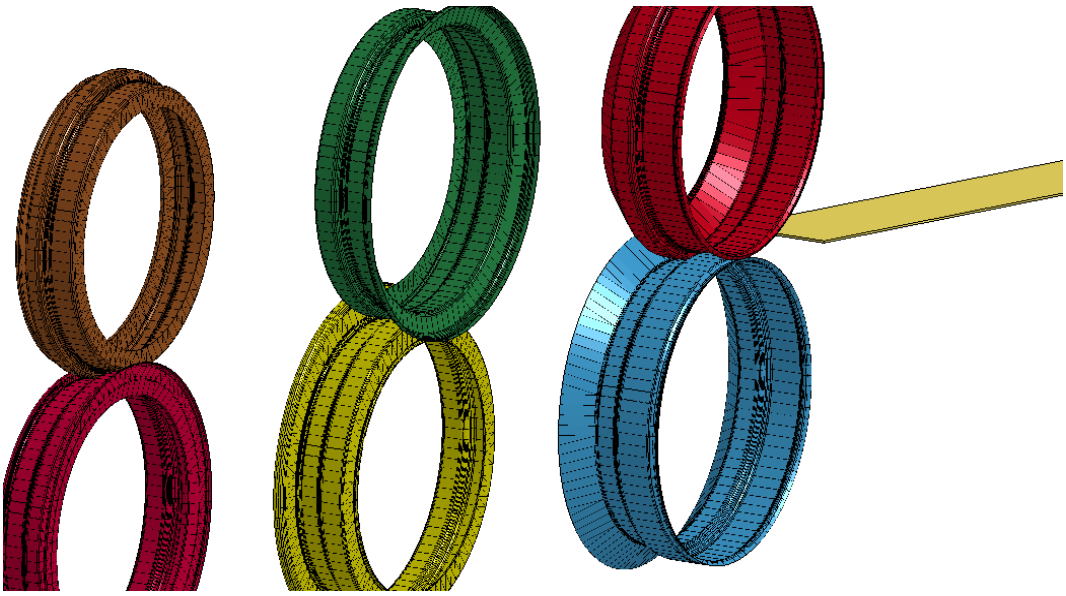

Figure 6-1: Example of a roll forming FE-model

The large deformation between each forming step does not always automatically catch the leading edge. Sometimes extra boundary conditions are required at the leading strip edge, when entering a roll gap. This can be handled by extending some of the tool surfaces to 'catch' the incoming profile or add boundary conditions to some nodes on the leading edge. In production the operators ensure the extra boundary conditions when the machine is threaded with a new strip. This is generally the most difficult issue in carcass roll forming FEA setup: ensuring correct profile entry into each forming step roll gap.

6.4 Simplified winding model

Figure 6-2 shows the simplified winding model including only the roll formed profile, WT1 and the mandrel. WT2 is not shown but is essential to prevent localised bending of the profile (described in 4.3.4) and keep the profile on the mandrel during winding. When necking and fracture appears in the carcass process it occurs during the first part of the winding operation, where the tongue is kept in an open position. The simplified winding model allows investigation of the strain distribution during this part of the process – especially around weld relief zone. Early models included a full roll formed profile but later ones only use the QT-side of the profile as shown in Figure 6-3, because only the strain distribution in the tongue is of interest. Boundary conditions applied to the half-profile is indicated in Figure

6-4 with descriptions in Table 6-3. The boundary conditions on the tongue are set to emulate that the WTs are holding it upright.

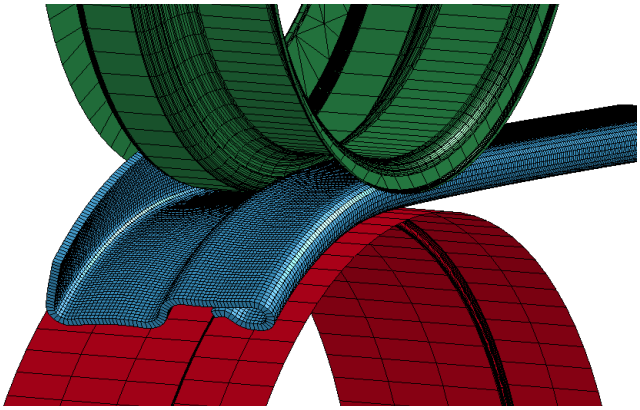

Figure 6-2: Simplified winding showing a 1.5mm carcass profile wound onto a 6” mandrel

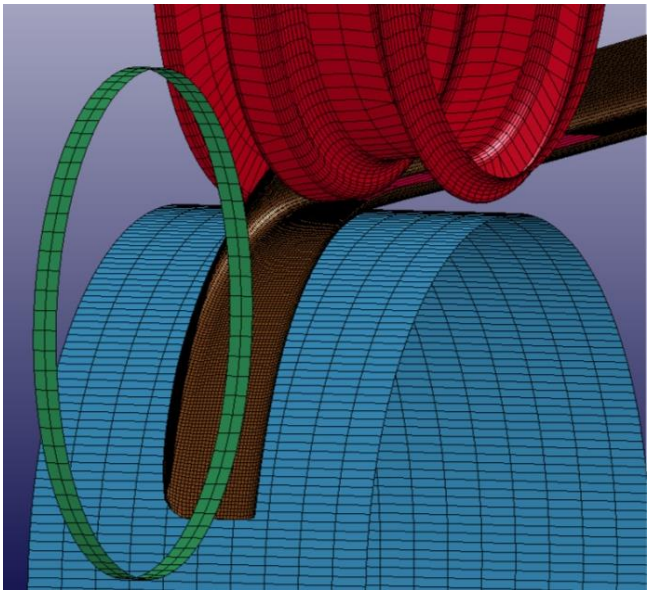

Figure 6-3: Simplified winding of half-profile (QT) wound onto a 4” mandrel

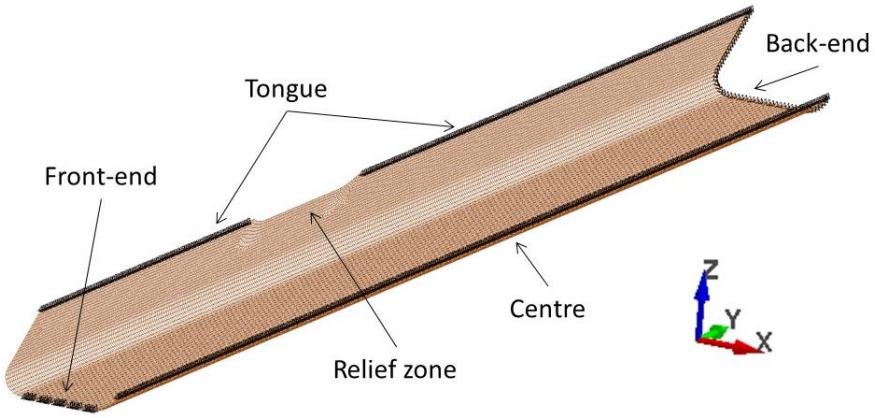

Figure 6-4: Boundary conditions on the QT-side of the carcass profile – this specific profile has a relief zone included

Table 6-3: Strip boundary conditions relating to Figure 6-4

Boundary	Condition
Front-end	Tied to mandrel
Back-end	Locked in z- and x-direction
Tongue	Locked in x-direction
Centre	Locked in x-direction

Roll formed profiles were imported into the winding model to include strain history of the material but comparisons with profiles without pre-strain history did not show different results as regards the tongue, whereby most simulations were done with profiles of standard dimension without strain history. This seems only viable for the present investigations as full interlocking of two profiles with the degrees of freedom allowed to the profile during winding necessarily will be influenced by the strain history from roll forming.

The mandrel is set to rotate at 30RPM (similar to normal carcass production speed) and boundary conditions are set on the leading profile edge to be ‘fixed’ onto the mandrel ensuring that the profile is pulled onto the mandrel as it rotates. Before entry under WT1 guides help steering the profile correctly under WT1 and onto the mandrel.

6.5 Three-point-bend model

The physics of winding a carcass profile onto a mandrel is similar to a three-point bending, exemplified by the localised bending failure mode described in 4.3.4. A simulative three-point-bend test was constructed (Chapter 7) and consequently a FEA model of this was made, see Figure 6-5. This very simple model allows fast setup of simulation settings especially for thicker strip sizes on relatively small mandrels, where winding onto the mandrel in the winding model is sometimes problematic. Boundary conditions are similar to those in the winding model with the addition that the nodes initially in contact with the mandrel are locked to it - otherwise the profile will buckle into a ‘v’ shape. The deformation starts at the initial contact point and moves on either side toward each bending roll. A direct comparison with the winding model in Figure 6-6 show that the deformation is similar, and that the three-point-bending is a good approximation to winding - at least regards the strain distribution in the tongue, when it is open on the mandrel.

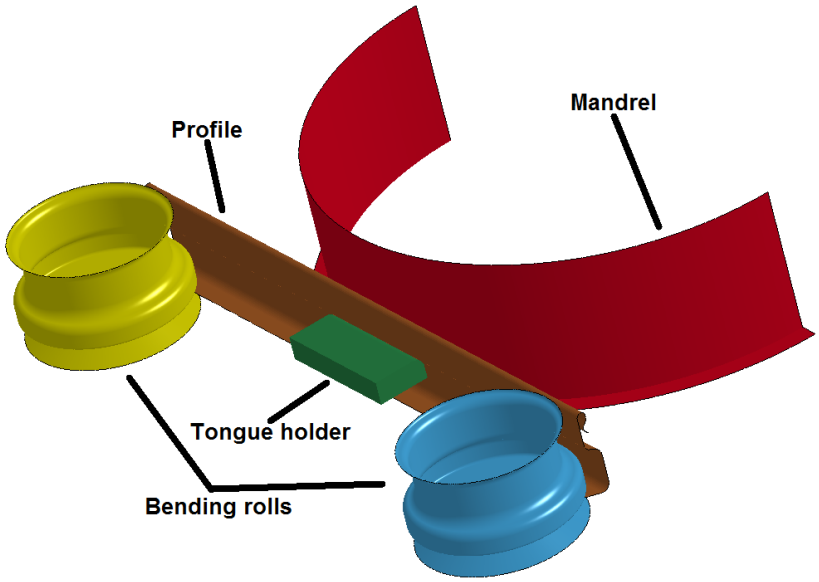

Figure 6-5: Three-point-bending FEA model

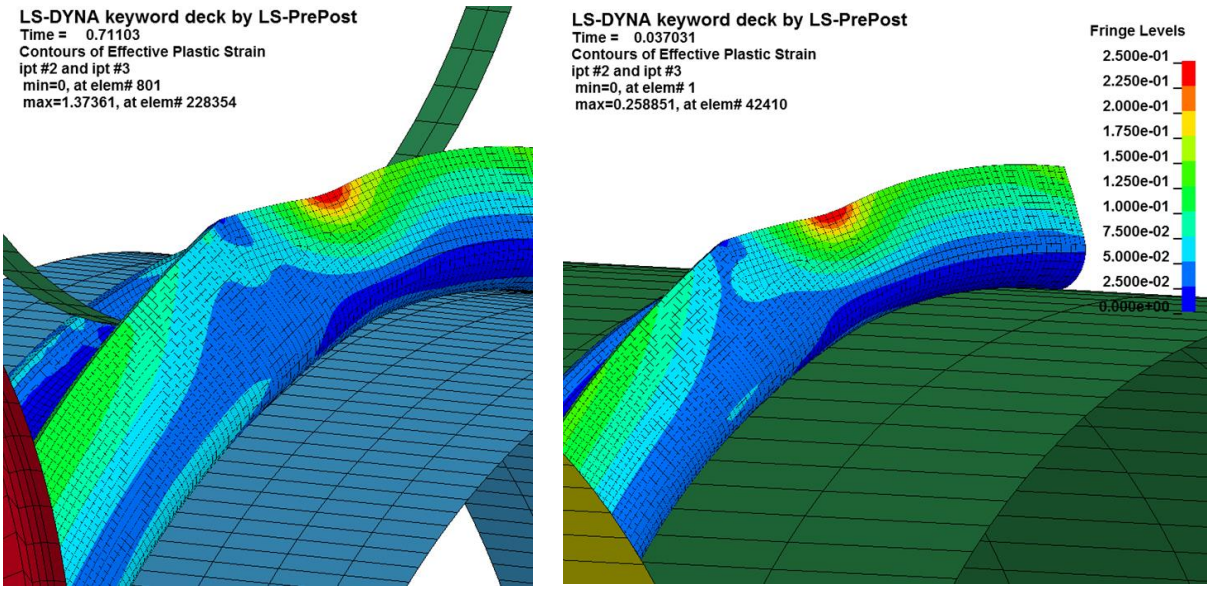

(a) (b)

Figure 6-6: Comparison of effective plastic strain in tongue / relief zone between simplified winding (a) and three-point-bend (b)

6.6 Convergence study

Precision and performance are the keywords to a convergence study where the objective is an optimisation of model parameters to obtain a desired precision within the shortest simulation time. The focus is on mass scaling, mesh size and Gauss integration points, where evaluation is made through comparison of strain distribution on profile cross-sections. Convergence is assumed to be achieved, when two levels of a factor produces similar results; both

levels of that factor leads to a converged result. Both roll forming and simplified winding is studied and common convergence parameters are established at the conclusion.

Simulations ran on an Intel® Core™ i5 M540 CPU (2.53GHz) with 4GB of memory and 64-bit Windows 7 installed. The solver was LS-DYNA version 971R5.0 double precision 64-bit version.

6.6.1 Mass scaling

For easy interpretation and discussion of the results from this convergence study, mass scaling is defined as a multiplier constant relating to the initial critical time step. This means that the notation "*50x mass scaling*" corresponds to 50x the initial critical time step, which does not directly tell anything about the added mass to each element. Selective mass scaling is applied to all the models in the convergence study. The motivation for using mass scaling is clearly seen from Table 6-4 where total CPU time is greatly improved.

Table 6-4: Effect of mass scaling on total CPU time for roll forming

Mass scale	Total CPU time
1x	311 hours
10x	26 hours
50x	11 hours
100x	8 hours
200x	6 hours

The roll forming results are seen in Figure 6-7 showing the effective plastic strain across strip width. The strain values displayed in the figure all correspond to the profile after leaving the final roll gap, and a global time, where equilibrium in the strip is reached, is chosen. This global time is the same for all directly comparable solutions. Mesh size of the workpiece in the present investigation is 0.75 mm along the width of the strip and 3 mm longitudinal to the strip. It is noticed that the solutions of 200x and 100x mass scaling have started to drift especially at the tongue edge (width position ~90 mm). It is important to ensure convergence at the tongue edge as the strains and strain paths of this section are important for determination of limit strains during the winding operation. Based on the results, it is concluded that convergence in roll forming is achieved at 50x mass scaling. The same result was achieved for the winding model, where only the strains at the tongue where evaluated.

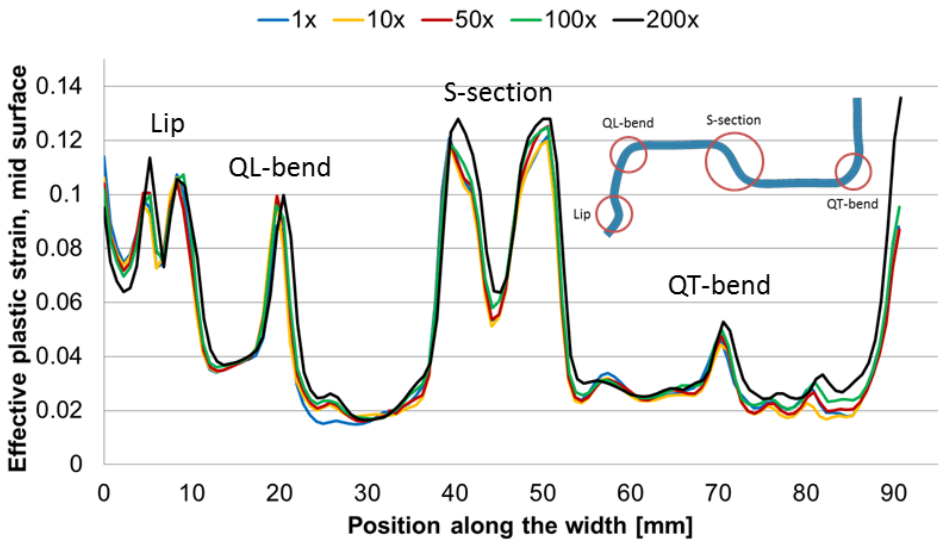

Figure 6-7: Effect of mass scaling in roll forming; effective plastic strain (mid-surface) across strip width

6.6.2 Element size

Strip and mandrel size vary from production to production, wherefore a normalised element size is determined, so that a fitting mesh is made for the specific combination that is studied. In roll forming the transverse element size is most important, whereas in winding it is the longitudinal one. The convergence study is therefore split into those two parts. By keeping mass scaling as a constant factor, the absolute time step scales with mesh size, which implies that the scaling factor is the same for all models, whereas the absolute time step varies. Table 6-5 show the effect of mesh size on CPU time in the roll forming simulation. Because carcass profiles are normally standardised, the mesh size is given as a mesh size factor that is multiplied with the strip width to obtain the mesh size in [mm].

Table 6-5: Effect of transverse mesh size on total CPU time for roll forming

Transverse mesh size factor (strip width) [-]	Total CPU time
0.0015	178 hours
0.003	60 hours
0.006	20 hours
0.008	8 hours
0.015	4 hours

The transverse mesh size factor, based on the roll forming analysis, was found to converge at 0.003 * strip width [mm], see Figure 6-8. The slight deviations in the curves can be explained by the difference in strip position in the roll gap due to the mesh size. Actually all three curves are very similar only the 0.006mm * strip width [mm] deviates a little at the lip; posi-

tion = 0. In fact such a fine mesh is not needed across the whole strip width as the fine mesh is only necessary in the bends and at the lip in particular. An optimised approach include finer mesh at the bends during roll forming but this path was not pursued because of increased focus on winding without including strain path from roll forming.

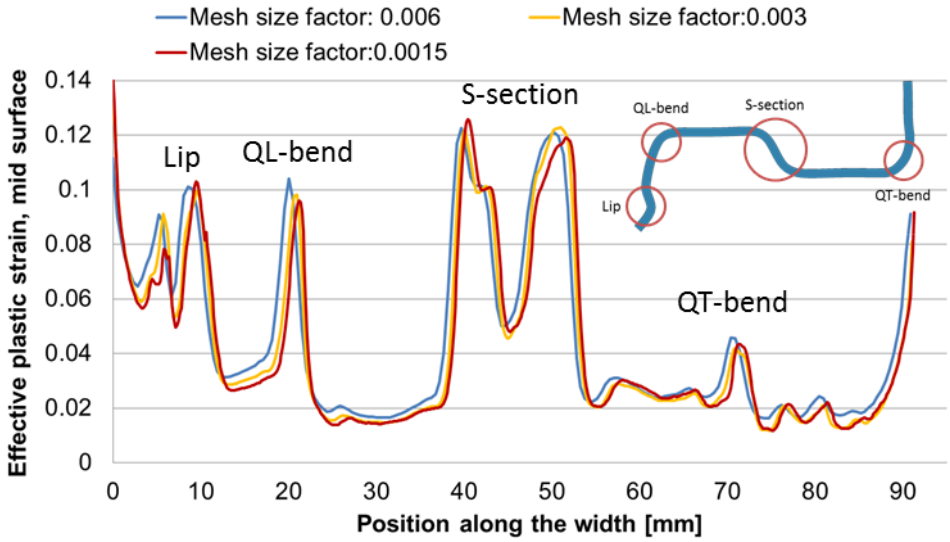

Figure 6-8: Effect of mesh size in roll forming indicated by mesh size factor; effective plastic strain (mid-surface) across strip width

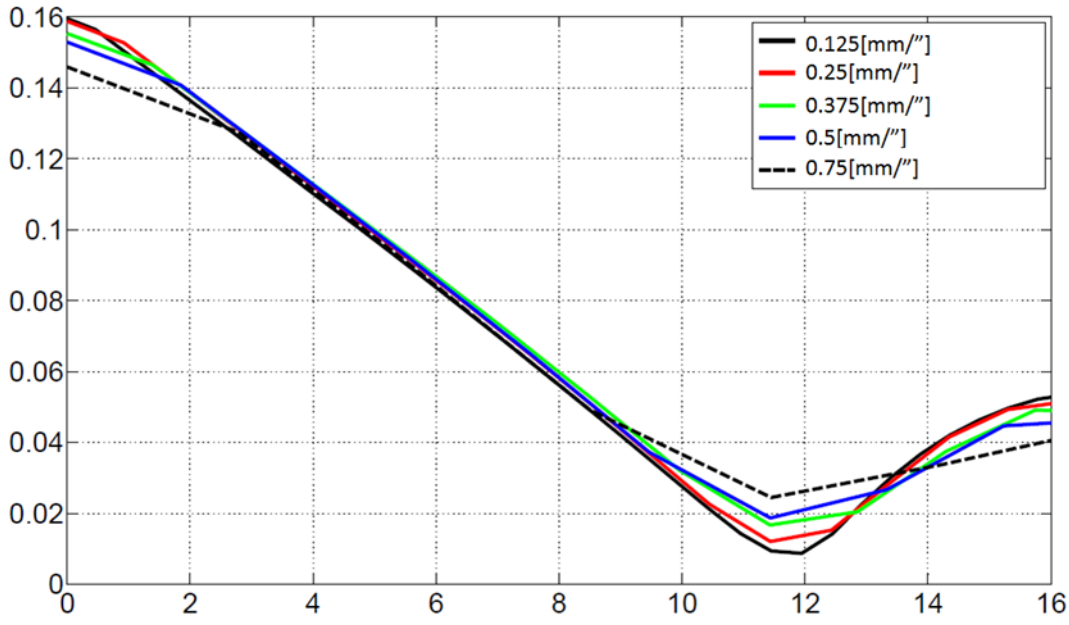

Figure 6-9: Effect of mesh size in winding shown as function of mandrel size [mm/"]; effective plastic strain (mid-surface) on the tongue [31]

The effective plastic strain at the tongue is shown in Figure 6-9 for mesh size winding convergence. It is seen that longitudinal element size converges at mesh size factor 0.25 [mm/"] – multiplying the mesh size factor with mandrel size in inches provides the proper mesh size. Because only the tongue strains are of interest in the winding simulations convergence is only

sought for this part of the profile. For a model including interlocking one might expect that a convergence study could be difficult due to the contact issues that could arise.

6.6.3 Integration points

The number of integration points through thickness has an effect on springback evaluation and stress/strain distribution through the thickness. Values for mass scaling and mesh size are chosen based on the convergence study:

- Mass scaling = 50x
- Mesh size: Transverse = 0.003 * strip width [mm]; Longitudinal = 0.25mm * mandrel diameter [“]

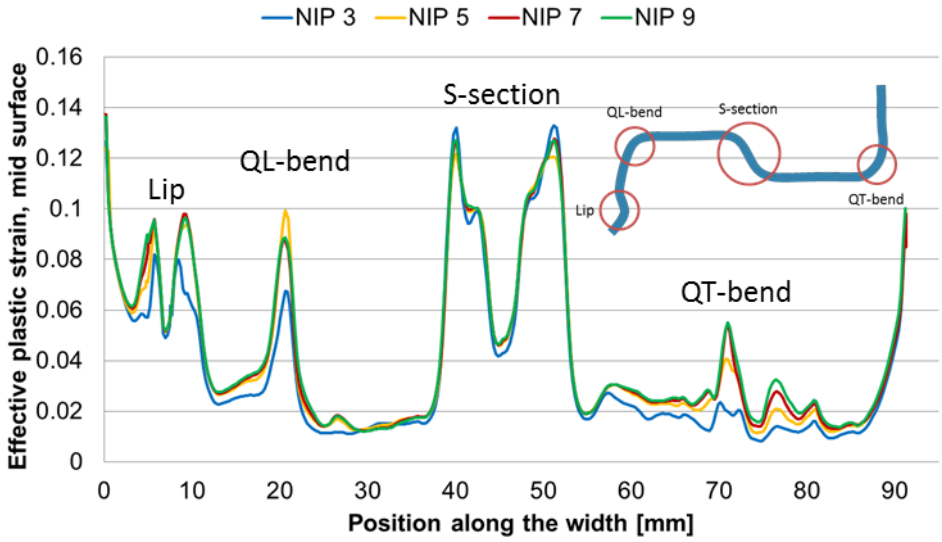

Figure 6-10: Effect of number of integration points in roll forming; effective plastic strain (mid-surface) across strip width

An odd number of integration points are chosen as this will always ensure an integration point at the sheet’s mid-surface. The mid-surface effective plastic strain for through thickness integration points of 3, 5, 7 and 9 is illustrated in Figure 6-10. The conclusion is that through thickness integration points of 7 and 9 have converged, which corresponds to the results from the winding simulation.

6.7 Converged parameters

- Mass scaling = 50x initial critical time step
- Mesh size: Transverse = 0.003mm * strip width [mm]; Longitudinal = 0.25mm * mandrel diameter [“]
- Gauss integration points = 7

6.8 Validity of shell elements in the current investigations

As mentioned earlier plane stress conditions must be met for the use of shell elements (i.e. when the thickness of the plate is much smaller than the in-plane dimensions). With some rather small bending radii of the carcass profile the assumption of plane stress might be invalid. Although some shell elements do have the potential to account for through thickness stresses such as element formulation 25 and 26 in LS-DYNA®, trial simulations showed stability problems with these element formulations, wherefore they were not further explored.

An investigation into the stress state of the bends is performed with 2D plane strain elements.

6.8.1 2D plane strain FEA of lip- and QL-bend

The 2D model is set to emulate the deformation at the lip- and QL-bend performing the deformation of a corresponding geometry by a punch and die, see Figure 6-11. The bend radii are set for a strip thickness of 1.8 mm.

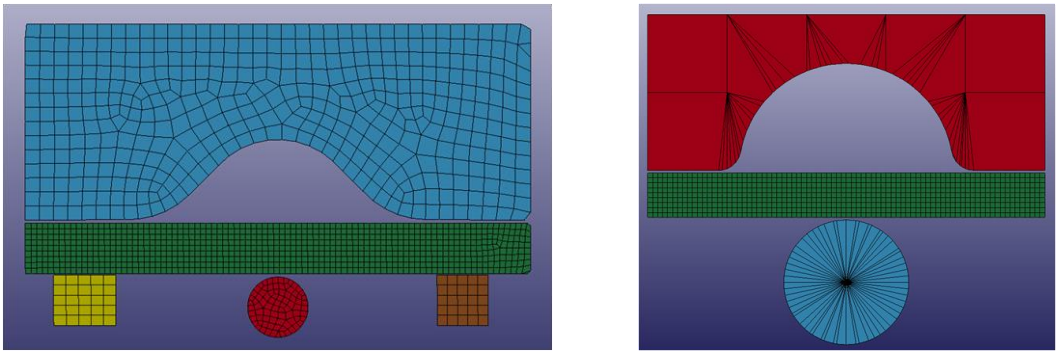

(a) (b)

Figure 6-11: (a) 2D model of the lip-bend where the punch (red) is moved upwards; (b) 2D model of QA-bend where the punch (blue) is moved upwards

The stress states before elastic relaxation are shown in Figure 6-12. The stresses are indicated according to the local element coordinate system. The through thickness stresses show only compressive peaks in the two contact points with the punch. Comparing these through thickness stresses to the transverse and longitudinal stresses it does not seem as an invalid assumption to assume plain stress since, apart from the contact points, the thickness stress is negligible. However, for full interlocking winding models with roll formed profiles the mandrel size-effect earlier mentioned could cause a three-dimensional stress situation that would not be representable with shell elements. Because of the lack of such a model, it is not further pursued but should be kept in mind for future FEA winding models.

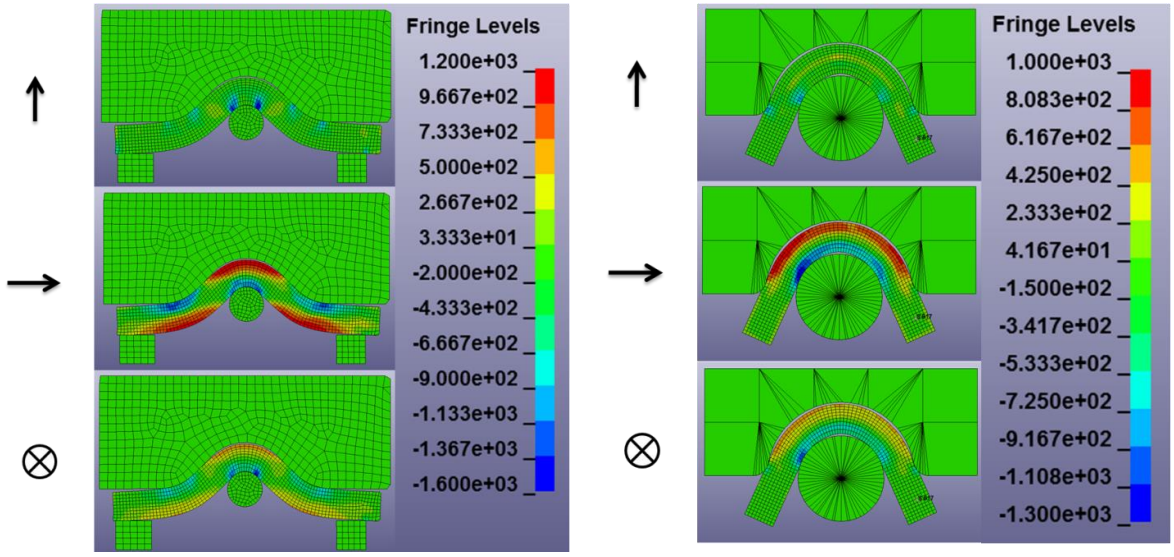

(a) (b)

Figure 6-12: Stress distribution according to local element coordinate system indicated by the arrows; (a) for the lip-bend and (b) for the QL-bend

Chapter 7 Simulative testing

Simulative testing is an efficient method of carrying out parametric studies in a controlled environment and eliminating unsuited parameters before production testing, which is often time consuming and costly. One of the tasks in this project was the development of a simulative test and the present chapter describes the important factors in the design, validation procedures and the use of the simulative test equipment to perform studies with simple, bent profiles.

7.1 Design

Because of formability issues in the winding stage attention was focused on a simulative winding test. Initial designs were all centred on simplified but still true winding of a profile that would ensure interlocking between two profiles. This, however, implied quite complex equipment, which did not correspond to the desire of simplicity of the test. The final choice ended up being a three-point-bend test that simulates how the roll formed profile is wound onto the mandrel with main focus on the strains in the profile tongue. Obviously the dynamics of the three point bend is different from continuous winding, but the simplicity is ideal and it allows offline testing of welding parameters and weld reliefs before testing the most promising solutions in the production machine.

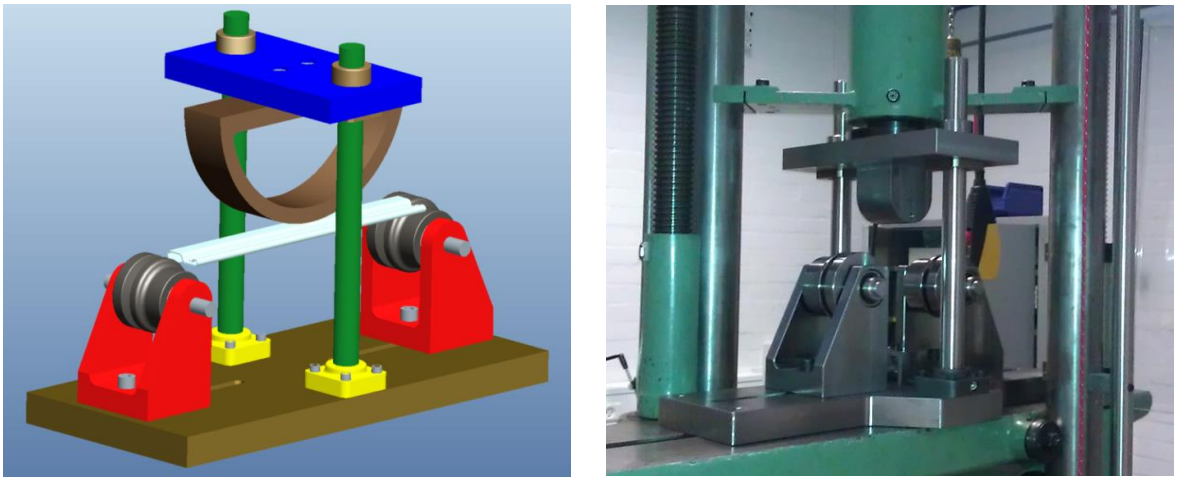

(a) (b)

Figure 7-1: Simulative three-point-bend test for winding simulation; (a) CAD model and (b) equipment mounted in the Mohr Federhaff press at DTU-MEK

Figure 7-1 shows the design which include: a moveable interchangeable mandrel, two contoured bending rolls (also interchangeable) suitable for the profile tested. In its present design the equipment is designed for a Mohr Federhaff 60 ton universal press in the laboratory of

DTU-MEK. Instrumentation consists of a load washer installed at the mandrel base and a draw wire sensor for displacement measurements.

7.1.1 Profile boundary conditions

To prevent localisation during bending boundary conditions needs to be applied to the profile in order for it to stay in contact with the mandrel during bending. The present solution is simple and involves a bracket and a restraining bolt fixing the profile to the mandrel as well as keeping the tongue open at this point, see Figure 7-2. This method of restricting tongue deformation is not perfect, which is evident from the following results.

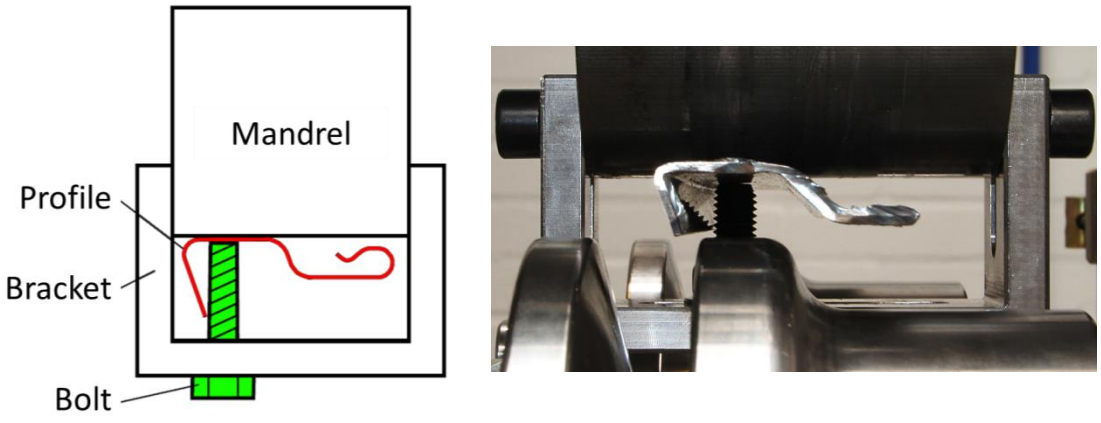

(a) (b)

Figure 7-2: Profile boundary conditions on the mandrel peak contact point; (a) illustration of profile fixation and (b) actual fixation of a simplified profile

7.2 Validation of test

Because strains at the tongue edge are of main interest for formability investigations the simulative test is compared to production strains at this position. An initial investigation showed that the simulative test gave similar strains in the FE-model as in production but an error in grid size measurements was found, which meant that the actual strain was in fact lower as seen in Table 7-1. The problem is the boundary conditions of the tongue during bending, since the bolt only supports the tongue at the initial contact with the mandrel. The result is that the tongue is free to reduce strains during bending by closing, leading to lower strains in the tongue edge away from the bolt position. The problem is visually seen in Figure 7-3, where the tongue at the bolt is kept in its original upright position, whereas the further away from the bolt the tongue closes more and more, which is confirmed by the plot of the measured major strain shown in Figure 7-4. Thus the problem consists of the strain varying on the tongue depending on measurement position with respect to the restraining bolt. This complicates strain comparison with production, since the strain is only proper at the bolt but bending of the tongue around the bolt is similar to carcass winding. The tongue would similarly close in carcass winding if not for the winding tools positioned around the mandrel keeping the tongue in the desired upright position. Because of the difference in boundary conditions the

profile deformation dynamics in the simulative test vary from that in the carcass production, where the strains are reduced by reducing tongue height and increasing QT, whereas the simulative test allows the tongue to close instead. Another effect of this change in process dynamics is that the mandrel size effect on profile geometry (reported in Chapter 3) is less pronounced in the simulative test.

Figure 7-3: Position at which the bolt keeps the tongue in an upright position; it can be seen how the tongue closes away from the restraining bolt position resulting in lower strains away from there

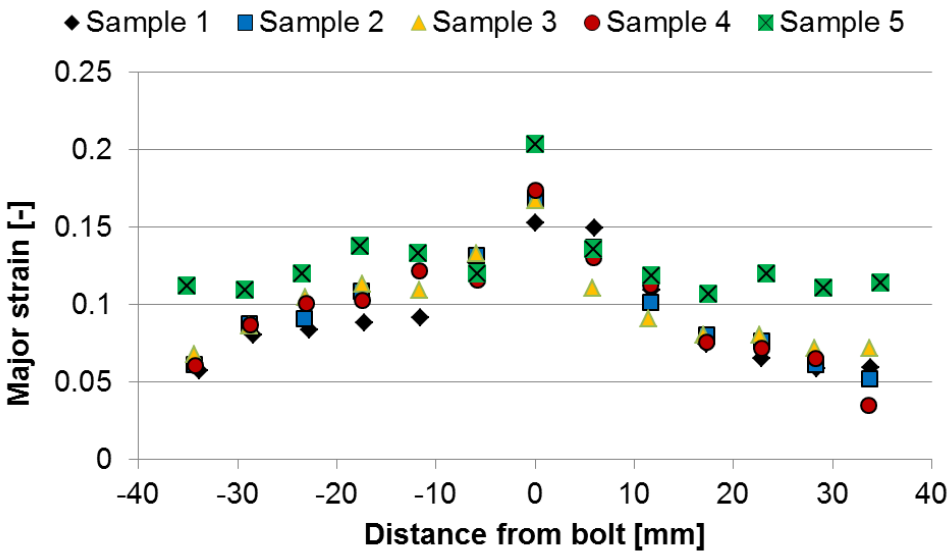

Figure 7-4: Major strain measured around the bolt (position '0') for 5 roll formed profiles; the tongue closes away from the bolt thereby reducing the major strain

Another issue related to strain measurements was the choice of grid for the simulative test, which was 5 x 5mm square grid provided by a rubber stamp and printing ink (paragraph 5.4.1). Minor strains are difficult to measure with this particular grid technique in the test, wherefore comparisons are only done for the major strains. This is not optimal, as no information is thereby about strain path. However, early measurements with a 3 x 3mm square grid

rubber stamp (this particular grid was damaged during the present validation procedure) showed the strain path of EN 1.4162 roll formed profiles in the simulative test to follow uni-axial strain path, which is also indicated by the FEA models.

Table 7-1: Comparison between production test, simulative bend test and FEA of the simulative test for a 1.1mm profile on 4” mandrel. The strain for the simulative test is measured 5mm from the bolt

	ε_{major}	Std. deviation
Carcass production	0.16	0.01
Simulative test	0.1	0.02
FEA, simulative test	0.14	-

The reason for the higher strains in the FEA compared to the simulative test is found in the manner of tongue deformation during bending at high strains. The FEA shows similar values as in the production strains but the three-point-bends performed in the laboratory test resulted in lower strains. Figure 7-5 (a) shows a 1.5mm roll formed profile bent on a 4” mandrel in the simulative test overlaid with the corresponding FEA profile mid-surface. The boundary conditions for the FE-model are corresponding to the test, but the tongue is not similarly closed. It shows that the FE-model does not allow the tongue to close and introduce a curvature, which might be a result of the choice of shell elements. FEA and test results for a 6” and 8” are comparable so it seems that for higher strain the FE-model encounters some problems, see Figure 7-5 (b). This behaviour needs further investigation in future work.

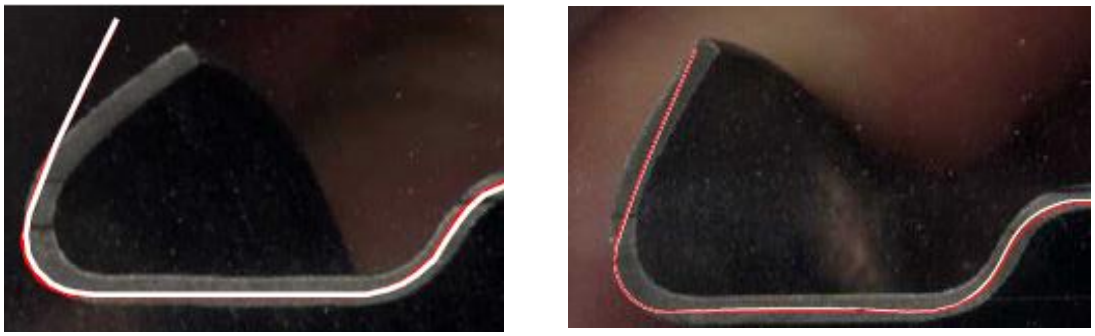

(a) (b)

Figure 7-5: Comparison of 1.5mm profile and FEA on a; (a) 4” mandrel and (b) 6” mandrel

7.2.1 Discussion

The simulative test seems promising as a tool to perform parametric studies of weld and relief zone fracture during the carcass winding stage although the tongue boundary conditions in present form of the test do not match those of the carcass winding. Even if the strain level is not fully comparable to that in production, it is still possible to perform parametric studies on the equipment to find optimised parameters for production. In the long run it is desirable to improve the simulative test to emulate production regarding maximum strain in

the tongue. This calls for a better way of applying proper boundary conditions to the profile and further validation must be performed.

7.3 Simplified profiles

The reason for introducing simple, bent profiles (made by air- and v-bending) in the simulative test is to facilitate manufacturing of test profiles, since getting roll formed profiles from carcass production is time consuming and thus costly, as production is on hold, while acquiring the profiles. This investigation was performed in the simulative test to investigate, if deformation behaviour of simple profiles and roll formed from carcass production are comparable. The error in tongue boundary conditions are accounted for by measuring and comparing strains at the same distance from the restraining bolt – 5mm away.

7.3.1 Profile design

Figure 7-6 shows the proposed test designs of the simple profiles, where the dimensions of the tongue are comparable to those of the roll formed carcass profile. The designs were chosen based on a FEA study, in which they showed promising results compared to the actual carcass profile. Table 7-2 shows the strain measurements on the tongue edge measured 5mm from the restraining bolt. It is noticed that the results are similar regarding major strains of the tongue, which indicates that even if deformation on the mandrel vary for the different profiles the final strains in the tongue are comparable. Profile 1-1 is the simplest, but twisting of the profile during testing (and in the FEA of the test) is not in accordance with the winding operation, where no twisting appeared. The strains measured in the tongue are, however, similar to that measured in the other profiles. Based on this result, it was chosen to continue with profile 2-1 because of the simplicity with only two bends and satisfactory behaviour in the simulative test regarding geometry and strains.

Table 7-2: Major strain measurement (5mm from the restraining bolt) on simple profiles bent in the simulative test: 1.1mm profiles on a 4” mandrel

Profile	ε_{major} (average)	Std. deviation
1-1	0.12	0.005
2-1	0.12	na
2-2	0.11	0.013
3-1	0.11	0.005
3-2	0.12	0.003
4-1	0.11	0.003

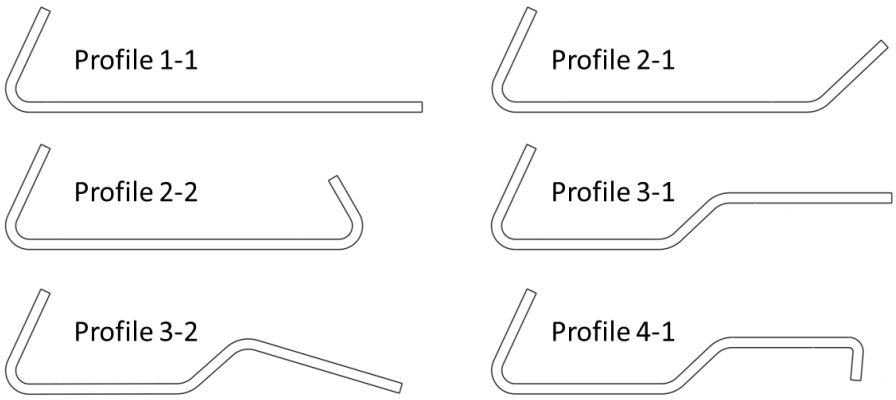

Figure 7-6: Design of simplified profiles with notation x-y (x indicates the number of bends and y design no.)

7.3.2 Comparison with roll formed profiles

The simplified bent profile 2-1 and the roll formed (RF) 1.1mm profiles from carcass production were compared in the simulative test with a 4" mandrel. The profiles include welds and strains are compared in the tongue and across the weld. The material is all taken from the same coil and the welded strips for the simple profile were welded with the same procedure as the one used for the roll formed profiles.

Figure 7-7 shows a comparison of major strains measured on the tongue edge and across the weld. The major strains in the tongue are similar, which is a satisfying result for profile 2-1. Notice that the strain level across the weld is higher for the roll formed profile although the strain at the tongue edge is similar. Since the strips are welded in the same setup at the same time, it is likely that the difference is caused by the roll forming stage. The weld zone is mechanically softer than the parent material (paragraph 8.1) therefore the longitudinal strains in the tongue during roll forming might cause geometrical non-homogeneity, much like the Marciniak-Kuczynski theoretical model for necking [50], causing earlier strain localisation during bending/winding in case of the roll formed profile.

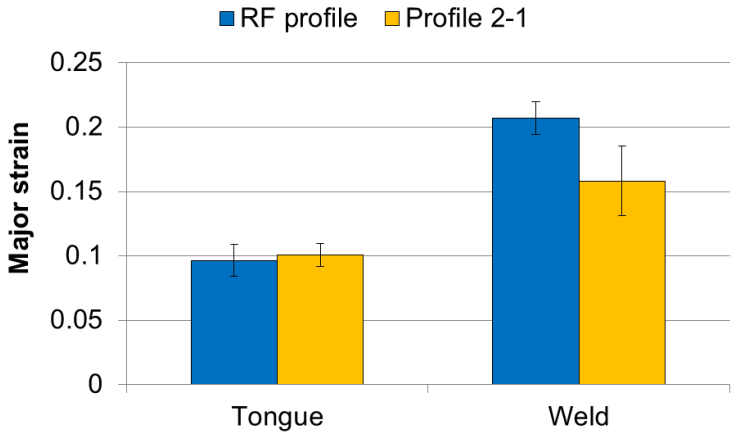

Figure 7-7: Strains in the tongue and across weld on 1.1mm roll formed and simple profiles on 4" mandrel. The error-bars indicate standard deviation

7.3.3 Results and discussion

In normal carcass production the carcass dimensions tested here are prone to weld fracture without the presence of relief zones. The lower strains in the tongue obtained in the simulative test further ensure that the strains are below the critical level, which explains why none of the welds fractured during the simulative test. The effect of the weld zone as regards the strain distribution herein is described in more detail in Chapter 8.

Simplified profiles seem to be a viable alternative to roll formed profiles in the simulative test, as the strains in the tongue are similar. However, it is important to note that the process path of the roll formed profile are causing strain localisation in the weld for the specific profile tested here, wherefore parametric studies between simple profiles are possible but they could show incorrectly higher tongue strains before weld fracture than in an actual roll formed profile. This is an effect that requires further investigation during future studies with the simulative test and simplified profiles.

With proper boundary conditions it seems likely that the tongue deformation in the simulative test will simulate that of carcass winding and thus enabling offline formability assessment of welding parameters, weld relief zones and other parameters affecting tongue fracture.

Chapter 8 Carcass process formability

The motivation for investigating formability in carcass production is to understand process requirements and how they relate to material forming limits. Production studies have shown that formability issues are confined to the winding stage with fracture of the tongue, when it is kept open during the first revolution before it is interlocked, and tongue buckling during interlocking. Attention is focused on fracture and the effect of welds and weld relief zones, as tongue buckling is known to be manageable by tool settings through a change in strain path/gradients. This chapter cover the process demands and material capability as regards to fracture by evaluating strains in production and FEA during winding and comparing them with the material data already acquired in Chapter 5.

8.1 Weld fracture

Weld fracture is the largest formability problem in carcass production especially when utilising duplex grade stainless steels. The ferritic- / austenitic duplex structure of the material is difficult to retain after welding, which result in an unbalanced microstructure that is believed to cause lack of ductility and toughness [10]. In the following it is shown that geometric and mechanical in-homogeneity of the weld zone is causing strain localisation almost from onset of tensile loading. Welded strips of EN 1.4162 lean duplex stainless steel were subjected to tensile testing and strain measurements of the weld fracture were made using GOM ARAMIS 4M strain measurement system. The investigation was further supported by hardness testing and material thickness measurements across the welds.

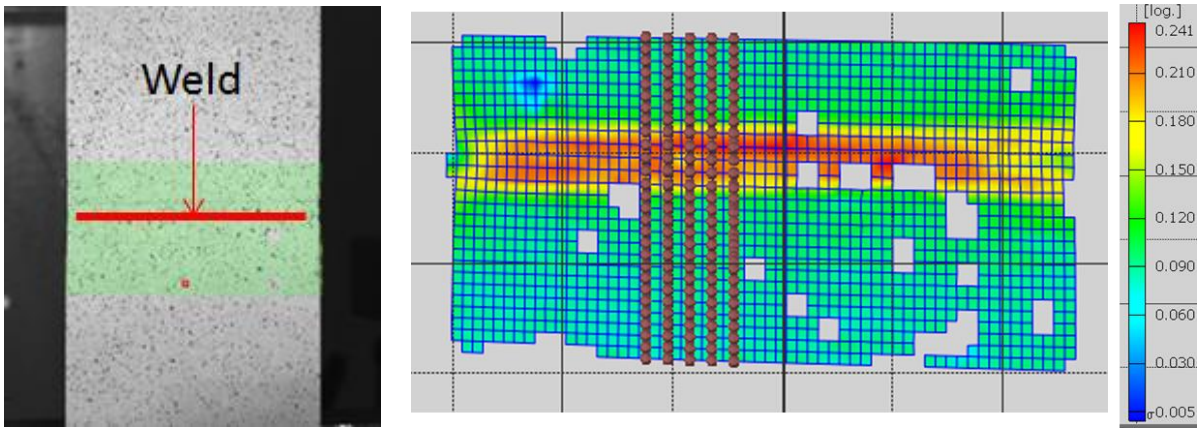

(a) (b)

Figure 8-1: ARAMIS results from tensile testing a 1.2mm welded strip; (a) last frame of specimen before fracture and (b) strain calculations across the weld just before fracture (the holes in the grid are facets not recognised by ARAMIS) – the brown dotted lines indicate the strain measurements across the weld

Figure 8-1 (a) show the speckled pattern around the weld of a tensile specimen, where slight, diffuse necking can be observed around the weld. This is also indicated by the strain distribution around the strip edge in (b); seen by the lower strains compared to the centre of the strip where the material is more constricted. Figure 8-2 shows how the longitudinal (major) strains, calculated in ARAMIS across the weld, develop from tensile test start to the last frame before weld fracture. Strain localisation is seen at the weld almost from onset of yielding causing the strains in the weld zone to be constantly higher throughout the test – rather similar to the Marciniak-Kuczynski strain localisation model [50]. The result is weld fracture at strip strain, ε_{nom}, in the homogeneous deformation zone that is much lower than parent material forming limit which for EN 1.4162 is ε_{major} = 0.4 (FLC tensile point). Although the strain localises across the weld, the homogeneous strain in the specimen still increase throughout the test. The rate of strain increase from frame to frame is just smaller than in the weld.

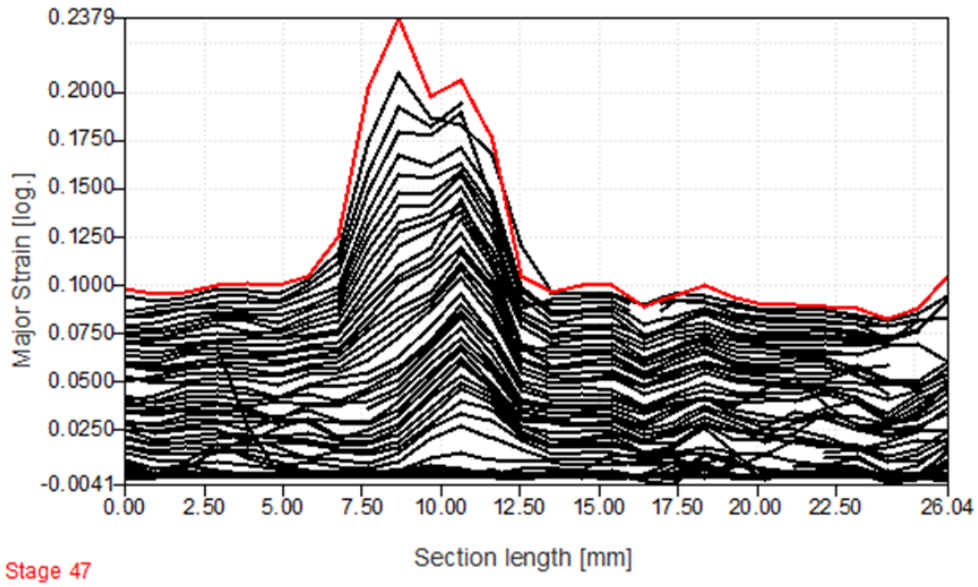

Figure 8-2: Longitudinal strains across weld seam where each line is the strain for each frame measured by ARAMIS – the red line is the strains for the frame just before weld fracture. The weld is positioned between 6mm and 12.5mm

The average major strain results from the tensile tests are shown in Table 8-1. They all show the same trend as Figure 8-2; the homogeneous strains in the strip are much lower than the strains across the weld, which implies that the homogeneous strains are far from the formability capabilities of the parent material. Weld fracture occurs at homogeneous strain ε_{major} = 0.1 suggesting that strains near to or above this level contains a risk of weld fracture. The strain localisation at the weld signify that one must be cautious, as even if fracture does not occur, there is still a risk of severe thinning at the weld before stress reversal, when the tongue is closed. When the tongue is closed, the weld will appear normal, without thinning, but damage to the material structure may have occurred.

Table 8-1: Average major strains from tensile test of EN 1.4162 with welds just before fracture. Strains were measured with a GOM ARAMIS 4M system

	ε_{major} [-]	std. deviation [-]
Homogeneous	0.10	0.01
Across weld	0.27	0.05

8.1.1 Strain localisation in weld zone

Weld fracture always occur in the transition zone between weld seam and the HAZ which is also the case for the tensile tested strips in the present investigation, see Figure 8-3. To investigate the background for thus hardness tests as well as thickness measurements across the weld are analysed.

Figure 8-3: Fracture at transition from weld seam to HAZ during tensile testing correlating to weld fracture during carcass winding

Figure 8-4 show the hardness test results for three welded duplex materials, where 100% indicate the parent material hardness. The graph clearly shows similarity in the HAZ and weld seam hardness's for the three materials, which all are lower than the parent material hardness. This explains the strain localisation in the weld zone, as this region creates an in-homogenous deformation zone, where strain localisation is initiated due to earlier yield onset than in the parent material.

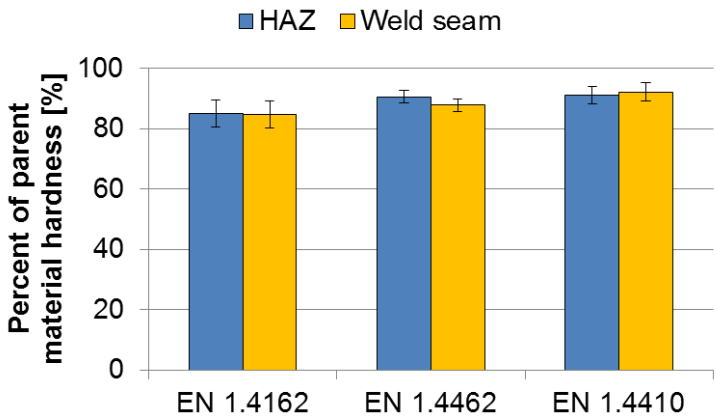

Figure 8-4: Vickers hardness (HV10) measurements; average hardness in HAZ and weld seam for several strip sizes is displayed as percentage of the respective parent material hardness. Error bars show standard deviation

The thickness measurements for 1.1mm and 1.2mm strips are shown in Figure 8-5, which indicates a trend of the weld seam being thicker than the HAZ and the parent material. This seems to be the contributing factor to necking in the HAZ / weld seam transition since similar hardness appears of the two zones.

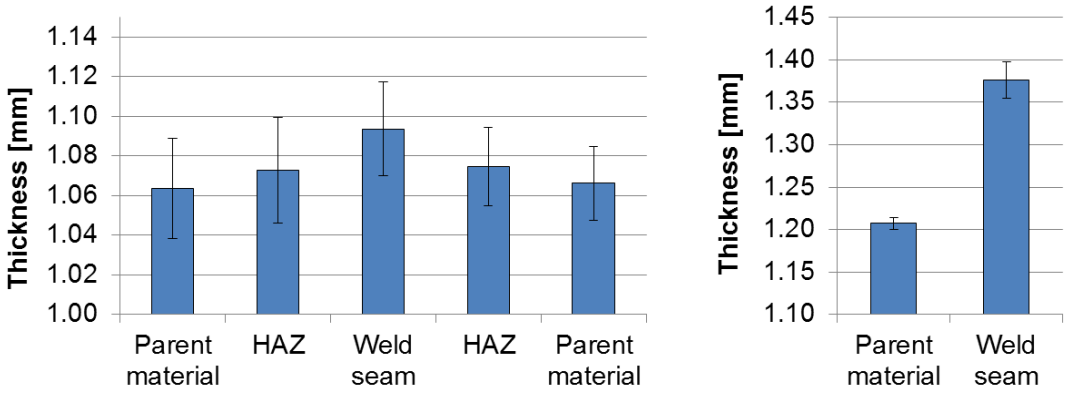

Figure 8-5: (a) Thickness measurements across weld for 1.1mm strip with Alicona InfiniteFocus, where the large standard deviation show the difficulty in optical measurements on a strip edge. (b) Thickness measurements with micrometre gauge on the weld seam and parent material for a 1.2mm strip

8.1.2 Simulative testing of welded profiles

Profiles of 1.1mm (RF profiles) and 1.7mm (simple profiles 2-1) with welds were bent onto 4" and 6" mandrels respectively in the simulative test to simulate necking and possibly fracture of the welds during winding deformation. The reason to use the simulative test is that it is fast, which implies that multiple tests can be carried out within a short time (10 minutes per sample), whereas a similar test in the production equipment would easily require 1-2 hours per winding sample. Figure 8-6 and Figure 8-7 show necking on either side of the weld seam in the transition to the HAZ for 1.1mm and 1.7mm profiles, respectively, which corresponds to the above mentioned hardness and thickness measurements. The necking occurring in the simulative test proves that the test can be used for weld optimisation, where different weld procedures and treatments can be tested for comparison. This makes it possible to optimise weld formability to increase the maximum possible, homogeneous strains towards that of the parent material.

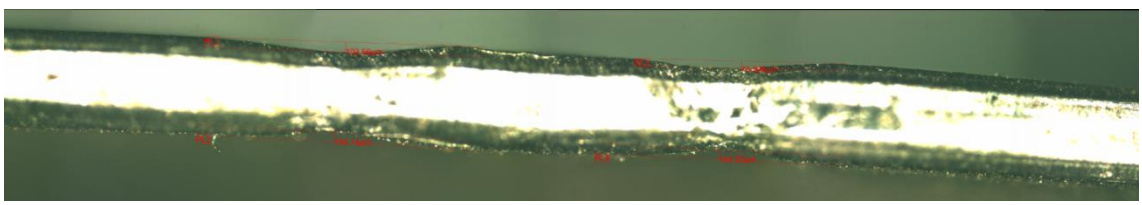

Figure 8-6: Necking at weld on either side of the weld seam in transition zone to HAZ – 1.1mm RF profile

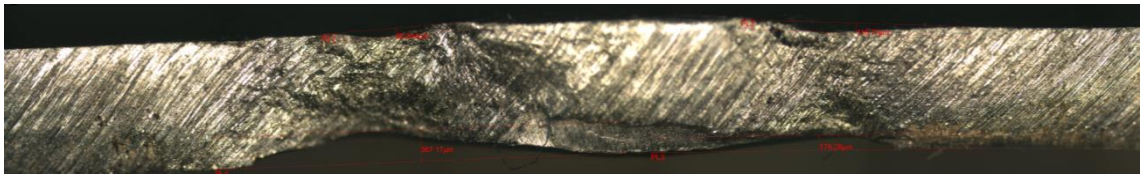

Figure 8-7: Necking at weld on either side of the weld seam in transition zone to HAZ – 1.7mm simple profile 2-1

8.2 Tongue strains

The strains at tongue edge during carcass production are important for formability evaluation of the parent material, weld zone and even for the design of the relief-cut, as is discussed later in this chapter. A general evaluation of production strains can be difficult as they depend on profile shape, tongue length and height over the mandrel as well as mandrel size. This is in turn complicated by the degrees of freedom during winding that allow the profile to change geometry during winding as reported in Chapter 3. Production tongue edge strains are measured for two specific carcass productions and the results are compared with FEA simple winding models to evaluate strain prediction with FEA of carcass winding.

Because of process lubricant and severe contact between tool and profile, laser marked grids (1x1mm size) were used for production strain measurements at the tongue during the initial part of winding, where the tongue is held in upright position. A short section of strip provided with the grid was welded to the coil, and winding was stopped once the grid section was winded on the mandrel. The sample was subsequently cut from the carcass, and strains were measured using transparent, flexible rulers. Figure 8-8 shows a typical carcass winding sample. Since the profile is interlocked, minimal springback occurs of the wound profile.

Figure 8-8: Typical carcass winding sample cut out of carcass for manual strain measurements with flexible rulers

8.2.1 FEA strain estimates

Winding of the same carcass dimensions as in the production samples were simulated in LS-DYNA® using the simple winding model. Standard geometry for the roll formed profile is used and wound on mandrels of nominal size. Weld relief zones are included in the simulations, but weld strains are only evaluated in the location next to the weld excluding the weld zones themselves. Model parameters regarding mass scaling and mesh size are determined by the convergence study in Chapter 6.

Figure 8-9 show a side view of the tongue during winding. Note that the weld relief is wound onto the mandrel before the weld itself, thus creating a relief zone towards the weld, where the tongue edge strains are lower than tongue edge strains for the rest of the profile. One of the things noted from the first FEA winding models including relief-cut is the strain concentration at the bottom of the relief-cut, which explains, why the relief-cut sometimes fracture during high strain productions (large profile on a relative small mandrel). The relief-cut is further investigated in paragraph 8.3.

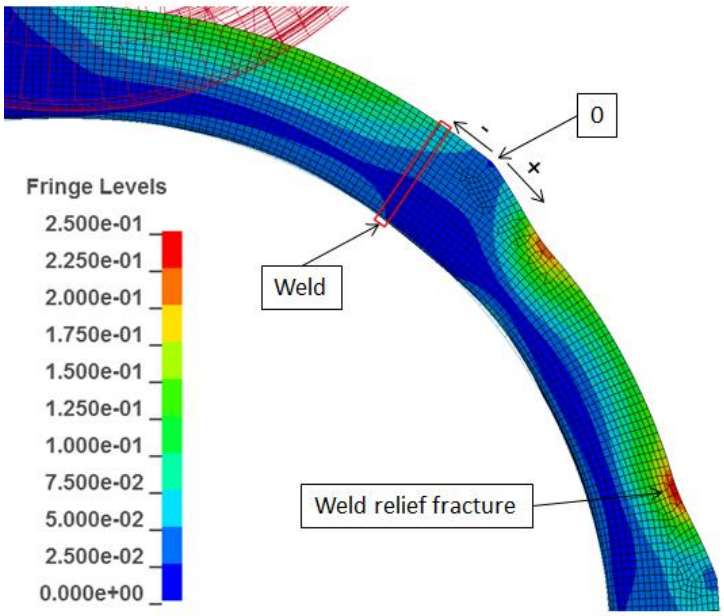

Figure 8-9: Side view of the tongue and relief zone. Fringe colours indicate equivalent plastic strain, zero is the position of the weld relief zone and +/- the direction towards relief-cut and weld respectively

8.2.2 Production strains

A 1.1mm profile 4” carcass and a 2.2mm profile 6” carcass were produced with EN 1.4162. The 4” carcass includes both weld and relief-cut measurements, while the 6” carcass did not have proper grid at the weld, wherefore weld strains are not included for that sample. It is challenging to get the grids aligned perfectly with the strip edge, which can complicate minor strain measurements at the edge. In such cases the strain ratio was measured for the

next grid point closer to the mandrel, and the strip edge minor strain was then calculated based on volume constancy and the knowledge about the major strain. The comparison with FEA is made at three significant points:

- Maximal strain at the relief-cut
- Strain at the outer edge of the tongue
- Strain at the weld

Figure 8-10 and Figure 8-11 show the strains for the 4" and 6" carcass respectively, where the uni-axial FLC point for EN 1.4162 and estimated strains from the simple winding FEA are included. As earlier mentioned the weld strains are not across the welds but instead in the grid next to the weld and towards the relief zone. It would also not be correct to compare weld seam strains with corresponding FEA position as material softening effect is not included in the FEA, so proper strain distribution around the weld cannot be expected.

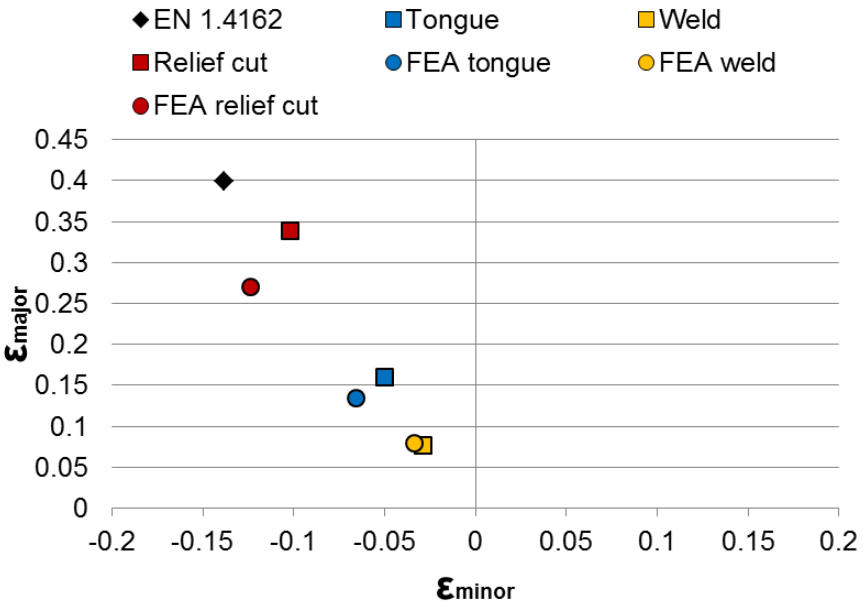

Figure 8-10: Production strains from a 4" carcass made with a 1.1mm profile (average values) compared with FEA result. The black square is the uni-axial FLC point for EN 1.4162 found in Chapter 5

The measured production strains follow the same slope as in uni-axial tension. The difference in slope between the production measurements and FEA results can be explained by material anisotropy. The FEA strain path is different, which is contributed to the isotropic hardening material model ($\varepsilon_{minor} = -0.5*\varepsilon_{major}$), whereas in reality the material behaves anisotropic as seen from the material characterisation in Chapter 5. The inaccuracy is without major consequence, since the FEA investigation focuses on qualitative comparison of different relief-cut geometries, and the FEA predictions of tongue edge major strains are generally within acceptable limits except for the relief-cut that deviates up to 20% for the 4" carcass. In this case the relief-cut maximum is lower for the FEA model, which can be explained by the fact that

during production, the strain might localise at the relief-cut, whilst being wound onto the mandrel because of the smaller second moment of inertia that the relief-cut introduces in the profile. In contradiction to this the FEA boundary conditions do not allow the profile to localize during winding. Otherwise the comparison between weld relief, tongue and relief-cut strains in simple winding FEA and production measurement is satisfactory, and the FEA model seems valid for rough strain predictions and otherwise suitable for parametric studies. The result is satisfactory as the FEA shows the same influence of the weld relief-cut on the surrounding strains as the production measurements.

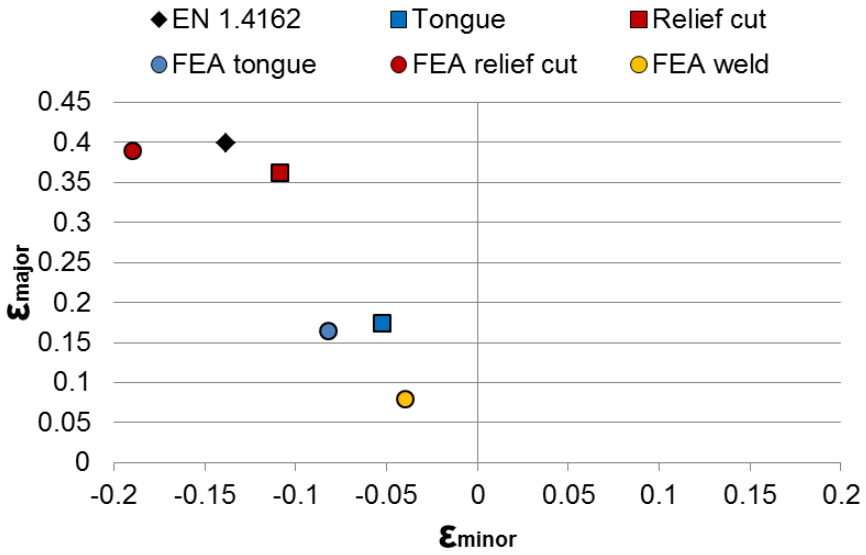

Figure 8-11: Production strain from a 6" carcass made with a 2.2mm profile (average values) compared with FEA result. The black square is the uni-axial FLC point for EN 1.4162 found in Chapter 5

An interesting result from this analysis, which should be noted, is that it is the relief-cut that is the limiting feature as regards necking and fracture during winding, since the maximum strains in the relief-cut are more than a factor two larger than the homogeneous strains in the tongue. The result of this is that the feature introduced to reduce strains in the weld zone demands more formability in the parent material than in the tongue during normal carcass winding. During the two production tests relief-cut fracture was not an issue, as also indicated by the FLDs. But the relief-cut strains are close to the limit strains, which implies that production with higher tongue strains than the investigated could cause problems with relief-cut fracture. Optimisation of relief-cuts by optimising weld zone relief whilst minimising strains in the relief-cut itself is performed later in this chapter.

Finally it is noted that FEA predictions and 4" carcass strain measurements at the weld are below $\varepsilon_{major} = 0.1$, which indicates that the relief-cut has effectively reduced the homogeneous strains below the critical strain, which in paragraph 8.1 indicated weld fracture for EN 1.4162.

8.2.3 Tongue neutral point estimate

For a theoretical estimate of tongue edge strains the position of tongue neutral point is required. This is possible to calculate from the production measurements. Figure 8-12 show the dimensions needed for tongue edge longitudinal / major strain calculations and eq. (8-1) show the method. The neutral point position on the tongue is determined by the np_{factor}.

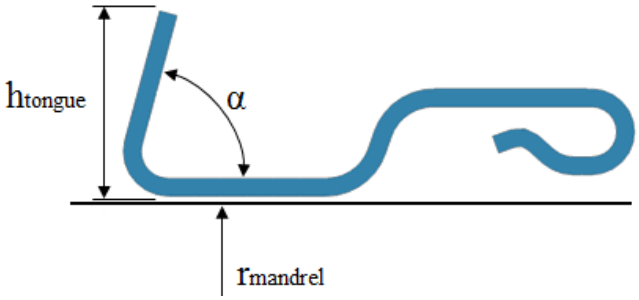

Figure 8-12: Dimensions for tongue strain calculations

$$\varepsilon_{major,tongue} = \ln\left(\frac{r_{mandrel} + h_{tongue}}{r_{mandrel} + (h_{tongue} \cdot np_{factor})}\right) \quad (8\text{-}1)$$

Based on production strain measurements the neutral point factor (np_{factor}) is calculated to 0.22 of the tongue height, see Table 8-2. This factor can be used for a quick estimate of tongue strains but it does not account for tool setup and changes in process dynamics. It can, however, be used as an indication of, when problems may arise in production regarding fracture in the weld and relief zone. Both FEA winding and bending models are in agreement with each other and shows the np_{factor} to be 0.24. This indicates that the FEA models are lacking tension in the carcass profile during bending, which is present in the production and is the likely cause for the lower FEA strain estimates.

Table 8-2: Estimate of tongue neutral point during winding based on production measurements of strain and tongue height

Carcass profile	h_{tongue} [mm]	ε_{major} [-]	$r_{mandrel}$ [mm]	h_{np} [mm]	np factor [-]
1.1mm - 4"	11.8	0.16	50.8	2.5	0.22
2.2mm - 6"	19.9	0.17	76.2	4.6	0.23
Average	-	-	-	-	0.22

Utilizing the np_{factor} of 0.22 and comparing the tongue edge major strains with the global strains at fracture for EN 1.4162, an estimate of weld fracture limits is possible by assuming standardised profile sizes and nominal mandrel sizes. Figure 8-13 shows the theoretical estimation of weld fracture for EN 1.4162. Further weld fracture investigations on more duplex materials and sheet thicknesses will allow a more general theoretical weld fracture estimate.

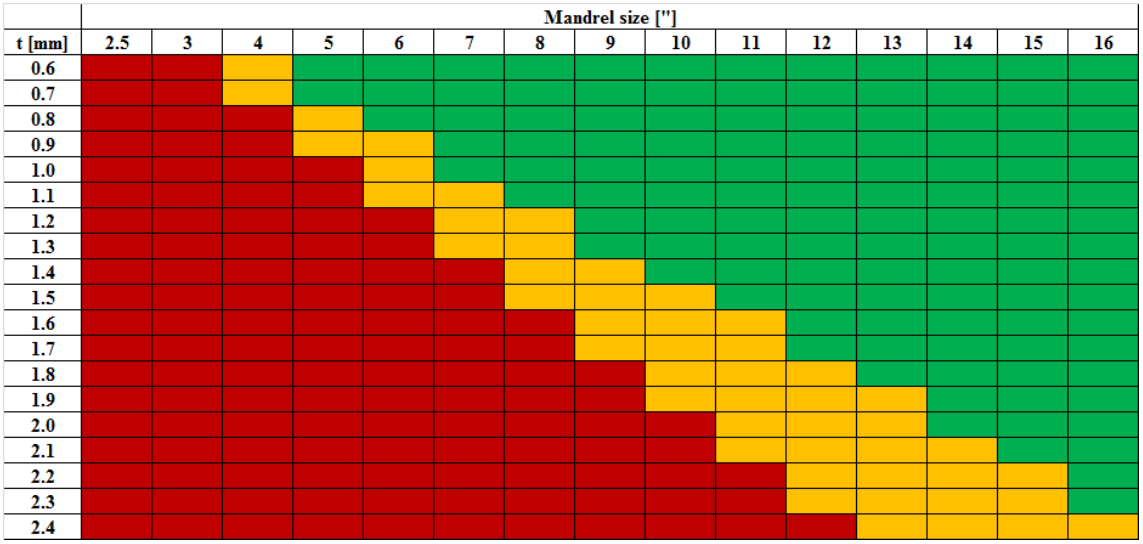

Figure 8-13: Theoretical estimation of EN 1.4162 weld fracture diagram as a function of strip thickness and bore diameter. Green indicates strain below fracture limit, yellow is in the uncertainty zone and red is likely to cause weld fracture

8.3 Weld relief-cut

Weld relief-cuts can be introduced when reduced formability of the weld zone leads to problems with fracture during winding of the carcass profile. The relief-cut works by mechanically weakening the tongue prior to the weld as the profile is being wound onto the mandrel, as illustrated in Figure 8-9. The result is a zone succeeding the relief-cut where strains are lower, the so-called relief zone, compared to the surrounding material and the weld is positioned in this zone to prevent fracture. Figure 8-14 show the parameters in a typical weld relief-cut.

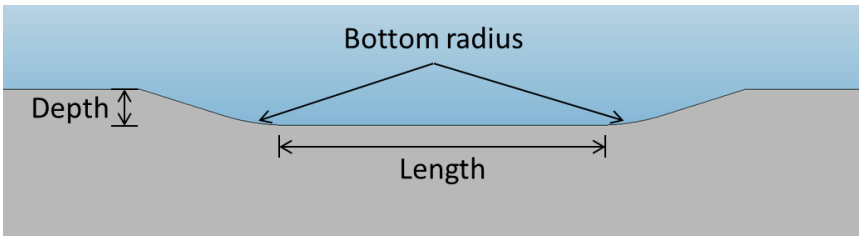

Figure 8-14: Typical weld relief-cut parameters

As indicated by Figure 8-10 and Figure 8-11 the relief-cut creates the necessary relief zone, which lowers the strains around the weld thereby preventing weld fracture, but the consequence is much higher strains in the relief-cut than in the rest of the tongue, which may cause relief-cut fracture instead, see Figure 8-15 (a). Another effect is folding or buckling at the leading relief-cut edge - Figure 8-15 (b) - which is caused by the change of the second moment of inertia across the relief-cut and contact points between tongue and QL-surface during closing of the carcass profile. Under normal winding conditions the material at the tongue is pulling itself under WT1 during closing but when the relief-cut is present closing may be in-

terrupted and later start again at the bottom of the relief-cut, since the shorter tongue of the relief cut is more resistant towards bending. This creates a fold when the WT comes into contact after passage of the relief-cut and closing of the tongue starts again. Folding is influenced by the winding strains at the tongue (folding is normally only seen in high strain productions) and the relief-cut geometry.

(a) (b)

Figure 8-15: Weld relief-cut failure. (a) Fracture at bottom corner of the relief-cut between WT1 and WT2 during winding and (b) folding at weld relief zone due to interrupted bending of the tongue

8.3.1 Relief-cut influencing parameters

One of the initial goals of the project was to investigate the relief-cuts to improve the knowledge on the strain distribution around the relief-cut in order to facilitate optimisation of the relief-cut geometry. Initially the relief-cut was positioned outside the HAZ approximately 5mm from the weld seam. This was subsequently changed due to the investigations documented in paragraph 8.3.2. From initial relief zone FEA investigations it was realised that maximum relief is found at the relief-cut edge as indicated by Figure 8-16, where the relief is shown as percent of the nominal tongue edge ε_{major} strain during FEA simple winding, 0% indicating no relief.

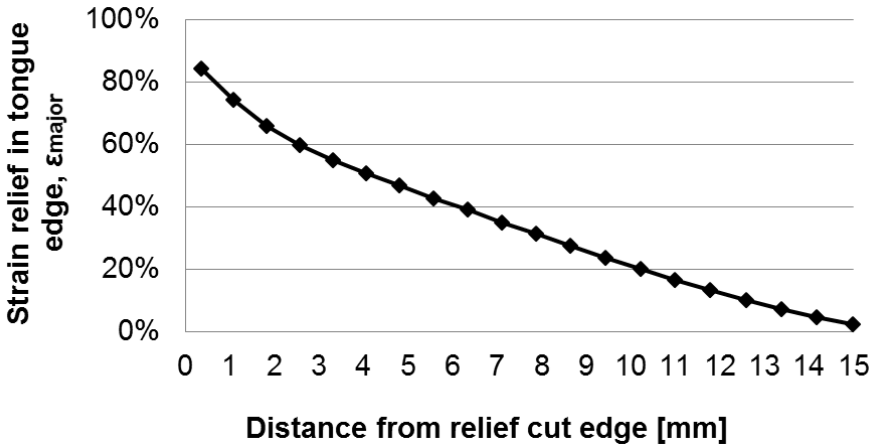

Figure 8-16: Relief effect in percentage of nominal tongue strains as a function of distance from relief-cut; '0' designates the relief-cut edge facing the weld (0% imply no relief) – result is based on a 1.0mm profile 4" carcass

FEA is used for an investigation of the relief-cut parameters shown in Figure 8-14, and design of experiments (DOE) is utilized to determine the influential parameters regarding relief zone and maximum relief-cut strains. The design is a fractional factorial with one centre point [33] – the parameters are shown in Table 8-3. The winding model is a 1.1mm profile on a 4" mandrel. The results are evaluated with regards to the tongue major strain at the weld position (5mm from the relief-cut) and maximum strain in the cut thus observing the effect of the relief-cut and the formability requirements of the relief-cut.

Table 8-3: Relief-cut parameter variation

Run Order	Depth [mm]	Bottom radius [mm]	Length [mm]
1	3	20	20
2	2.5	30	15
3	3.5	10	15
4	2.5	10	25
5	3.5	30	25

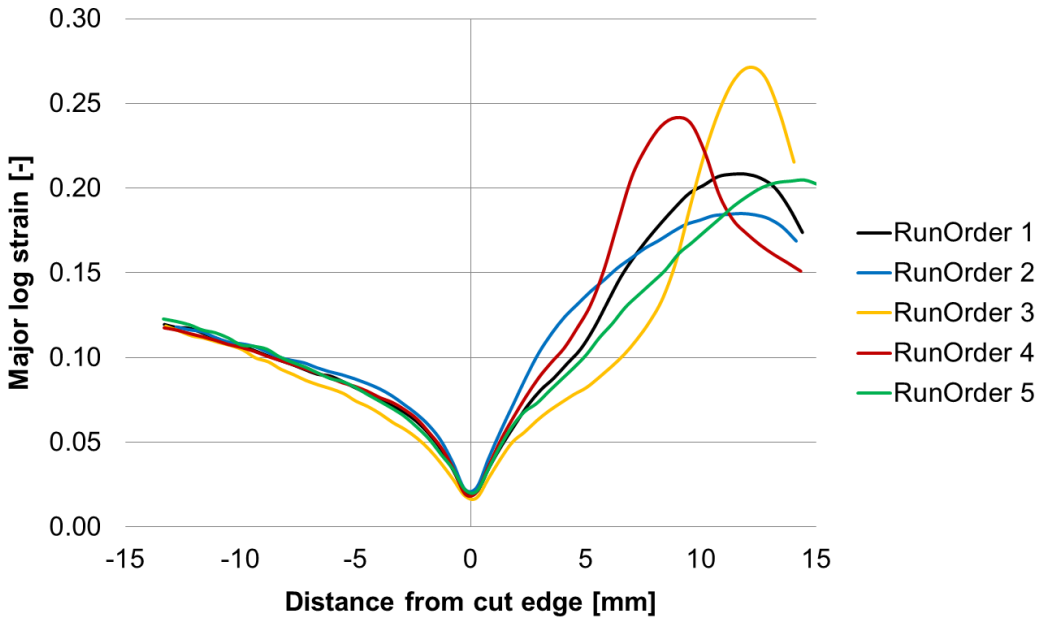

Figure 8-17: Major strain for the 5 relief-cut geometries (1.1mm profile 4" mandrel) shown as a function of distance from the relief-cut edge. Positive and negative direction is specified in Figure 8-9

Figure 8-17 shows the major strains at the tongue edge as a function of the distance from the relief-cut edge facing the weld. Negative distance is towards the weld and positive distance is into the relief-cut, see Figure 8-9 for visual clarification. The distance is the curve line distance on the tongue edge, wherefore the strain positions can be directly compared on the tongue in negative direction, whereas the position of the strain in the cuts in positive direction cannot be directly compared. This is not a problem because it is the maximum value of the

major strain in the cut that is of importance. The small difference between the results and the subsequent analysis in 8.3.2 indicate that the parameter variation is probably too small as regards the depth of cut, but it still gives an indication of the main influencing factors. The five DOE relief-cuts reveal a similar trend that the lowest strain is found exactly at the cutting edge. The strains towards the weld i.e. in negative direction vary little between the five cuts. But the maximum strains at the relief-cut changes significantly with regards to relief-cut geometry. The largest influence on weld relief is the distance to the cut. Optimum relief is locating the relief-cut at the transition between the weld and HAZ.

Plots of the main effects evaluated with the software Minitab® are found in Figure 8-18 and Figure 8-19:

- Depth of cut shows minimal effect on the relief-cut maximum strain (likely due to the small range chosen 2.5mm – 3.5mm), whereas relief is improved by deeper relief-cut
- Larger bottom radius significantly reduces the relief-cut maximum strains. This shows the effect that larger strains in the relief-cut will cause a larger relief zone towards the weld
- The length of relief-cut does not seem to affect the maximum strain in the cut, whereas it is noted that shorter length improves the weld relief. However, one must be cautious as moving the bottom radii closer together will result in strain localisation at the middle of the relief-cut, which may cause strain localisation during winding onto the mandrel as explained in paragraph 4.3.4

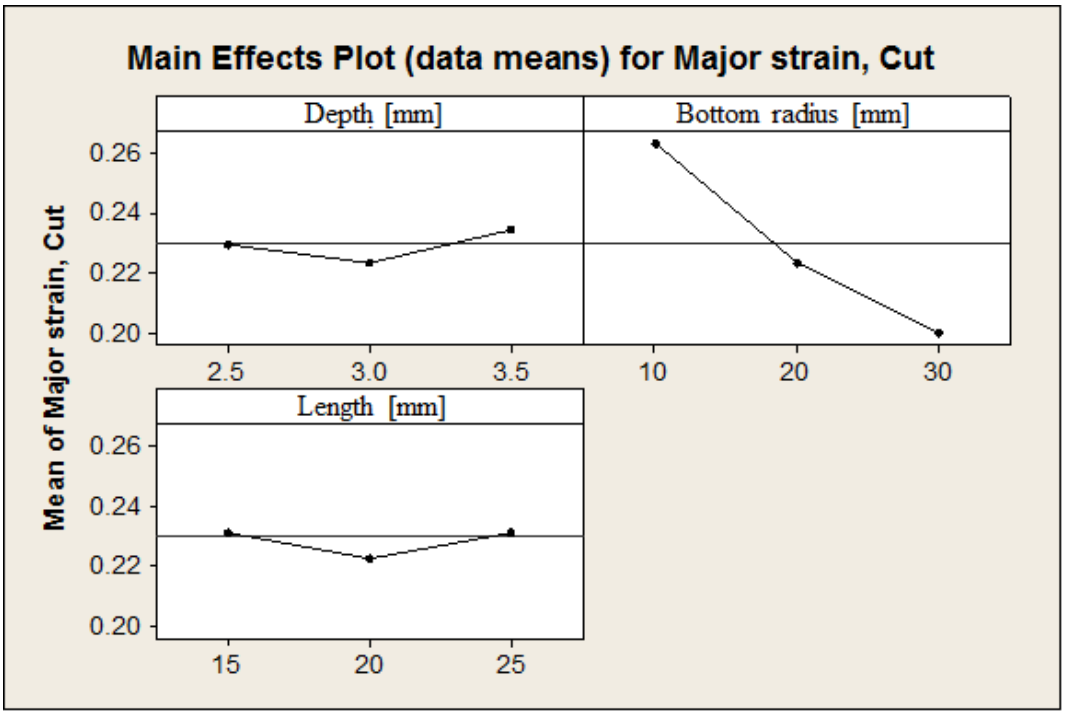

Figure 8-18: Main effects plot for major strain maximum in the relief-cut zone

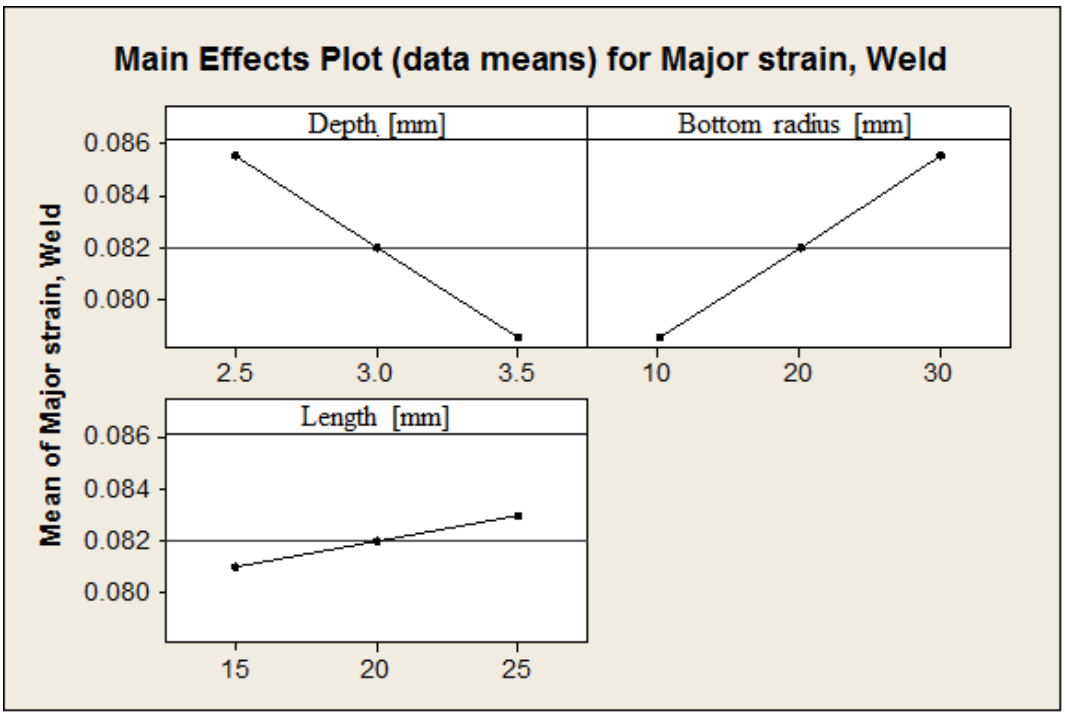

Figure 8-19: Main effects plot for major strain at the weld – 5mm from the relief-cut

8.3.2 Optimising relief-cut

Issues on relief-cut fracture in production initiated an analysis of possible optimisation of the relief-cut to lower the maximum strain whilst still ensuring sufficient weld relief. Similar to the above, simple FEA winding models with different relief-cut geometries are simulated – again using the 1.1mm 4" mandrel model. It has been empirically determined that too deep relief-cut will result in fracture in the relief-cut zone, which shows the depth to be an important factor to be investigated again, although for reduced depths compared to the above investigated.

The following geometries are investigated:

- Relief-cut depth 1 x strip thickness
  - Bottom radius 10 (1t_r10)
  - Bottom radius 30 (1t_r30)
- Relief-cut depth 2 x strip thickness
  - Bottom radius 30 (2t_r30)

The results are shown together with those of a standard weld relief-cut in Figure 8-20. As before the results indicate that moving the relief-cut close to the weld yields the best weld relief. From the selected values an optimal cut is 2t_r30, where good relief is achieved together with minimal strain impact in the relief-cut. The 1t_r10 cut is also good, as the maximum strains in the cut are lowered. This proves that the range of relief-cut depth in the former investigation was to narrow. A beneficial effect of a reduced weld relief-cut is the smaller change in second

moment of inertia over the relief-cut, which ensures that it is more resistant towards strain localization when wound onto the mandrel. The standard weld relief-cut ensures the best relief but with the highest strains in the relief-cut as a consequence.

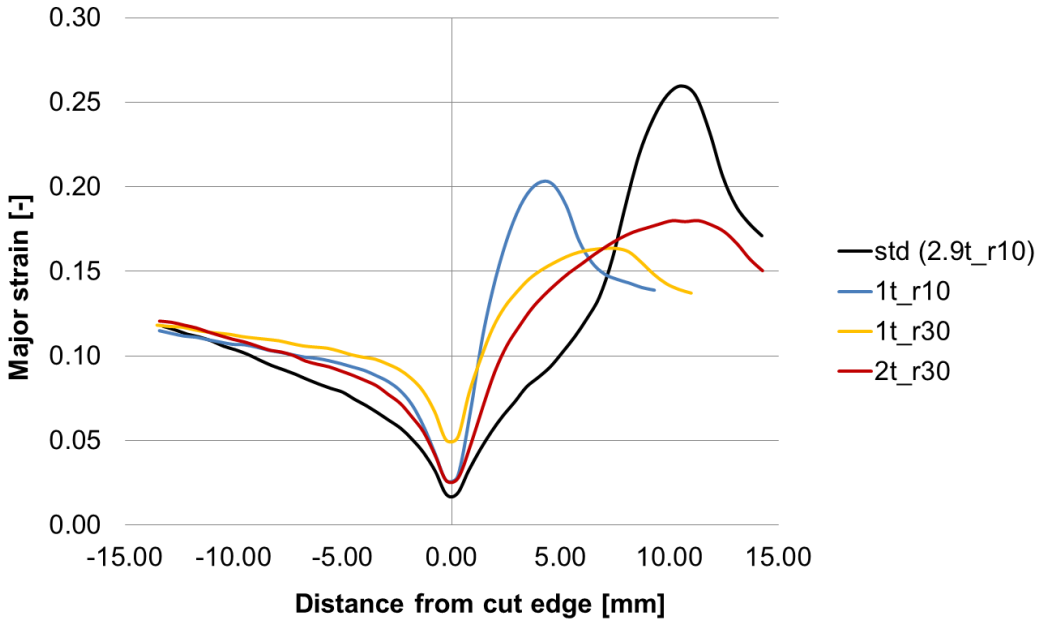

Figure 8-20: Major strain for the relief-cut depth and bottom radii variation as a function of distance from the relief-cut edge (1.1mm profile and 4" mandrel). A standard weld relief-cut is included for reference

Due to lead time on manufacture of new cutting tools the 1t_r10 relief-cut was selected, since the only change is the depth of cut and the result was positive:

- 1.7mm profile, 6" carcass: During production start-up 11 out of 20 standard weld relief-cuts fractured between WT1 and WT2 as they were being wound onto the mandrel. The standard weld relief-cut is shown in Figure 8-21. Using the above results it was decided to make the weld relief-cut 1t deep (1t_r10) and move its edge to the weld / HAZ transition zone, see Figure 8-22. Afterwards 4,900m carcass was produced without any weld or weld relief-cut fractures
- 1.4mm profile, 8" carcass: During production the standard relief-cut fractured during winding. The weld relief-cut was moved towards the weld and only cutting 1t deep (1t_r10). Afterwards 2,800m carcass was produced without any weld or weld relief-cut fractures

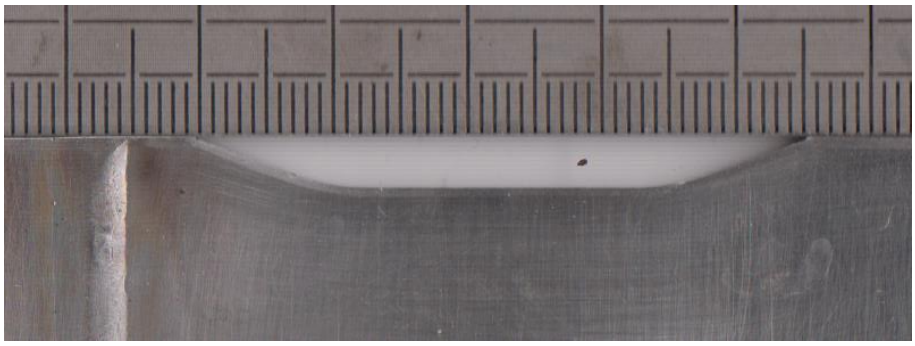

Figure 8-21: 1.7mm profile with standard weld relief-cut

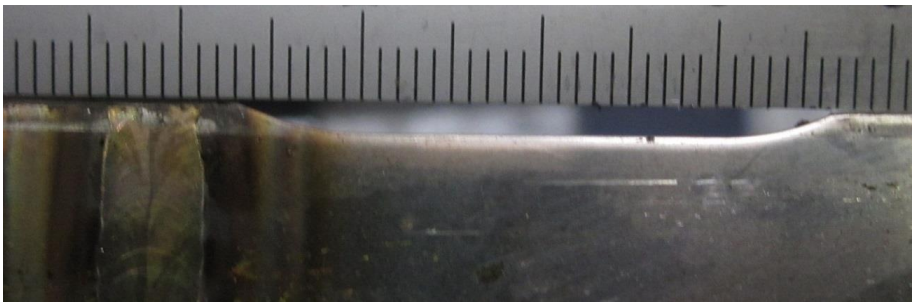

Figure 8-22: 1.7mm profile with optimised weld relief-cut

8.4 Results and discussion

One of the limiting factors in carcass production is the formability of the welds between coils, which are required to do continuous carcass production. The investigations have shown that material inhomogeneity caused by the strain localisation at the weld during tensile testing, where the strains in the non-homogenous zone increase faster than in the parent material. For EN 1.4162 homogeneous $\varepsilon_{major} \approx 0.1$ resulted in weld fracture, which is far from the duplex stainless steel forming limits thus limiting the use of the material's formability. One way to solve this problem is by introducing a weld relief zone, but the use of relief zones introduces new failure mechanisms to the carcass process. A better solution would be to improve weld formability, and the present investigations shows that improvement can be obtained by homogenising the weld according to the parent material either by mechanical hardening or heat treatment of the weld zone. The goal is to obtain weld strains similar to the homogeneous strains in the tongue during winding. Improving weld formability could also allow the use of less ductile materials with higher yield strength, which would improve carcass collapse resistance, as it was noted that normal tongue strains are far from the stainless steels forming limits.

FEA of the strain distribution at tongue and relief-cuts showed good correlation with the production strain measurements. The results showed that the simple FEA winding model is an effective tool for parametric studies of the straining in the weld relief zones. Production results and FEA data both showed that maximum strains during winding occur in the weld relief-cut and are more than a factor 2 larger than the homogeneous strains in the tongue during

winding. As a result the use of weld relief-cuts to solve weld fracture cause much higher strains in the process, sometimes on the limit of material formability thus resulting in fracture, in the relief-cut zone.

FEA investigations of the influencing parameters of the carcass weld relief-cut reveals that changing of the cut design has little effect on the relief zone next to the relief-cut, but has significant effect on the maximum strains in the cut itself. Maximum relief is achieved at the edge of the relief-cut. Locating the relief-cut edge at the boundary between the weld and HAZ provides maximum relief and ensures that the weld does not fracture. Using the presently available cutting tools, with bottom radius r10 and bottom length 20mm, an improved weld relief-cut is achieved by cutting only 1 x strip thickness deep (1t_10). However, more optimal solutions are obtainable such as cutting 2 x strip thickness with bottom radius r30.

The relief-cut modelled in this investigation was subjected to a controlled deformation onto the mandrel due to the boundary conditions in order to study the influencing parameters of the relief-cut. However, in reality the winding deformation may be less well defined in production. Even though damage due to the cutting and the HAZ are not accounted for in the modelling the strain behaviour of the FEA is still believed to give valuable results.

Finally increased carcass process formability can be obtained by changing the profile rolling process path. A reduction of tongue strains by partly closing the profile thereby decreasing the tongue height during winding. The challenge is that the profile must still be able to interlock with itself.

Chapter 9 Tribology in carcass production (swarf and scoring)

Compared to other sheet forming processes such as deep drawing and ironing, where large contact loads and surface expansion lead to severe tribological conditions, roll forming has relatively low contact loads and almost no surface expansion. Roll forming process kinematics, however, entails relative sliding between tool and workpiece in the roll gap and with long productions series, sometimes many kilometres, tool life due to wear is an important issue [51]. In carcass production the severity is slightly increased due to fewer forming steps available in the roll forming stage and also the sliding contact between stainless steel in the interlock requires a lubricant with sufficient lubricity.

Increase in tool life may be obtained through optimization of the tribo-system allowing longer production series before pick-up of workpiece material on the tool surface with subsequent scoring of workpiece surfaces, the series of mechanisms normally referred to as galling [11, 52]. Effective lubrication of stainless steel demands sufficient lubricant viscosity at the actual process temperature as well as efficient boundary lubrication. In severe stainless steel forming processes mineral oils with chlorinated paraffin additives are generally used [11, 52]. However, due to adverse effects on human health, still increasing restrictions are introduced via legislation on the use of these additives [53]. Some promising new environmentally benign lubricants have been developed that allow successful production in stainless steel [11, 54].

The tribological focus from a carcass production standpoint is on swarf, scoring/galling and tool life. Investigation and optimisation of the influencing factors for these effects is the motivation of this chapter which expands on the conference paper [55]. The performance of alternative lubricants is compared with the currently applied by combining simulative laboratory tests with production trials and FEA for determination of contact stress distribution evaluation.

9.1 Carcass tribo-system evaluation

The analysis phase of the investigation is carried out to understand the failure modes by reason of tribo-system failure and performance of the existing system. The solution to the latter is performing comparative studies in a simulative tribo-test to understand how tool, workpiece and lubricant are performing as a system. The investigations are based on the carcass production tribo-system: stainless steel (austenitic and duplex), Cr-Mo-V powder metallurgical (PM) high-speed tool steel and biodegradable, cold pressed, rapeseed oil that has boundary lubricating properties [56].

9.1.1 Simulative tribo-test

Simulative tribo-testing is performed in order to evaluate carcass tribo-system performance and understand the process conditions. Lubricant performance is assessed with the Strip-Reduction-Test (SRT) that has proven reliable for testing and ranking tribo-systems [57, 58, 59]. The SRT is a severe tribo-test that simulates the conditions in ironing, i.e. high surface pressure and surface expansion, by drawing a metal strip under a fixed circular cylindrical tool thus reducing the strip thickness. The equipment is illustrated in Figure 9-1. Test evaluation is done by determining the critical sliding length, defined as the point where galling initiates, resulting in scoring of the workpiece surface. The equipment applied allows for a maximum sliding length of 300mm [58, 59]. The goal is to compare the applied rapeseed oil with two other lubricants as well as investigating workpiece effects as a result of yield strength and surface condition. The assumption for using the test is that a tribo-system that performs well under the severe conditions in the SRT will also perform well in less severe carcass production conditions. But factors such as interface temperatures are certainly important in the SRT but not in carcass production, due to lower contact forces and rotating tools.

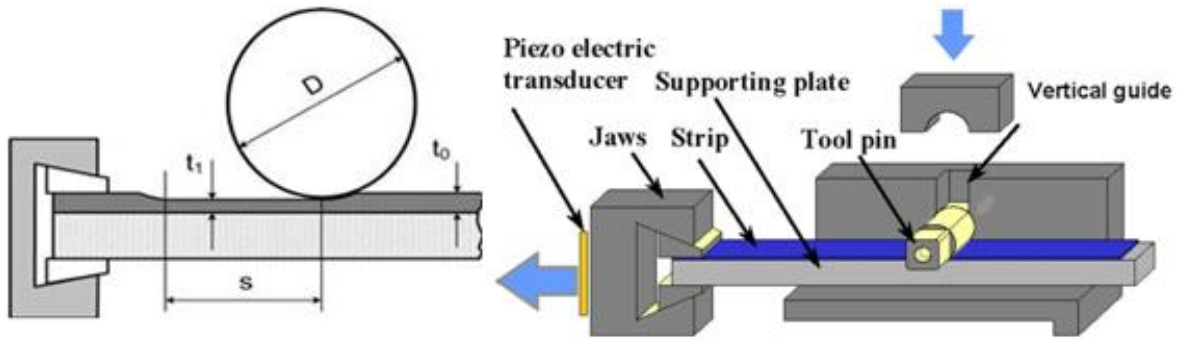

Figure 9-1: Schematic outline of the strip reduction test [57]

Table 9-1: Lubricants tested in the strip reduction test

Lubricant	Viscosity @ 40 ºC [cSt.]	Description
A	44.9	Cold pressed rapeseed oil without additives
B	150	Mineral oil with EP-additives
C	-	Thin polymer film (60 % water)

The lubricants included in the test are described in Table 9-1. The three lubricants are all environmentally benign containing no chlorines. A is the rapeseed oil applied presently, B is a mineral oil with ExtremePressure (EP) -additives that have shown to be a good alternative to chlorinated paraffin oils in severe deep drawing [11] and C is a water based thin polymer film lubricant.

The tool and workpiece materials are listed in Table 9-2. The SRT tools were polished to an average roughness value known to provide good testing conditions [11]. Two lean duplex

stainless steel grades were included with two different surface conditions to test the effect of this. The roughness values are acquired with a Taylor Hobson Surtronic 25 surface finish measurement system and treated with the software Sursam 7.4. Plane glass measurements identify the smallest measurable roughness values (Ra = 0.006, Rz = 0.105). Furthermore calibration measurements are performed with a certified roughness standard for calibration of the measured values of tools and strips. Every roughness value is an average of at least 5 measurements on the same surface.

Table 9-2: Description of strip reduction test workpiece and tool materials

Steel grade	Surface condition	Description
EN 1.4162	EN 2E, brushed: Ra = 0.219µm, Rz = 1.954µm	Lean duplex stainless steel, 1.0mm
UNS S82011	EN 2B, bright annealed: Ra = 0.169µm, Rz = 1.102µm	Lean duplex stainless steel, 1.0mm
EN 1.4401	EN 2B	Austenitic stainless steel, 0.7mm
Cr-Mo-V PM tool steel	Polished: Ra = 0.033µm, Rz = 0.25µm	Hardened to 63HRC. Composition [wt%]: C2.1, Si1.0, Mn0.4, Cr6.8, Mo1.5, V5.4

9.1.2 Strip reduction test results

The results of the lubricant test is shown in Figure 9-2 (a); indicating that the thin polymer film lubricant is not a viable alternative to the rapeseed oil, since galling was initiated immediately. The rapeseed oil had a mean critical sliding length of 23mm, whereas the mineral oil with EP-additives performed best with a mean critical sliding length of 90mm. The result indicates that a mineral oil with EP-additives may improve galling resistance but performance of the rapeseed oil is not bad considering that it is a pure vegetable oil without any additives. In carcass production lubricant removal is not an option and heating of the carcass in the subsequent polymer extrusion process heats up the lubricant together with its additives significantly, which may cause problems to the operator in production. Also since the SRT is a quite severe tribo-test it does seem that the vegetable oil performance is acceptable in carcass production, wherefore significant improvements may not be achieved through the change of lubricant.

The result of rapeseed oil performance on the two different workpiece materials is shown in Figure 9-2 (b) - critical sliding length is 105mm for EN 1.4401 compared to 23mm for EN 1.4162. The difference in lubricant performance is significant but the poor performance of EN 1.4162 in the test is mostly caused by higher yield strength of the material leading to higher interface temperatures in the test causing the lubricant to break due to lower lubricant film thickness [11]. But in actual carcass production the performance difference is not expected to be large, due to the fact that interface temperatures are not critical in carcass production. However, difference in the surface quality could have an influence on lubricant entrapment,

also during roll forming, and as a result the surface quality was investigated for two different surface qualities for lean duplex stainless steels.

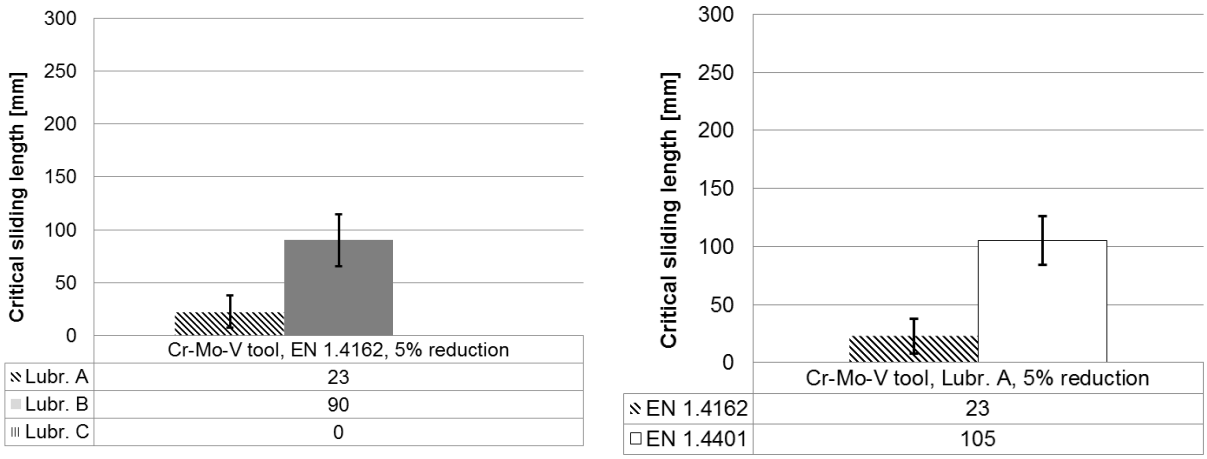

(a) (b)

Figure 9-2: SRT screening results at 5% reduction showing mean critical sliding length and standard deviations for (a) lubricant test on EN 1.4162 and (b) a comparison between EN 1.4401 and EN 1.4162

9.1.3 Strip surface quality

The effects of lay caused by brushing of the sheet on lubrication in SRT have been reported in [60] where a lay perpendicular to the sliding direction improve tribo-system performance because of better lubricant retainment in tool / workpiece interface. In carcass production several types of stainless steels are used implying the use of different surface qualities, which can have an effect on the tribo-system performance. For that reason two lean duplex stainless steels with similar mechanical strength but different surface quality were tested in the SRT. Table 9-2 describes the two materials. Reduction was 5% as before and lubricant B was used for the test.

Figure 9-3 shows the results in SRT by way of sliding load with four repetitions for each material. The 2E surface is able to retain sufficient lubrication enabling 120mm sliding length before galling cause an increase in the sliding load. It is clear that the 2B surface is not able to retain sufficient lubricant during pressure build-up at the initial reduction of the strip before sliding and as a result galling starts immediately, which is seen by the increase in sliding load from the beginning of the test. Because the two materials exhibits the same mechanical properties, i.e. yield strength and strain hardening exponent, the difference in the test results seems to be contributed from the surface quality, where the 2E brushed surface seems better at retaining lubricant during pressure build-up.

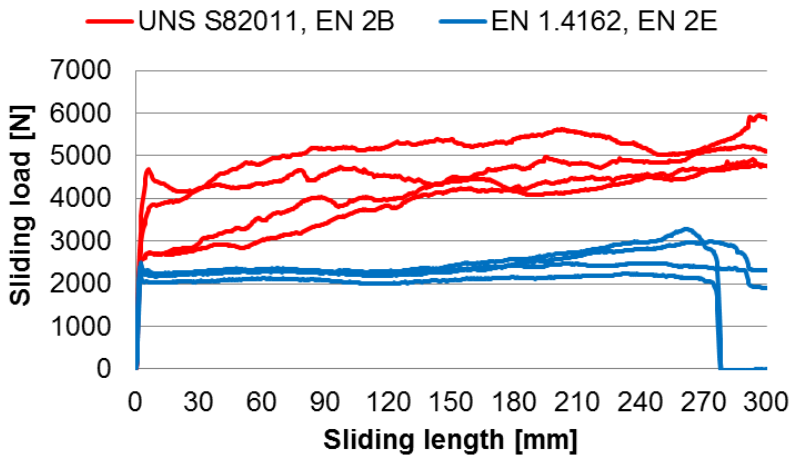

Figure 9-3: Loads during SRT of two lean duplex surfaces. Each surface quality has four repetitions 5% reduction tested with lubricant B

3D surface measurements were done on both strip surfaces, which explains the SRT results as seen in Figure 9-4. Because the 2E surface is brushed along the sliding direction it was initially assumed that this would allow lubricant to escape during the test but the 3D measurements show a different story. It is actually the bright annealed 2B surface that has the directional lay of the surface thus allowing the lubricant to escape during pressure build-up and the result is immediate galling. The carcass process is not as severe but in the roll forming stage production direction, like in the SRT, is along the length of the surface lay and it seems likely that the tribo-system with a 2B surface also would perform worse than a 2E surface resulting in earlier onset of pickup and galling.

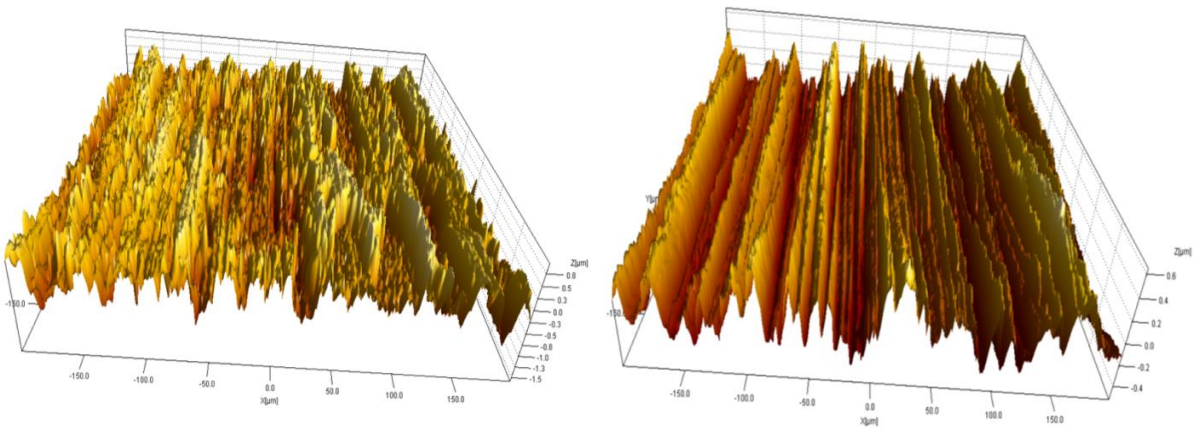

(a) (b)

Figure 9-4: 3D surface measurements; (a) 2E surface and (b) 2B surface. The directional 2B surface seems to be unable to retain sufficient lubrication during pressure build-up thus allowing the lubricant to escape

9.2 Production study

The attention in the production study is to identify the tribological problems that may be present in carcass production and typical matters such as tool wear, swarf and scoring are investigated. But also conditions in the interlock, where strip surface quality might be an issue, as described in paragraph 4.2.4.

9.2.1 Tool roughness measurements

Roughness measurements on critical tool features and surfaces are difficult with skid contact as well as no-contact profilometry due to surface curvature and length. Evaluation of tool roughness is therefore performed using replicas of the surface and performing optical roughness measurements with a 3D optical measurement device, InfiniteFocus from Alicona Imaging. Replicas are made with RepliSet-GF1 from Struers A/S. Figure 9-5 show a couple of replicas of a polished RF tool used for optical roughness measurements. Investigations into surface characterisation using replica technology have shown that this technique has a replication degree of 95-96%, thus being a useful technique for measuring difficult specimens [61]. A replica was made of a roughness calibration artefact and measured in the Alicona InfiniteFocus; the results are compared to the roughness artefact certificate values in Figure 9-6, where good correlation between replica and certificate values is obtained.

Some tool surfaces, generally non-forming surfaces, allow tactile roughness measurements. A Taylor Hobson Surtronic 25 roughness measurement device was utilised for stylus roughness measurements. Data analysis is performed with the software Sursam 7.4. Measurements on plane glass ensure data for background noise, and the device was calibrated using a certified roughness standard.

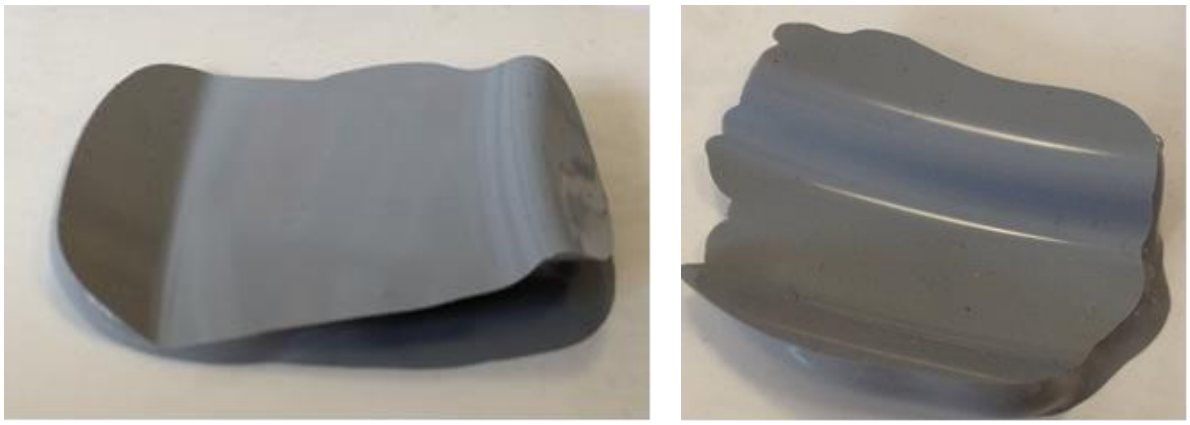

(a) (b)

Figure 9-5: Replica of RF tool surfaces; (a) surface in contact with tongue and (b) s-bend surface where pickup usually form

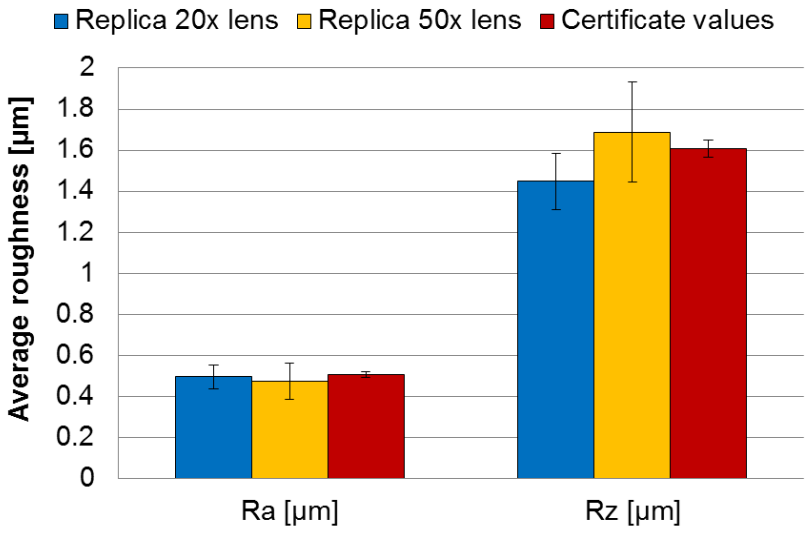

Figure 9-6: Roughness measurement of a replica calibration artefact made in Alicona InfitineFocus at 20x and 50x magnification. Certificate values for the original artefact is included

9.2.2 Pickup development

Pickup is cold welding of workpiece material to the tools due to insufficient tribo-system performance and in carcass production pickup usually is located at curvatures / bends such as depicted in Figure 9-7 (a). Close-up on pickup in a stereo microscope can sometimes give the impression that the tool surface is damaged as there is no colour difference between the two materials under the microscope as seen in Figure 9-7 (b).

Table 9-3: Tool surface conditions in the production test

Tool set	Tool steel	Surface condition	Description
TA	Cr-Mo-V PM steel	Turned: Ra = 0.20µm Rz = 1.15µm	Hardened to 63HRC
TB	Cr-Mo-V PM steel	Polished: Ra = 0.04µm Rz = 0.18µm	Hardened to 63HRC

Two tool surface conditions are tested with the purpose of determining tribo-system performance and the rate at which pickup will form on the tools. A four step roll forming tool set was selected due to the severity in forming between each step. Table 9-3 show some details for the two tool set designated TA and TB. Tool set TA has an acceptable surface; turned and slightly abraded with grit 1,500 abrasive paper. Tool set TB has a finer surface; turned, abraded, and polished with diamond paste.

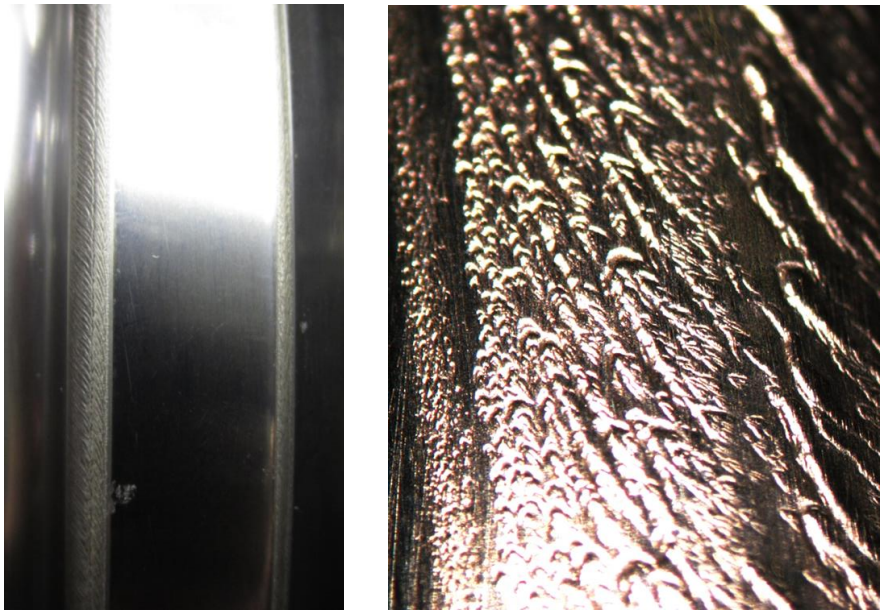

(a) (b)

Figure 9-7: (a) Pickup on roll forming tool where the s-section and tongue is bent and (b) close up on pickup in a stereo microscope - which sometimes look like tool damage because the stainless steel look like the tool material

Tool set TA showed slight pick-up on bending curvatures of the tools after a few km's production, but there were no significant scoring of the strip / profile. At 77km profile production pick-up was clearly noted on bending curvatures, but no further increase in pick-up was seen after 198km production, Figure 9-8 (a). Extended chipping of tool material in the critical zone that forms the lip was observed after 198km indicating fatigue of the tool surface, Figure 9-8 (b).

The fine polished surface of tool set TB does not significantly improve tribo-system performance as pick-up does form and evolves similarly to TA. And again once the pick-up had reached a certain level no further development appeared. After 250km strip had passed through tool set TB a single chip had come off in the critical zone that forms the lip, thus fine polishing seems to have improved chipping resistance as only one chip appeared, Figure 9-8 (c), which corresponds to literature [62]. In fact the chip looks different as it is much deeper and could indicate a problem with the tool material at this specific location.

An interesting observation is the maintained constant amount of pick-up, which forms on bending curvatures, without any severe scoring of the workpiece. In severe metal forming processes pick-up normally continues to develop after initialization, leading to severe galling [11]. In carcass production it is likely that an equilibrium state is reached, where pick-up is repeatedly formed on and removed from the tool surface. The pickup is easily removed by slight abrasion with emery paper; another indication that the pickup is not severe. It could; however, affect tool life through increased wear.

Besides the aforementioned pickup on bending curvatures, non-critical tool surfaces exhibit signs of improvement from abrasion against the strip surface, indicating that tool polishing is only required on specific critical curvatures / surfaces.

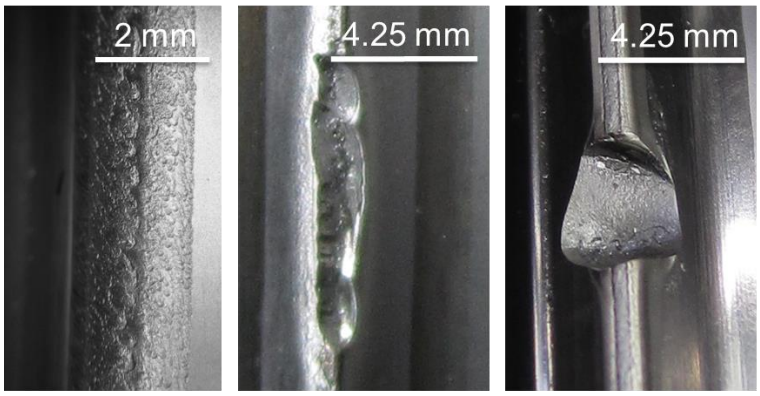

(a) (b) (c)

Figure 9-8: (a) Pick-up on bending curvature. Tool chipping from TA (b) and TB (c)

9.2.3 Tool wear

The above indication, that pickup does not develop past a certain amount, raises the question, whether or not pickup is in fact constant or if there is some sort of wear on the tools caused by constant pickup formation and removal – visually seen as a constant amount of pickup. Selected tools with pickup that had been extensively applied in production were investigated by pickup removal with emery paper and then inspected under a stereo microscope.

The tools exhibited signs of damage under the pickup and it seemed like material was pulled out of the surface suggesting adhesive wear, see Figure 9-9. It does not seem likely that this damage is caused by the emery paper due to the direction and size of the damage. A reasonable explanation is that pickup is continuously formed and removed on the tribological critical tool features resulting in adhesive tool wear.

Tool chipping as seen from the test with tool sets TA and TB is certainly influenced by the adhesive wear caused by pickup and the cyclic load, which roll formed tools experiences. On both tool sets the same tool feature was fractured by chipping, a low cycle fatigue mechanism also indicated by the number of tool revolutions or cycles for each tool set; TA ~470,000 and TB ~600,000. Figure 9-10 illustrates estimated contact stresses by 2D FEA with LS-DYNA®; (a) initial contact and (b) contact at roll gap centre. Maximum von Mises stresses are obtained at the roll gap centre ~1,000 [MPa], which is about 37.8 % of the tools compressive strength. These stress values and number of cycles does not give reason to suspect serious danger of fatigue. However, small contact area and stress development in each cycle, where a single contact evolves into two, could cause alternating sub-surface shear stresses leading to crack formation and growth [63]. The pick-up formation causing friction increase, which is not accounted for, may furthermore affect tool fatigue life through wear and stress concentration as well as the adhesive wear on the tool.

(a)

(b)

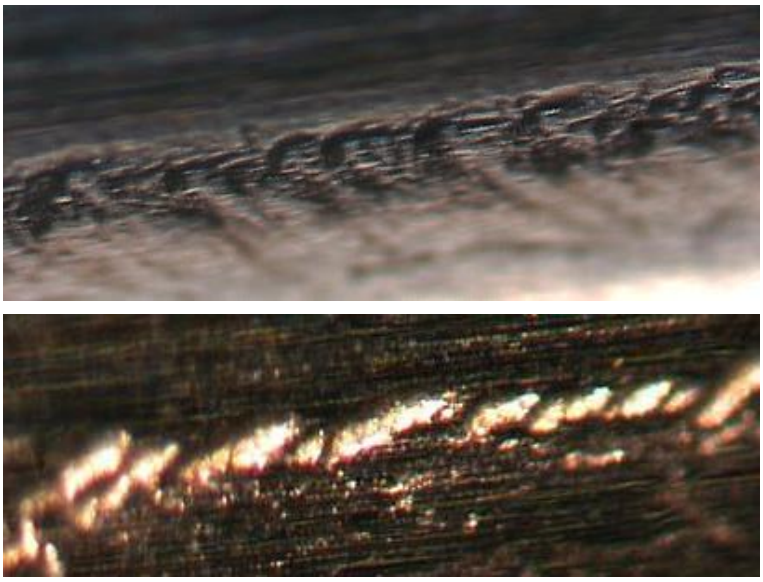

Figure 9-9: Pickup removed on tool surfaces showing damage by material torn from the tool; (a) at s-bend and (b) at QT-bend

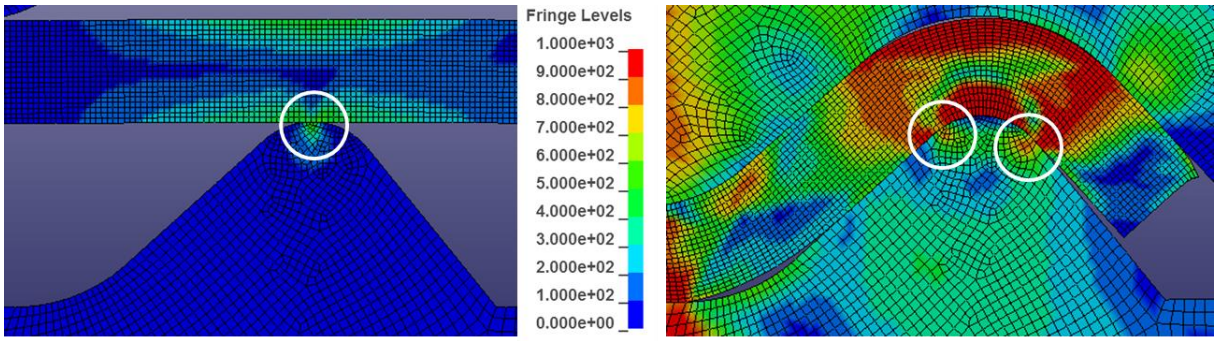

(a) (b)

Figure 9-10: Fringe plot of von Mises stresses [MPa] in lip-forming feature in the production study. Initial contact (a) and (b) contact at roll gap centre. The white circles mark contact stress concentration with workpiece

9.2.4 Interlock issues

Friction between the tongue edge and the lip and the respective surfaces in contact during interlocking is a determining factor in obtaining a smooth interlocking, without gunshots and tongue buckling. Paragraph 4.2.4 mentions oxide residues on the strip surface to cause problems in the interlocking due to increased friction in the stainless steel to stainless steel contact. A similar situation was encountered during testing of the lean duplex 2B and 2E surfaces (Table 9-2) where the 2E surface performed without any problems but when the 2B surface was introduced, in the same machine setup, gunshots were noticed representing a friction increase. Because the initial interlock contact is between tongue edge, lip edge and QT-surface and QL-surface respectively, see Figure 3-6, it does not seem likely that the effect is lack of lubricant entrapment as the case was in the SRT investigation but rather mechanical locking due to the directional 2B surface. Figure 9-4 (b) shows the directional surface topography, where the tongue needs to traverse across the peaks and valleys thus possibly mechani-

cally locking the tongue and thereby causing an increase in static friction, which is released each time the gunshot is heard.

This difference in performance between the two lean duplex surfaces was not further explored due to lack of time, but it is certainly an interesting subject for further investigation.

9.3 Swarf and scoring

Swarf and scoring is often the result of tribological problems in carcass production and the different failure mechanisms are already mentioned in Chapter 4. This paragraph attempts at describing the different situations encountered for swarf and scoring to occur and how to solve the problems.

9.3.1 Swarf and scoring due to galling

Even though pickup normally does not develop beyond a critical level, some tool edges or tools sets do have unfortunate conditions that cause enough pickup to form resulting in scoring of the strip surface and causing galling swarf. The problem is the relative sliding between tool and workpiece from roll gap entry to roll gap centre, wherefore it is a problem located at the tongue- or lip-sections of the profile. When pickup forms on the tools it acts like an abrading surface scoring the profile and creating the so-called galling swarf. Figure 9-11 shows an example of scoring of the tongue, which can generate the galling swarf.

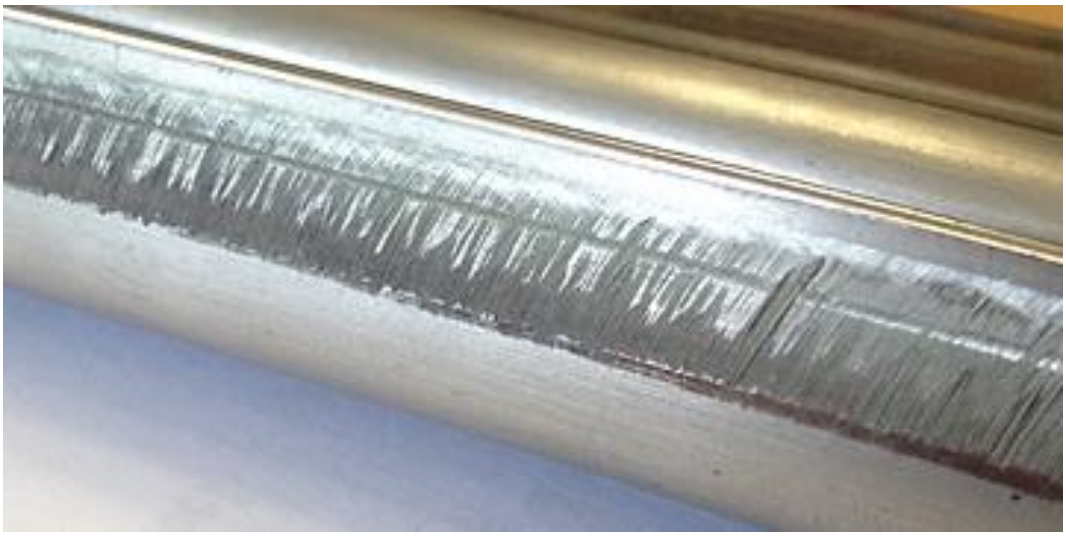

Figure 9-11: Scoring of the tongue from pickup on a forming curvature and the relative sliding motion between tool and workpiece through the roll gap

Successful solution to this problem is to improve tribo-system performance such that tool pickup is impeded and such an attempt is done with a tool coating - described later in this chapter.

9.3.2 Swarf due to strip-edge contact

Figure 9-12 show the typical length of edge swarf generated in the roll forming stage. In many cases the problem occurs because of incorrect tool designs that allow undesired tool contact with the strip/profile edge. In severe cases this contact can create a burr on the strip edge whilst generating swarf as the following case study reports.

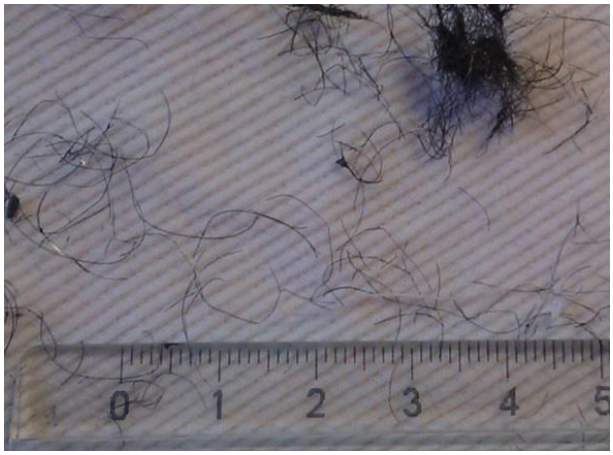

Figure 9-12: Edge swarf generated in the roll forming stage from tool contact

In a test tool set for a 1.1mm carcass profile swarf was noted in the roll forming stage, see Figure 9-13. Swarf originated from the lip edge, which was in contact with the tool when entering the roll gap. A strong indication hereof is a burr that was introduced on the lip-edge, which was not present on roll gap entry. Swarf was also found in the preceding RF step 2, but its origin was not immediately clear due to lack of tool and strip edge contact and no signs of excessive galling. However, judged by the location and the size of swarf, it is likely that it is accumulated edge swarf generated in RF step 3. The trail of swarf towards RF step 2 from step 3 is also a strong indication that the swarf found in step 2 originates from step 3, which due to rotation of the roll forming line during production ends up in step 2. The cause of edge swarf was severe tool and strip edge contact, where the profile enters the roll gap of RF step 3. A small edge radius on the tool generated swarf on contact with the lip-edge and a sharp burr on the profile, which could become a problem during winding.

Figure 9-13: Edge swarf in roll forming caused by high normal pressure between tool curvature and workpiece

The problem was solved by increasing tool step 3 radius in contact from R2.0mm to R5.0mm. Figure 9-14 shows the change of tool radius, which decreased the contact load and allowed a more smooth entry of the profile into the roll gap. With this modification the burr, which was created at the lip-edge, was significantly reduced and, since then no sign of edge swarf generation in the roll forming line has occurred.

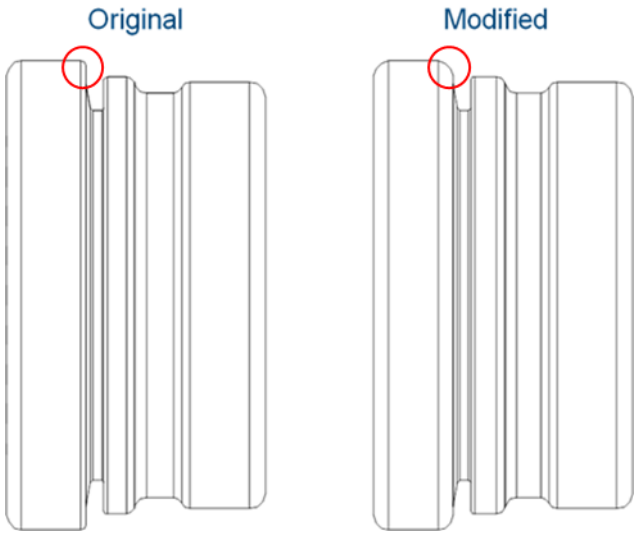

Figure 9-14: Roll forming tool modification of tool radius due to edge swarf

9.4 Tribo-system optimisation

From the above investigations improvement of the tribo-system performance which impedes pickup on the tools, is beneficial in relation to: galling swarf, scoring and adhesive wear on the tools. The focus is on improving tool performance since although introduction of a more potent lubricant might solve the tribological issues, it would be more costly, as rapeseed oil is quite inexpensive, and it could have adverse environmental side-effects in the following extrusion process were the carcass is heated causing lubricant fumes.

Fine polished tools did not improve tribo-system performance satisfactorily thus either using anti-seizure tool steels such as Vancron® 40 [64] or applying a coating are possibilities. In ironing investigations it was found that Vancron® 40 was better than traditional PM tool steels, but the use of coatings with low friction were considerably better at impeding pickup on forming tools [11]. An AlCrN coating was selected for production trials; tool surface preparation was done at the coating company by polishing the turned surface, coating and final polishing of the coating.

Figure 9-15 shows the coated tools (1.1mm profile) indicated by the grey tint. The tools were mounted for several production runs in succession. The calculated amount of strip that has passed through the tools were 678km.This result is very promising as the tools did not show any signs of pickup and no significant signs of tool wear or damage – a clear improvement to the earlier results without coating, see Figure 9-16 (a). The exception is the contact points

with the strip edges, where the edge burr damages the coating, but this is not important to the process and can be allowed, see Figure 9-16 (b). The matter can be resolved by avoiding strip edge contact by tool design or improving the edge quality. Absence of tool chipping does point towards adhesive wear of the tool during pickup / pickup removal being a significant factor in tool chipping.

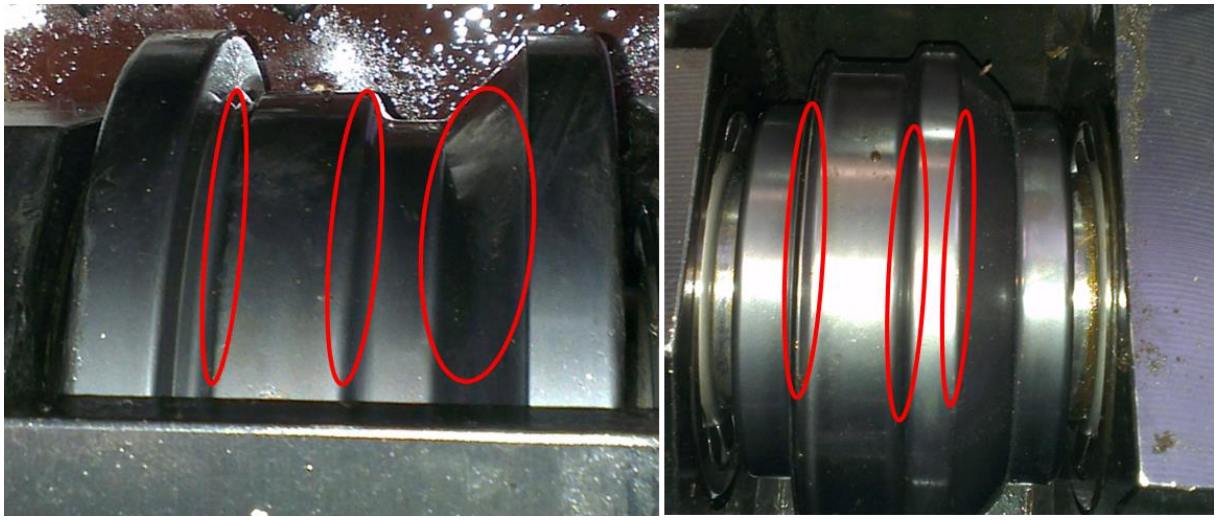

Figure 9-15: Roll forming tools coated with AlCrN where the red circles indicate critical curvatures or surfaces that are monitored for pickup and wear

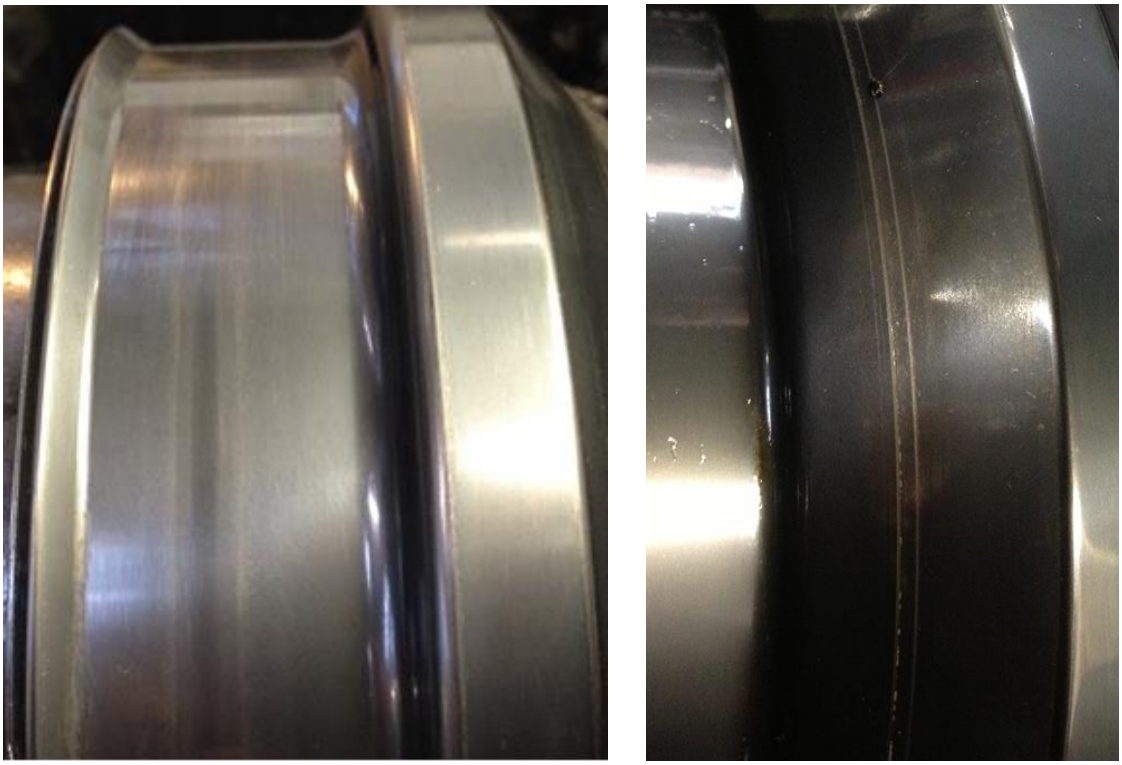

(a) (b)

Figure 9-16: Coated 1.1mm RF tools after 678km strip has passed through; (a) lip- and s-bend tool features normally showing pickup and (b) damage of coating due to wear from strip edge burr

9.5 Results and discussion

The investigation of the carcass tribo-system has revealed some interesting results. Among those the galling tendency in the roll forming stage that develops until a certain amount after which it stabilises. Tribological conditions are found to be challenging in the carcass production, most likely due to the limited space that restricts deformation to be performed in fewer steps than is recommended for normal roll forming processes. Furthermore small contact areas lead to critical loads thus increasing demands to lubricant performance. High flow stress and inappropriate surface lay of the workpiece material may also increase lubrication demands. All these factors influence the tribo-conditions in carcass production and reduce the efficiency of the lubricant.

Proper tool design can solve most problems with edge swarf by minimizing strip-edge and tool interaction during production. But it still demands proper strip de-burring to minimize edge swarf issues in carcass production.

Fracture by chipping off local areas of the critical bending zone was identified as a tool failure mode in production. Tool polishing seemingly improved fracture resistance but only by application of tool coating chipping was prevented, which indicates that adhesive wear is a main contributing factor to tool chipping in carcass production.

Fine polished tool surfaces did not ensure proper lubrication with rapeseed oil, but the use of an AlCrN coating for the roll forming tools significantly improved pickup resistance and tool life. Longer tool life may be possible as a worn coating can be refurbished if the substrate material is not damaged.

Chapter 10 Conclusion

The subject of this PhD-project has been the carcass production process for flexible pipe systems with focus on generating fundamental knowledge about the combined process of roll forming and winding of stainless steel profiles with the objective to ensure improved production. The focus has been on the carcass process winding stage, as this is the most challenging stage of carcass production. The topics investigated in this work were as follows.

10.1 Failure modes and mechanisms

An extensive production study was performed by following closely the production during quality issues and process failures, the so-called 'Gemba' methodology. Most failures regarding process and design deviation occur during the winding stage where tongue fracture, interlock failure, localised bending as well as other geometric deviations and scoring of the carcass profile are issues. Most of the failure mechanisms are caused by errors in tool setup and erroneous tool design but also issues regarding tribo-system performance and material / weld formability are a concern.

An investigation into geometry change during winding by measurement of the profile dividing point movement was seen to depend on maximum profile stresses and strains at the profile outer sections during winding. Smaller mandrel size with the same carcass profile resulted in increased dividing point movement. The cause of the free-form bending in winding is due to the interlocking between two profiles, in which the profiles are the forming tools. The condition allow the profiles certain degrees of freedom thus enabling them to minimise stresses and strains during winding by adjusting the profile geometry. The mechanism is that the profile outer parts are moved closer to the neutral plane thus minimising the deformation energy resulting in dividing point movement where QL is increased and QT is decreased causing profile 'a-symmetry'. By trial and error this dividing point movement was successfully accounted for by changing the profile geometry in the roll forming stage, which demonstrates that tool designers must account for the process dynamics from the final profile and backwards through the process to the roll forming stage.

10.2 Finite element analysis

A combined roll forming and helical winding model including interlock deformation was not pursued due to experience from initial process investigations, where the complexity of the carcass winding process was deemed to be too sensitive to be properly simulated with FEA. Instead roll forming, simple winding models and a three-point-bend model were simu-

lated with the general purpose software LS-DYNA®. Initial studies included a convergence study, where parameters for numerical stability were determined:

- Mass scaling = 50x initial critical time step
- Mesh size: Transverse = 0.003mm * strip width [mm]; Longitudinal = 0.25mm * mandrel diameter [“]
- Gauss integration points = 7

The behaviour and simplicity of the simple winding models showed strain values and distribution similar to production measurements, and they were successfully used in evaluation of weld relief-cut functionality.

For the three-point-bend model the strains were higher than those in the actual simulative test even with similar boundary conditions of the two. The problem is that the FEA does not show closing and curving of the tongue during bending on the mandrel as it is observed during the simulative test. Thus the behaviour of the shell elements did not respond to reality, where the tongue is free to move without boundary conditions. However, this was not further pursued in the present investigation, since comparisons with the production test require boundary conditions holding the tongue in an upright open position.

10.3 Simulative testing

A simulative three-point-bend test emulating the conditions during carcass winding was constructed and used for testing welds and relief zones. The simulative test showed promising results as regards to weld investigations but the lack of proper tongue boundary conditions during bending made it difficult to attain strain levels similar to those in production.

For a faster evaluation of tongue strains during winding simple v-bent profiles were compared to roll formed profiles. It was found that a simple profile with two bends is sufficient to attain deformation and strains comparable to the roll formed profiles, although there was a deviation between the roll formed and simple profiles as regards the strains across the welds. The simulative test strains across the weld was higher for the roll formed profiles than the simple ones. This is likely due to an effect from the roll forming stage, where longitudinal stretching might have influenced the weld zone. This effect is not included in simple bent profiles.

10.4 Formability and forming limits

Flow curves were obtained for the austenitic and the three duplex grade stainless steels; EN 1.4404, EN 1.4162, EN 1.4462 and EN1.4410. Full left-hand-side forming limit curves were attempted for all four materials by tensile testing of notched specimens, but problems with the samples gave limit strains measurements much lower than expected – likely due to the dimensions of the material in the notch. As a result only the uni-axial tension points were reliable. This is, however, acceptable for use in carcass process formability analysis,

since the necking and fracture in the profile tongue during winding occurs after uni-axial loading.

Weld fracture in duplex stainless steels is a problem in carcass production and strain measurements across welded EN 1.4162 lean duplex stainless steel during tensile testing showed that strain increases faster in the weld zone than the homogeneous strains in the parent material. Fracture in the weld zone occurs at an average homogeneous strain of 0.1, whereas the average fracture strain in the weld zone is 0.27. Furthermore, fracture was found to occur at the transition from weld seam to HAZ. Hardness tests and thickness measurements across welds indicated lower material hardness in the weld and the HAZ, and since the weld seam is thicker than the HAZ the fracture appears in the transition zone.

Weld relief zones can be introduced, when weld fracture is a concern, but production strain measurements and FEA analysis showed that cutting a relief zone for the welds demands more of the parent material in the relief-cut. The maximum strains in the relief-cuts are more than twice as large as the nominal strains in the tongue edge during winding. FEA investigations of the relief zone showed that maximum relief is found directly at the relief-cut edge and that bottom radius and depth of cut influenced the maximum strains in the relief-cut. This leads to optimised use of existing relief cutting tools by moving the relief-cut next to the weld seam and only cutting 1 x strip thickness deep.

The nominal strains in the tongue during winding are far from the tested stainless steels forming limits so with increased formability in the welds it is possible to improve utilisation of the material by increasing yield strength at the expense of formability / ductility.

10.5 Tribology

Simulative testing with the strip-reduction-test showed that biodegradable rapeseed oil is an acceptable lubricant for the carcass process although a better non-chlorinated mineral oil where found. It was also shown that for two lean duplex stainless steels surface quality EN 2E brushed surface had better lubricant retainment capabilities than the 2B bright annealed surface, the latter having a longitudinal directional surface lay allowing lubricant to escape during pressure build-up. This was furthermore observed to have a negative impact on interlock friction conditions, where stainless steel is in contact with stainless steel.

Swarf was found to originate from two mechanisms: edge swarf and galling swarf. Edge swarf is a result of strip edge in severe contact with tools or another strip edge during interlocking, where large swarf is removed, sometimes resulting in a large burr forming on the strip edge. Galling swarf is smaller originating from pickup on the tool surfaces and subsequent scoring of the profile surface during roll gap entry in the roll forming stage. Edge swarf was successfully removed by increasing tool curvature in contact with the strip edge thereby lowering contact pressures, when the strip enters the roll gap.

Tool chipping was found on some roll forming tools where pickup formation, adhesive wear and cyclic contact loads caused low-cycle fatigue. Chipping resistance was improved by fine polishing of the tools.

Pickup is an issue on the roll forming tools, but it does not develop beyond a critical amount. Analysis of tool surfaces under the pickup showed signs of adhesive wear on the tools, which may explain the low-cycle chipping problem.

An AlCrN coating showed promising results in production testing as it was used to produce more than 650km EN 1.4162 stainless steel strip without any indications of tool wear or pickup formation, a vast improvement to non-coated tool performance.

Chapter 11 Future work

This project has treated a number of interesting subjects related to carcass production and the knowledge generated in the project is useful as a foundation for future optimisation of the carcass process. In the following suggestions are given on how to proceed with carcass process optimisation.

11.1 Failure modes and mechanisms

The buckling tendencies are not investigated in detail in this work but it was concluded that a change in profile path and strain gradient would in some cases solve the problem. Parametric studies of profile size, mandrel size and process path should be made in order to estimate the influence of these parameters on the tongue buckling tendency. A proper FE-model with satisfactory interlock deformation could be a first stage of investigation of tongue buckling phenomena.

The mandrel size-effect during winding should be investigated further on direct-feed machines, where profile back-tension and controlled angling of the incoming roll formed profile are both possible. This would allow determination of the influencing parameters to the interlock profile geometry and dividing point movement.

11.2 Finite element analysis

Although the results obtained with shell elements in simplified FE-models were satisfactory, it was a problem to obtain proper interlock deformation between two profiles, since the dividing point movement was not evident. This is likely due to the lack of super-imposed stresses on the profile during interlocking, which needs to be included in future simulations. This might also warrant re-consideration of using shell elements as the use of 3D stress solid elements might be better suited for the task.

An evaluation of the CAE software Copra$^{@}$ RF for use in tool design and optimisation is proposed, to study, how well the software can predict interlock deformation and dividing point movement during winding.

11.3 Simulative test

An improved fixture for applying the right boundary conditions to the tongue during bending needs to be constructed in order to have proper strain distribution in the simulative test corresponding to the carcass winding as regards tongue strains.

The deformation of more combinations of profile and mandrel sizes should be performed and evaluated to determine whether the simple profile deformation in the simulative test is satisfactory.

11.4 Formability and forming limits

Weld fracture investigations should be extended to include more strip thicknesses and materials for a more thorough investigation of the homogeneous strains at weld fracture.

Weld performance could be improved by either heat treatment or strain hardening to increase weld formability during winding. The goal should be to minimise the effect of the non-homogenous zone at the weld. Initial studies can be performed in the simulative test with simple profiles.

Optimised strain paths during winding, which includes interlocking with more closed roll formed carcass profiles should be sought. These should minimise stresses and strains during winding and could solve some of the specific problems in the winding stage.

11.5 Tribology

A further investigation of tribological issues in the carcass interlocking process is warranted to verify, whether or not interlocking problems due to surface lay and quality of the stainless steel can be solved by using a more effective lubricant, thereby proving if the cause is mechanical friction or lack of lubricant entrapment in the interlock.

Minimum quantity lubrication for the carcass process should be explored in light of the promising results with the AlCrN coating, which could solve problems with excessive lubricant in the subsequent processes.

References

[1] "American Petroleum Institute - API Specification 17J," [Online]. Available: http://www.api.org/publications-standards-and-statistics/standards/whatsnew/publication-updates/new-exploration-and-production-publications/api_spec_17j. [Accessed 05 11 2014].

[2] National Oilwell Varco, "Floating production systems: Dynamic flexible risers," [Online]. Available: http://fps.nov.com/subsea/flexibles/dynamic-flexible-risers. [Accessed 17 09 2014].

[3] Z. Chen, R. L. Reuben and D. G. Owen, "The deformation mechanics of interlock tubes," *Strain,* vol. 28, no. 3, pp. 99-106, August 1992.

[4] G. T. Halmos, Roll Forming Handbook, Boca Raton, Florida: CRC Press - Taylor & Francis Group, LLC, 2006.

[5] A. G. Neto and C. d. A. Martins, "A Comparative Wet Collapse Buckling Study for the Carcass Layer of Flexible Pipes," *JOURNAL OF OFFSHORE MECHANICS AND ARCTIC ENGINEERING-TRANSACTIONS OF THE ASME,* vol. 134, no. 3, 2012.

[6] Y. Zhang, B. Chen, L. Qiu, T. Hill and M. Case, "State of the art analytical tools improve optimization of unbonded flexible pipes for deepwater environments," in *Proceedings of the 2003 offshore technology conference*, Houston, Texas, USA, 2003.

[7] U.S. Energy Information Administration, "Analysis & Projections," 09 09 2014. [Online]. Available: http://www.eia.gov/forecasts/ieo/world.cfm. [Accessed 19 09 2014].

[8] "PreSalt.com," [Online]. Available: http://www.presalt.com/en/understanding-2/130-petrobras-and-the-pre-salt.html. [Accessed 24 08 2014].

[9] M. Imai, Gemba Kaizen: A Commonsense Approach to a Continuous Improvement Strategy 2/E, USA: McGraw-Hill Education, 2012.

[10] S. S. M. Tavares, C. Scandian, J. M. Pardal, T. S. Luz and F. J. da Silva, "Failure analysis of duplex stainless steel weld used in flexible pipes in offshore oil production," *Engineering*

Failure Analysis, vol. 17, no. 6, pp. 1500-1506, 2010.

[11] P. S. Nielsen, K. S. Friis and N. Bay, "Testing and modelling of new tribo-systems for industrial sheet forming of stainless steels," *Proceedings of the Institution of Mechanical Engineers, Part J: Journal of Engineering Tribology,* vol. 225, no. 10, pp. 1036-1047, 2011.

[12] S. M. Panton, S. D. Zhu and J. L. Duncan, "Fundamental deformation types and sectional properties in roll forming," *International Journal of Mechanical Sciences,* vol. 36, no. 8, pp. 725-735, 1994.

[13] Z. Marciniak, J. L. Duncan and S. J. Hu, Mechanics of Sheet Metal Forming, Great Britain: Butterworth-Heinemann, 2002.

[14] P. S. Nielsen, M. S. Nielsen and N. Bay, "Size effects in winding roll formed profiles: a study of carcass production for flexible pipes in offshore industry," in *Proceeedings of the 15th Bi-annual International Sheet Metal Conference (SheMet13)*, Belfast, Northern Ireland, 2013.

[15] K. Lange, Handbook of metal forming, Dearborn, Michigan: Society of Manufacturing Engineers, 1985.

[16] W. F. Hosford and R. M. Caddell, Metal forming, Mechanics and matallurgy 2/E, Englewood Cliffs: PTR Prentice Hall, 1993.

[17] J. Rodrigues and P. Martins, Tecnologia Mecânica Vol 2 , Tecnologia da Deformação Plástica - 2nd edition (in Portuguese), Escolar Editora, 2010.

[18] D. F. Eary and E. A. Reed, Techniques of Pressworking Sheet Metal: An Engineering Approach to Die Design, University of Michigan: Prentice-Hall, 1974.

[19] "Wikipedia - pigging," [Online]. Available: http://en.wikipedia.org/wiki/Pigging. [Accessed 23 08 2014].

[20] T. Wanheim, B. G. Ravn and N. Bay, Teknologisk Plasticitetslære, Lyngby: Institut for Mekanisk Teknologi - Danmarks Tekniske Universitet, 2008.

[21] H. J. Kleemola and M. A. Nieminen, "On the Strain-Hardening Parameters of Metals," *Metallurgical Transactions,* vol. 5, pp. 1863-1866, 1974.

[22] D. Banabic, Sheet Metal Forming Processes, Berlin: Springer-Verlag Berlin Heidelberg, 2010.

[23] H. J. Kleemola and J. O. Kumpulainen, “Factors influencing the forming limit diagram: Part I - The experimental determination of the forming limits of sheet steel,” *Journal of Mechanical Working Technology,* vol. 3, pp. 289-302, 1980.

[24] W. Müschenborn and H. -M. Sonne, "Influence of the strain path on the forming limits of sheet metal (in German)," *Arch. Eisenhüttenwesen,* vol. 46, no. 9, pp. 597-605, 1975.

[25] V. Hasek, “Research and theoretical description concerning the influences on the FLDs,” *Blech Rohre Profile,* vol. 25, pp. 213-220, 285-292, 493-499, 617-627, 1978.

[26] H. J. Kleemola and J. O. Kumpulainen, “Factors influencing the forming limit diagram: Part II - Influence of sheet thickness,” *Journal of Mechanical Working Technology,* vol. 3, pp. 303-311, 1980.

[27] K. Janssens, F. Lambert, S. Vanrostenberghe and M. Vermeulen, “Statistical evaluation of the uncertainty of experimentally characterized forming limits of sheet steel,” *Journal of Materials Processing Technology,* vol. 112, no. 2-3, pp. 174-184, 2001.

[28] “Wikipedia - screen printing,” [Online]. Available: http://en.wikipedia.org/wiki/Screen_printing. [Accessed 30 07 2014].

[29] GOM, “www.gom.com,” [Online]. Available: http://www.gom.com/3d-software/aramis-software.html. [Accessed 01 08 2014].

[30] “www.asametech.com,” [Online]. Available: http://www.asametech.com/. [Accessed 01 08 2014].

[31] J. T. Henckel, “Procestekniske analyser af carcass-fremstilling til fleksible rør,” Technical University of Denmark, Dept. of Mech. Engn., Lyngby, 2011.

[32] GOM Optical Measuring Techniques, “FLC Computation v6.1.1. and higher,” GOM mbh, Braunschweig, 2009.

[33] D. C. Montgomery, Design and Analysis of Experiments, Hoboken: John Wiley & Sons, 2009.

[34] S. N. Rasmussen and B. G. Hansen, “Et nyt ekstensometer og databearbejdningsprogram til trækprøvning af tyndplade,” in *DMS-møde, MM.86.06*, Lyngby, 1986.

[35] M. Lindgren, “Experimental and Computational Investigation of the Roll Forming Process,” Universitetstryckeriet, Luleå, 2009.

[36] M. O. Görtan, D. Vucic, P. Groche and H. Livatyali, “Roll forming of branched profiles,” *Journal of Materials Processing Technology,* vol. 209, no. 17, pp. 5837-5844, 2009.

[37] J. Larrañaga, L. Galdos, L. Uncilla and A. Etxaleku, “Development and validation of a numerical model for sheet metal roll forming,” *International Journal of Material Forming,* vol. 3, no. 1, pp. 151-154, 2010.

[38] J.-J. Sheu, “Simulation and optimization of the cold roll-forming process,” in *Materials Processing and Design: Modeling, Simulation and Applications NUMIFORM 2004*, Columbus Ohio, 2004.

[39] J. Paralikas, K. Salonitis and G. Chryssolouris, “Investigation of the effects of main roll-forming process parameters on quality for a V-section profile from AHSS,” *The International Journal of Advanced Manufacturing Technology,* vol. 44, no. 3-4, pp. 223-237, 2009.

[40] M. S. Tehrani, H. M. Naeini, P. Hartley and H. Khademizadeh, “Localized edge buckling in cold roll-forming of circular tube section,” *Journal of Materials Processing Technology,* vol. 177, no. 1-3, pp. 617-620, 2006.

[41] W. J. T. Daniel and P. A. Meehan, “Implicit Finite Element Study of Non-steady Effects in Cold Roll Forming,” in *Proceedings of the 5th Australasian Congress on Applied Mechanics*, Brisbane, 2007.

[42] M. A. Sheikh and R. R. Palavilayil, “An assessment of finite element software for application to the roll-forming process,” *Journal of Materials Processing Technology,* vol. 180, pp. 221-232, 2006.

[43] Anon., “COPRA® RF - Software for Roll Forming,” DataM Sheet Metal Solutions GmbH, [Online]. Available: http://www.datam.de/en/products-solutions/roll-forming/. [Accessed 27 08 2014].

[44] A. E. Tekkaya and P. A. F. Martins, “Acuracy, reliability and validity of finite element analysis in metal forming: a user's perspective,” *Engineering computations: International Journal for Computer-Aided Engineering and Software,* vol. 26, no. 8, pp. 1026-1055, 2009.

[45] L.-E. Lindgren and J. Edberg, “Explicit versus implicit finite element formulation in simulation of rolling,” *Journal of Materials Processing Technology,* vol. 24, pp. 85-94, 1990.

[46] J. O. Hallquist, LS-DYNA® theory manual, Livermore, California: Livermore Software

Technology Corporation, March 2006.

[47] Anon., »LS-DYNA Support,« LSTC Inc and DYNAmore GmbH, [Online]. Available: http://www.dynasupport.com/tutorial/ls-dyna-users-guide/elements. [Senest hentet eller vist den 26 08 2014].

[48] R. D. Cook, D. S. Malkus, M. E. Plesha and R. J. Witt, Concepts and Applications of Finite Element Analysis, John Wiley And Sons Ltd, 2001.

[49] L. Olovsson, K. Simonsson and M. Unosson, "Selective mass scaling for explicit finite element analyses," *International Journal for Numerical Methods in Engineering,* vol. 63, no. 10, pp. 1436-1445, 2005.

[50] Z. Marciniak and K. Kuczynski, "Limit strains in processing of stretch forming sheet metal," *International Journal of Mechanical Sciences,* vol. 9, pp. 609-620, 1967.

[51] A. S. Galakhar, J. D. Gates, W. J. T. Daniel og P. A. Meehan, »Adhesive tool wear in the cold roll forming process,« *Wear,* årg. 271, pp. 2728-2745, 2011.

[52] E. van der Heide and D. J. Schipper, "Galling initiation due to frictional heating," *Wear,* vol. 254, no. 11, pp. 1127-1133, 2003.

[53] European Parliament, Council. REACH, "EC Regulation No 1907/2006 of the European Parliament and of the Council," 2006.

[54] N. Bay, A. Azushima, P. Groche, I. Ishibashi, M. Merklein, M. Morishita, T. Nakamura, S. Schmid and M. Yoshida, "Environmentally benign tribo-systems for metal forming," *CIRP Annals - Manufacturing Technology,* vol. 59, no. 2, pp. 760-780, 2010.

[55] P. S. Nielsen, M. S. Nielsen and N. Bay, "Tribological study in roll forming of lean duplex stainless steel sheets," in *Proceedings of the 2012 International Deep-Drawing Research Group (IDDRG 2012)*, Mumbai, India, 2012.

[56] W. Chua and G. W. Stachowiak, "The growth of thin film lubricating films of plant oils," *Tribology Letters,* vol. 41, no. 2, pp. 451-462, 2011.

[57] J. L. Andreasen, N. Bay, M. Andersen, E. Christensen and N. Bjerrum, "Screening the performance of lubricants for ironing of stainless steel with a strip reduction test," *Wear,* vol. 207, no. 1-2, pp. 1-5, 1997.

[58] D. D. Olsson, N. Bay and J. L. Andreasen, "Prediction of limits of lubrication in strip reduction testing," *CIRP Annals Manufacturing Technology,* vol. 53, no. 1, pp. 231-234,

2004.

[59] J. L. Andreasen, B. Niels and L. De Chiffre, “Quantification of galling in sheet metal forming by surface topography characterization,” *International Journal of Machine Tool and Manufacture,* vol. 38, no. 5-6, pp. 503-510, 1998.

[60] B. Wadman, J. Eriksson, M. Olsson, E. Schedin, E. Madsen and N. Bay, “Influence of surface texture on the galling characteristics of lean duplex and austenitic strainless steels,” in *Proceedings of Duplex World 2010 Conference*, Beaune, France, 2010.

[61] S. Gasparin, H. N. Hansen and G. Tosello, “Traceable surface characterization using replica moulding technology,” in *13th International Conference on Metrology and Properties of Engineering Surfaces*, Twickenham, UK, 2011.

[62] W. D. Callister, Materials Science and Engineering: An Introduction, USA: John Wiley & Sons, Incorporate, 2003.

[63] W. A. Glaeser and S. J. Shaffer, “Contact Fatigue,” in *ASM Handbook, Volume 19: Fatigue and Fracture*, ASM International, 1996, pp. 331-336.

[64] Anon., “Uddeholm Vancron 40,” 01 2014. [Online]. Available: http://www.uddeholm.com/files/PB_vancron_40_english.pdf. [Accessed 09 09 2014].

Appendix A: Python script

The procedure is as follows:

1. Load the data file through the file menu
2. Select material model: either Hollomon or Swift
3. Input test/specimen description for the output file
4. Input initial specimen thickness [mm] – the width is not needed as this is read from the first line in the data file as it is measured by the equipment
5. Input modulus of elasticity [MPa]
6. Press ‘calculate’ to calculate engineering stresses and strains and receive a graphical representation of the engineering flow curve
7. Use sliders to cut away unwanted data; elastic region and region after onset of diffuse necking
8. Press ‘curvefit’ to calculate true stresses and strains and receive a graphical representation of the flow curve as well as curvefit parameters according to the selected material model
9. Press ‘export data’ to write the results to a file

```
# -*- coding: utf-8 -*-
"""
Created on Tue Dec 04 12:57:14 2012

@author: SoeNielsenP
"""
import wx
from wx.lib.plot import PlotCanvas, PlotGraphics, PolyLine, PolyMarker
import numpy as np
import csv
import scipy.optimize as so
import os
```

```
#Create empty lists for the test data
area = []
time = []
load_kp = []
delta_l = []
w1 = []
load_n = []
e_stress = []
l_strain = []
w_strain = []
t_strain = []
t1 = []
el_strain = []
pl_strain =[]
Sstress = []
Sstrain = []
stress = []
del_sp = 0
del_ep = 0
raw_t = []
raw_e = []
cb_str = []

#Fixed factors
g = 9.82 #Gravity [N/kg]
```

```
l0 = 39.82 #Initial length [mm] - fixed factor by testing equipment



#Plot raw data calculated from input file

def rawPlot(raw_t, raw_e, sp_plot, ep_plot):

    marker1 = PolyMarker(raw_t, legend='True stress', colour='black', marker='circle', size = 0.8)

    marker2 = PolyMarker(raw_e, legend='Engineering stress', colour='grey', marker='circle', size = 0.8)

    line1 = PolyLine(sp_plot, legend = 'Curvefit start point', colour = 'green', width = 2)

    line2 = PolyLine(ep_plot, legend = 'Curvefit end point', colour = 'red', width = 2)

    return PlotGraphics([marker1, marker2, line1, line2], "Raw data", "log strain [-]", "Stress [MPa]")


#Plot the data used for curve fit and the fit curve

def fitPlot(fitdata, fitline):

    line = PolyLine(fitline, legend = 'Fit curve', colour = 'red', width = 2)

    marker = PolyMarker(fitdata, legend='Fit data', colour='blue',

                marker='circle', size = 0.8)

    return PlotGraphics([marker, line], "Curvefit data", "Plastic log strain [-]", "True stress [MPa]")


class mwindow(wx.Frame): #Generic constructor

  def __init__(self, parent, title):

    wx.Frame.__init__(self, parent, title = title, size = (1000, 700))


    # Generate splitter window with two panels
```

```
self.sw = wx.SplitterWindow(self)
self.pnl1 = wx.Panel(self.sw, style = wx.SP_3D)
self.pnl2 = wx.Panel(self.sw, style = wx.SUNKEN_BORDER)
self.sw.SplitVertically(self.pnl1,self.pnl2,250)
#

#Set statusbar
self.statusbar = self.CreateStatusBar()
#

self.Centre() #Center the frame on screen
self.dirname=''

#Text fonts
font1 = wx.Font(12, wx.DEFAULT, wx.NORMAL, wx.NORMAL)
font2 = wx.Font(12, wx.DEFAULT, wx.NORMAL, wx.BOLD)
#

#Generate menubar and menu objects
menubar = wx.MenuBar() #Create a menubar object
filemenu = wx.Menu() #Create a menu object
aboutmenu = wx.Menu() #Create a menu object

menubar.Append(filemenu, 'File') #Tilføjer File til menubaren
menubar.Append(aboutmenu, '?') #Tilføjer About til menubaren
self.SetMenuBar(menubar) # Tilføjer menubaren til mwindow
```

```
#Filemenu open
fmopen = filemenu.Append(wx.ID_OPEN, "Open", "Open a LabView file")
self.Bind(wx.EVT_MENU, self.OpenF, fmopen)

#Filemenu quit
fmquit = filemenu.Append(wx.ID_EXIT, 'Quit', 'Quit application')
self.Bind(wx.EVT_MENU, self.Quit, fmquit) #Binding Quit to the event of clicking quit in the file menu

#About
about = aboutmenu.Append(wx.ID_ABOUT, 'Software', 'About this software')
self.Bind(wx.EVT_MENU, self.About, about)

#Generate input textboxes
#Input material information
mtrl_inf_txt = wx.StaticText(self.pnl1, label='Material and test information', pos=(10, 80))
mtrl_inf_txt.SetFont(font1)
mtrl_inf = wx.TextCtrl(self.pnl1, -1, pos = (10, 100), size = (235, -1))
mtrl_inf.Bind(wx.EVT_TEXT, self.InfText) #Get string

#Specimen thickness
mtrl_thk_txt = wx.StaticText(self.pnl1, label='Initial thickness [mm]', pos=(10, 140))
mtrl_thk_txt.SetFont(font1)
mtrl_thk = wx.TextCtrl(self.pnl1, -1, pos = (10, 160), size = (50, -1))
```

```
mtrl_thk.Bind(wx.EVT_TEXT, self.tNum)


#Modulus of elasticity
E_mod_txt = wx.StaticText(self.pnl1, label='Modulus of Elasticity [MPa]', pos=(10, 200))
E_mod_txt.SetFont(font1)
E_mod = wx.TextCtrl(self.pnl1, -1, pos = (10, 220), size = (70, -1))
E_mod.Bind(wx.EVT_TEXT, self.ENum)


#Start calculations button
go = wx.Button(self.pnl1, wx.ID_OPEN, 'Calculate!', (90, 260))
go.Bind(wx.EVT_BUTTON, self.StartC)


#Curve fit button
fit = wx.Button(self.pnl1, wx.ID_OPEN, 'Curve fit', (90, 400))
fit.Bind(wx.EVT_BUTTON, self.Fit)


#Write file button
fwrite = wx.Button(self.pnl1, wx.ID_OPEN, 'Export data', (10, 580))
fwrite.Bind(wx.EVT_BUTTON, self.WriteF)


#Create Combobox for selection of material model
lst = ['Hollomon', 'Swift']
self.cb = wx.ComboBox(self.pnl1, pos=(10, 30), choices=lst, style=wx.CB_READONLY)
```

```
matrmdl = wx.StaticText(self.pnl1, label='Select material model', pos=(10, 8))

matrmdl.SetFont(font2)


self.st = wx.StaticText(self.pnl1, label='', pos=(90, 30))

self.st.SetFont(font1)

self.cb.Bind(wx.EVT_COMBOBOX, self.OnSelect)


#Create sliders

sp_sld = wx.Slider(self.pnl1, value = 0, minValue = 0, maxValue = 3000, pos = (10, 320), size = (230, -1), style = wx.SL_HORIZONTAL)

self.Bind(wx.EVT_SCROLL, self.spSliderScroll, sp_sld)

wx.StaticText(self.pnl1, label='Curvefit start point: ', pos = (10, 300))

self.sp = wx.StaticText(self.pnl1, label='0', pos = (110, 300))


ep_sld = wx.Slider(self.pnl1, value = 0, minValue = 0, maxValue = 6000, pos = (10, 370), size = (230, -1), style = wx.SL_HORIZONTAL)

self.Bind(wx.EVT_SCROLL, self.epSliderScroll, ep_sld)

wx.StaticText(self.pnl1, label='Curvefit end point: ', pos = (10, 350))

self.ep = wx.StaticText(self.pnl1, label='0', pos = (105, 350))



#Create canvas' for plotting

#Canvas 1 on pnl2

self.canvas1 = PlotCanvas(self.pnl2, pos = (1, 1))

self.canvas1.SetInitialSize(size = (725, 280))

self.canvas1.SetEnableLegend(1)
```

```
    #Canvas 2 on pnl2
    self.canvas2 = PlotCanvas(self.pnl2, pos = (1, 280))
    self.canvas2.SetInitialSize(size = (725, 280))
    self.canvas2.SetEnableLegend(1)



    #Printing curvefit, anisotropy and yield stress results on panel2
    self.mp = wx.StaticText(self.pnl2, label = '', pos = (10, 565))
    self.mpr = wx.StaticText(self.pnl2, label = '', pos=(185, 565))
    self.lpr = wx.StaticText(self.pnl2, label = '', pos = (10, 590))
    self.r = wx.StaticText(self.pnl2, label = '', pos = (60, 590))
    self.ys = wx.StaticText(self.pnl2, label = '', pos = (230, 590))
    self.ysr = wx.StaticText(self.pnl2, label = '', pos = (330, 590))


#Which material model is the data fitted to?
def Fit(self, e):
    if cb_str == 'Hollomon':
        self.Hollomon(e)
    elif cb_str == 'Swift':
        self.Swift(e)
    else:
        print 'You have not selected a material model to fit the data to'


#Grabbing input from textboxes in the frame
def InfText(self, e):
```

```
        global inf
        inf = e.GetString()

    def tNum(self, e):
        global t0
        t0 = float(e.GetString())

    def ENum(self, e):
        global E
        E = float(e.GetString())

    #Dialog with program information
    def About(self, e):
        print 'ICFG Python script v1.0\n\nThis Python script is used for data analysis of tensile testing with ICFG tool at DTU-MEK building 427\n\nCreated by Peter Soee Nielsen\nEmail: psoe@mek.dtu.dk'

    #Quit program
    def Quit(self, e):
        self.Close()

    #Select file to be opened
    def OpenF(self, e):
        del l_strain[:]
        del w_strain[:]
        del t_strain[:]
```

```
        del l_strain[:]
        del t1[:]
        del area[:]
        del load_n[:]
        del stress[:]
        del e_stress[:]
        del el_strain[:]
        del pl_strain[:]
        del raw_t[:]
        del raw_e[:]
        dlg = wx.FileDialog(self, "Choose LabView data file", self.dirname, "", "*.lvm", wx.OPEN)
        if dlg.ShowModal() == wx.ID_OK:
            self.filename = dlg.GetFilename()
            self.dirname = dlg.GetDirectory()
            tstd = open(os.path.join(self.dirname, self.filename), 'rb')
            csv_read = csv.reader(tstd, dialect=csv.excel_tab)
            for line in csv_read:
                time.append(line[0])
                load_kp.append(line[1])
                delta_l.append(line[2])
                w1.append(line[3])
            tstd.close()
            dlg.Destroy()


    #Select file to write data to
```

```
    def WriteF(self, e):
        row1 = ['Material information:', inf]
        row2 = ['Strip initial thickness [mm]:', t0]
        row3 = ['Modulus of Elasticity [MPa]:', E]
        row4 = ['Yield stress [MPa]:', y_stress]
        row5 = ['R-value:', R]
        row6 = ['Curve fit start point index', del_sp]
        row7 = ['Curve fit end point index', del_ep]
        if cb_str == 'Hollomon':
            row8 = ['Results of curvefitting according to Hollomon:', 'C', 'n']
            row9 = ['', lsqresult[0], lsqresult[1]]
        elif cb_str == 'Swift':
            row8 = ['Results of curvefitting according to Swift:', 'C', 'n', 'b ']
            row9 = ['', lsqresult[0], lsqresult[1], lsqresult[2]]
        else:
            print 'Error: Material model is not selected'
        dlg = wx.FileDialog(self, "Choose filename to write data to", self.dirname, "", "*.txt", wx.SAVE)
        if dlg.ShowModal() == wx.ID_OK:
            self.filename = dlg.GetFilename()
            self.dirname = dlg.GetDirectory()
            wtstd = open(os.path.join(self.dirname, self.filename), 'wb')
            csv_write = csv.writer(wtstd, dialect=csv.excel_tab)
            csv_write.writerow(row1)
            csv_write.writerow(row2)
            csv_write.writerow(row3)
```

```
        csv_write.writerow(row4)
        csv_write.writerow(row5)
        csv_write.writerow(row6)
        csv_write.writerow(row7)
        csv_write.writerow(row8)
        csv_write.writerow(row9)
        wtstd.close()
        dlg.Destroy()


#Show selected ComboBox value
def OnSelect(self, e):
    global cb_str
    cb_str = e.GetString()
    if cb_str == 'Hollomon':
        self.st.SetLabel(u'\u03c3 = C * \u03f5^n')
    elif cb_str == 'Swift':
        self.st.SetLabel(u'\u03c3 = C * (b + \u03f5)^n')


def spSliderScroll(self, e):
    obj = e.GetEventObject()
    global del_sp
    del_sp = obj.GetValue()
    self.sp.SetLabel(str(del_sp))

    #Create points for visual determination of curvefit data
```

```
        sp_2pnt = [l_strain[del_sp], l_strain[del_sp]]
        end_2pnt = (len(l_strain) - del_ep) - int(1)
        ep_2pnt = [l_strain[end_2pnt], l_strain[end_2pnt]]
        sp_plot = zip(sp_2pnt, pnt)
        ep_plot = zip(ep_2pnt, pnt)

        #Plot rawdata on canvas1
        self.canvas1.Draw(rawPlot(raw_t, raw_e, sp_plot, ep_plot))

    def epSliderScroll(self, e):
        obj = e.GetEventObject()
        global del_ep
        del_ep = obj.GetValue()
        self.ep.SetLabel(str(del_ep))

        #Create points for visual determination of curvefit data
        sp_2pnt = [l_strain[del_sp], l_strain[del_sp]]
        end_2pnt = (len(l_strain) - del_ep) - int(1)
        ep_2pnt = [l_strain[end_2pnt], l_strain[end_2pnt]]
        sp_plot = zip(sp_2pnt, pnt)
        ep_plot = zip(ep_2pnt, pnt)

        #Plot rawdata on canvas1
        self.canvas1.Draw(rawPlot(raw_t, raw_e, sp_plot, ep_plot))

    #Calculation of stresses and strains
```

```
def StartC(self, e):
    #Calculate longitudinal strains
    global l_strain
    for number in delta_l:
        l_strain.append(np.log((l0+float(number))/l0))

    #Calculate width strains
    for number in w1:
        w_strain.append(np.log(float(number)/float(w1[0])))

    #Calculate thickness strains using Tuples
    global t_strain
    t_strain = [(-x-y) for x, y in zip(l_strain, w_strain)]

    #Calculate t1
    for number in t_strain:
        t1.append(t0*np.exp(float(number)))

    #Calculate area using tuples and converting lists to floats
    area = [x*y for x,y in zip(map(float, w1), map(float, t1))]

    #Convert load in kP to N
    for number in load_kp:
        load_n.append(float(number) * g)

    #Calculate true stresses
```

```
global stress
stress = [x/y for x, y in zip(load_n, area)]

#Calculate engineering stresses
for value in load_n:
    e_stress.append(value / area[0])

#Determine elastic strains
for number in stress:
    el_strain.append(number/E)

#Remove elastic strains from l_strain for pure plastic strain
global pl_strain
pl_strain = [x-y for x, y in zip(l_strain, el_strain)]

#Create points for visual determination of curvefit data
global pnt
pnt = [0, max(stress) + 100]
sp_2pnt = [l_strain[del_sp], l_strain[del_sp]]
end_2pnt = (len(l_strain) - del_ep) - int(1)
ep_2pnt = [l_strain[end_2pnt], l_strain[end_2pnt]]
sp_plot = zip(sp_2pnt, pnt)
ep_plot = zip(ep_2pnt, pnt)

#Raw data for plot
global raw_t
```

```
    global raw_e
    raw_t = zip(l_strain, stress)
    raw_e = zip(l_strain, e_stress)

    #Plot rawdata on canvas1
    self.canvas1.Clear() #Clear canvas for new plot
    self.canvas1.Draw(rawPlot(raw_t, raw_e, sp_plot, ep_plot))

    #Clear input lists such that a new file can be loaded
    del time[:]
    del load_kp[:]
    del delta_l[:]
    del w1[:]

#Swift curvefitting function
def Swift(self, e):
    Sstress = stress
    Sstrain = pl_strain

    #Remove unwanted section of data from file start and end
    del Sstress[0:del_sp]
    del Sstrain[0:del_sp]
    end = len(Sstress) #Define endpoint of the list
    del Sstress[end-del_ep:end]
    del Sstrain[end-del_ep:end]
```

```
xdata = np.array(Sstrain)
ydata = np.array(Sstress)

#Calculate sheet anisotropy
del w_strain[0:del_sp]
del t_strain[0:del_sp]
end_r = len(w_strain) #Define endpoint of the list
del w_strain[end_r-del_ep:end_r]
del t_strain[end_r-del_ep:end_r]
global Lankford_parameter
Lankford_parameter = [x/y for x, y in zip(w_strain, t_strain)]
global R
R = np.average(Lankford_parameter) #Average value for the Lankford parameter

#Function to fit data to
def Swift_func(xdata, C, n, b):
    return C*(b+xdata)**n

#Calculating the residuals
def Swift_residuals(p, ydata, xdata):
    C, n, b = p
    err = ydata-Swift_func(xdata, C, n, b)
    return err

#Function to evaluate least sqaures result
def Swift_eval(xdata, p):
```

```
    C, n, b = p
    return Swift_func(xdata, C, n, b)

p0 = [1000, 0.1, 0.1] #Initial guess for C, n & b

#Curve fitting to Swift using least squares
global lsq
lsq = so.leastsq(Swift_residuals, p0, args=(ydata, xdata), xtol=0.0001)
global lsqresult
lsqresult = lsq[0]

#Yield stress calculation based on fit curve - only possible for Swift's material model
global y_stress
y_stress = Swift_eval(0, lsq[0])
self.ys.SetLabel('Yield stress [MPa]:')
self.ysr.SetLabel(str(y_stress))

self.mp.SetLabel('Material parameter, Swift [C n b]:')
self.mpr.SetLabel(str(lsqresult))
self.lpr.SetLabel('R-value:')
self.r.SetLabel(str(R))

#Data used for fit
fitdata = zip(xdata, ydata)
#Plot rawdata + fit curve on canvas2
fitline = zip(xdata, Swift_eval(xdata, lsq[0]))
```

```
    self.canvas2.Draw(fitPlot(fitdata, fitline))



#Hollomon curvefitting function
def Hollomon(self, e):
    Hstress = stress
    Hstrain = pl_strain

    #Remove unwanted section of data from file start and end
    del Hstress[0:del_sp]
    del Hstrain[0:del_sp]
    end = len(Hstress) #Define endpoint of the list
    del Hstress[end-del_ep:end]
    del Hstrain[end-del_ep:end]

    xdata = np.array(Hstrain)
    ydata = np.array(Hstress)

    #Calculate sheet anisotropy
    del w_strain[0:del_sp]
    del t_strain[0:del_sp]
    end_r = len(w_strain) #Define endpoint of the list
    del w_strain[end_r-del_ep:end_r]
    del t_strain[end_r-del_ep:end_r]
    global Lankford_parameter
    Lankford_parameter = [x/y for x, y in zip(w_strain, t_strain)]
```

```
global R
R = np.average(Lankford_parameter) #Average value for the Lankford parameter

#Function to fit data to
def Hollomon_func(xdata, C, n):
    return C*xdata**n

#Claculating the residuals
def Hollomon_residuals(p, ydata, xdata):
    C, n = p
    err = ydata-Hollomon_func(xdata, C, n)
    return err

#Function to evaluate least sqaures result
def Hollomon_eval(xdata, p):
    C, n = p
    return Hollomon_func(xdata, C, n)

p0 = [1000, 0.1] #Initial guess for C & n

#Curve fitting to Hollomon using least squares
global lsq
lsq = so.leastsq(Hollomon_residuals, p0, args=(ydata, xdata), xtol=0.0001)
global lsqresult
lsqresult = lsq[0]
```

```
        #Yield stress - only possible for Swift's material model
        global y_stress
        y_stress = 0
        self.ys.SetLabel('')
        self.ysr.SetLabel('')

        self.mp.SetLabel('Material parameter, Hollomon [C n]:')
        self.mpr.SetLabel(str(lsqresult))
        self.lpr.SetLabel('R-value:')
        self.r.SetLabel(str(R))

        #Data used for fit
        fitdata = zip(xdata, ydata)
        #Plot rawdata + fit curve on canvas2
        fitline = zip(xdata, Hollomon_eval(xdata, lsq[0]))
        self.canvas2.Draw(fitPlot(fitdata, fitline))

app = wx.App() #Initializes GUI toolkit
frame = mwindow(None, 'ICFG tensile test - Data treatment and curvefitting') #Initilaze frame
frame.Show() #Show frame
app.MainLoop() #Run the GUI in continuous loop
```

Appendix B: Tensile test results

Test no.	Specimen	Material [EN]	Meas. t [mm]	Meas. w [mm]	Yield stress [MPa]	C	n	b	R_alpha
3.2	Tensile (0º)	1.4162	0.58	19.95	653	1461	0.241	0.037	0.99
73	Tensile (0º)	1.4162	0.58	19.97	666	1430	0.226	0.033	0.94
46	Tensile (0º)	1.4162	0.59	19.96	651	1406	0.227	0.035	0.83
3	Tensile (0º)	1.4162	0.6	20	650	1386	0.226	0.034	0.79
					655	1421	0.230	0.035	0.89
stdev					7	32	0.008	0.002	0.09
8	Tensile (0º)	1.4162	1.49	19.99	604	1328	0.233	0.034	0.81
24	Tensile (0º)	1.4162	1.49	19.99	605	1323	0.228	0.033	0.74
51	Tensile (0º)	1.4162	1.49	19.98	610	1316	0.221	0.030	0.76
					606	1322	0.227	0.032	0.77
stdev					3	6	0.006	0.002	0.04
10	Tensile (0º)	1.4162	2.46	20.02	-	-	-	-	-
10.2	Tensile (0º)	1.4162	2.49	19.99	577	1274	0.216	0.030	0.55
4	Tensile (0º)	1.4162	2.5	20.01	581	1269	0.208	0.027	0.55
63	Tensile (0º)	1.4162	2.5	20	578	1268	0.210	0.028	0.50
					579	1270	0.211	0.028	0.53
stdev					2	3	0.004	0.001	0.03
9	Tensile (45º)	1.4162	0.59	19.95	656	1358	0.213	0.037	1.08
11	Tensile (45º)	1.4162	0.59	19.97	662	1378	0.220	0.038	1.16
56	Tensile (45º)	1.4162	0.59	19.95	-	-	-	-	-
56.2	Tensile (45º)	1.4162	0.59	19.89	626	1310	0.184	0.021	1.15
					648	1349	0.205	0.032	1.13
stdev					19	35	0.019	0.009	0.05
54	Tensile (45º)	1.4162	1.48	19.96	611	1276	0.212	0.033	1.21
35	Tensile (45º)	1.4162	1.49	19.97	607	1279	0.215	0.033	1.10
39	Tensile (45º)	1.4162	1.49	19.97	591	1275	0.214	0.032	1.03
					603	1276	0.214	0.033	1.12
stdev					11	2	0.002	0.001	0.09
79.2	Tensile (45º)	1.4162	2.45	19.98	584	1207	0.195	0.028	1.02
18	Tensile (45º)	1.4162	2.47	19.97	588	1230	0.206	0.033	1.15
29	Tensile (45º)	1.4162	2.47	19.98	580	1227	0.196	0.028	1.20
79	Tensile (45º)	1.4162	2.48	20.02	-	-	-	-	-
					584	1221	0.199	0.030	1.12
stdev					4	13	0.006	0.003	0.09
26	Tensile (90º)	1.4162	0.6	19.8	641	1331	0.200	0.029	1.04
43	Tensile (90º)	1.4162	0.6	19.9	626	1306	0.193	0.028	1.21
2	Tensile (90º)	1.4162	0.61	19.95	625	1328	0.211	0.036	1.38
					631	1322	0.201	0.031	1.21
stdev					9	14	0.009	0.004	0.17
32	Tensile (90º)	1.4162	1.49	19.95	607	1312	0.207	0.029	0.97
66	Tensile (90º)	1.4162	1.49	19.97	606	1286	0.197	0.026	1.23
81	Tensile (90º)	1.4162	1.49	19.95	610	1286	0.197	0.025	1.07
					608	1295	0.200	0.026	1.09
stdev					2	15	0.006	0.002	0.13

55	Tensile (90º)	1.4162	2.45	20.09	626	1251	0.185	0.026	0.77
19	Tensile (90º)	1.4162	2.48	20.08	618	1233	0.173	0.022	0.85
42	Tensile (90º)	1.4162	2.48	20.06	632	1248	0.180	0.025	0.80
					625	1244	0.179	0.024	0.81
stdev					7	10	0.006	0.002	0.04
48	Tensile (0º)	1.4404	0.6	20	285	1364	0.431	0.025	0.84
71	Tensile (0º)	1.4404	0.61	20.01	289	1372	0.448	0.028	0.84
15	Tensile (0º)	1.4404	0.62	20	284	1361	0.453	0.029	0.81
					286	1366	0.444	0.028	0.83
stdev					3	6	0.012	0.002	0.02
49.2	Tensile (0º)	1.4404	1.43	19.97	298	1327	0.426	0.030	0.82
49	Tensile (0º)	1.4404	1.46	19.99	-	-	-	-	-
80	Tensile (0º)	1.4404	1.47	19.98	307	1329	0.427	0.031	0.82
27	Tensile (0º)	1.4404	1.49	19.98	585	1310	0.219	0.029	0.76
					303	1328	0.426	0.030	0.82
stdev					6	1	0.001	0.001	0.00
53	Tensile (0º)	1.4404	2.49	19.98	323	1309	0.417	0.034	0.83
76	Tensile (0º)	1.4404	2.49	19.99	316	1309	0.417	0.033	0.83
36	Tensile (0º)	1.4404	2.5	19.99	308	1376	0.452	0.040	0.73
					316	1331	0.429	0.036	0.79
stdev					8	39	0.020	0.004	0.06
77	Tensile (45º)	1.4404	0.6	19.95	280	1440	0.505	0.043	2.08
16	Tensile (45º)	1.4404	0.61	19.95	290	1453	0.536	0.051	2.07
31	Tensile (45º)	1.4404	0.61	19.95	295	1485	0.546	0.052	1.78
					288	1459	0.529	0.049	1.98
stdev					8	23	0.021	0.005	0.17
23	Tensile (45º)	1.4404	1.45	19.95	315	1485	0.533	0.060	1.30
5	Tensile (45º)	1.4404	1.47	19.95	295	1453	0.522	0.056	1.45
75	Tensile (45º)	1.4404	1.48	19.96	300	1313	0.436	0.037	1.54
					303	1417	0.497	0.051	1.43
stdev					10	91	0.053	0.012	0.12
12	Tensile (45º)	1.4404	2.48	20	324	1344	0.464	0.053	1.56
33	Tensile (45º)	1.4404	2.49	19.99	320	1392	0.495	0.058	1.53
40	Tensile (45º)	1.4404	2.5	19.98	303	1338	0.463	0.048	1.59
					316	1358	0.474	0.053	1.56
stdev					11	30	0.018	0.005	0.03
64	Tensile (90º)	1.4404	0.59	19.9	298	1432	0.480	0.038	2.16
69	Tensile (90º)	1.4404	0.59	19.91	307	1496	0.501	0.043	1.95
78	Tensile (90º)	1.4404	0.61	19.94	301	1442	0.509	0.045	2.40
					302	1457	0.497	0.042	2.17
stdev					5	35	0.015	0.004	0.22
17	Tensile (90º)	1.4404	1.46	19.96	315	1413	0.514	0.060	2.02
47	Tensile (90º)	1.4404	1.46	20	311	1393	0.505	0.058	1.88
50	Tensile (90º)	1.4404	1.47	19.98	307	1374	0.508	0.059	1.94
					311	1393	0.509	0.059	1.94
stdev					4	20	0.004	0.001	0.07
37.2	Tensile (90º)	1.4404	2.48	19.99	369	1320	0.445	0.060	2.10
41	Tensile (90º)	1.4404	2.48	19.98	337	1385	0.482	0.058	1.75
37	Tensile (90º)	1.4404	2.49	19.98	-	-	-	-	-
44	Tensile (90º)	1.4404	2.5	20.01	354	1425	0.516	0.073	1.71
					353	1377	0.481	0.064	1.85
stdev					16	53	0.035	0.008	0.22

22	Tensile (0º)	1.4410	0.77	19.99	813	1581	0.194	0.033	0.62
6	Tensile (0º)	1.4410	0.78	19.98	808	1546	0.186	0.031	0.61
7	Tensile (0º)	1.4410	0.79	19.99	797	1559	0.191	0.032	0.51
					806	1562	0.190	0.032	0.58
stdev					8	18	0.004	0.001	0.06
57	Tensile (0º)	1.4410	1.52	19.99	767	1553	0.199	0.031	0.55
70	Tensile (0º)	1.4410	1.52	19.99	753	1558	0.201	0.031	0.58
21	Tensile (0º)	1.4410	1.53	19.99	759	1559	0.205	0.034	0.55
					760	1556	0.202	0.032	0.56
stdev					7	3	0.003	0.002	0.02
61.2	Tensile (45º)	1.4410	0.77	19.91	828	1523	0.186	0.040	1.11
20	Tensile (45º)	1.4410	0.78	19.96	817	1502	0.183	0.037	1.10
61	Tensile (45º)	1.4410	0.78	19.95	-	-	-	-	-
74	Tensile (45º)	1.4410	0.78	19.94	812	1491	0.178	0.034	1.29
					819	1505	0.183	0.037	1.17
stdev					8	16	0.004	0.003	0.11
45	Tensile (45º)	1.4410	1.52	19.99	781	1480	0.196	0.040	1.20
59	Tensile (45º)	1.4410	1.52	19.98	772	1481	0.197	0.039	1.16
60.2	Tensile (45º)	1.4410	1.52	19.95	761	1467	0.188	0.036	1.37
60	Tensile (45º)	1.4410	1.53	19.96	-	-	-	-	-
					771	1476	0.194	0.038	1.25
stdev					10	8	0.005	0.002	0.11
34	Tensile (90º)	1.4410	0.78	19.98	875	1556	0.170	0.036	0.94
52	Tensile (90º)	1.4410	0.79	19.96	870	1539	0.175	0.040	1.00
68	Tensile (90º)	1.4410	0.79	19.87	851	1540	0.174	0.038	1.53
					865	1545	0.173	0.038	1.16
stdev					13	9	0.003	0.002	0.33
1	Tensile (90º)	1.4410	1.52	19.95	843	1576	0.196	0.044	1.10
38	Tensile (90º)	1.4410	1.52	19.98	859	1538	0.179	0.038	1.07
72	Tensile (90º)	1.4410	1.52	19.95	832	1529	0.180	0.037	1.21
					845	1548	0.185	0.040	1.13
stdev					14	25	0.010	0.004	0.07
14	Tensile (0º)	1.4462	0.67	19.98	725	1479	0.219	0.040	0.53
28	Tensile (0º)	1.4462	0.68	19.98	668	1474	0.226	0.039	0.44
58	Tensile (0º)	1.4462	0.66	19.86	698	1500	0.220	0.038	0.48
					697	1484	0.222	0.039	0.48
stdev					29	14	0.004	0.001	0.04
25	Tensile (45º)	1.4462	0.68	19.95	676	1428	0.241	0.054	1.40
65	Tensile (45º)	1.4462	0.68	19.91	659	1400	0.231	0.047	2.17
67	Tensile (45º)	1.4462	0.67	19.84	648	1430	0.232	0.047	1.44
					661	1419	0.235	0.049	1.67
stdev					14	17	0.006	0.004	0.43
13	Tensile (90º)	1.4462	0.69	19.9	750	1437	0.209	0.052	0.69
30	Tensile (90º)	1.4462	0.69	19.9	772	1438	0.194	0.045	0.71
62	Tensile (90º)	1.4462	0.68	19.83	-	-	-	-	-
62.2	Tensile (90º)	1.4462	0.68	19.93	765	1453	0.201	0.046	0.71
					762	1443	0.201	0.048	0.70
stdev					11	9	0.007	0.004	0.01

Appendix C: Uni-axial FLC points

Uni-axial FLD point EN 1.4404:

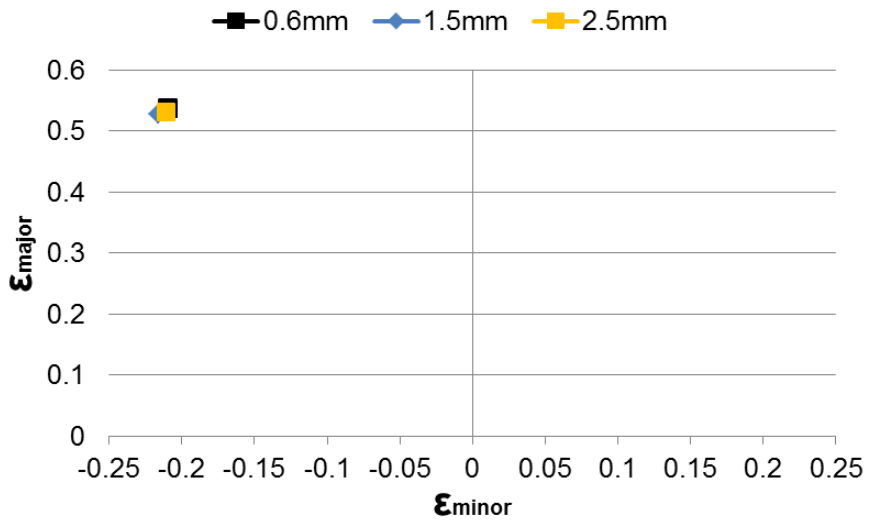

Uni-axial FLD point EN 1.4162:

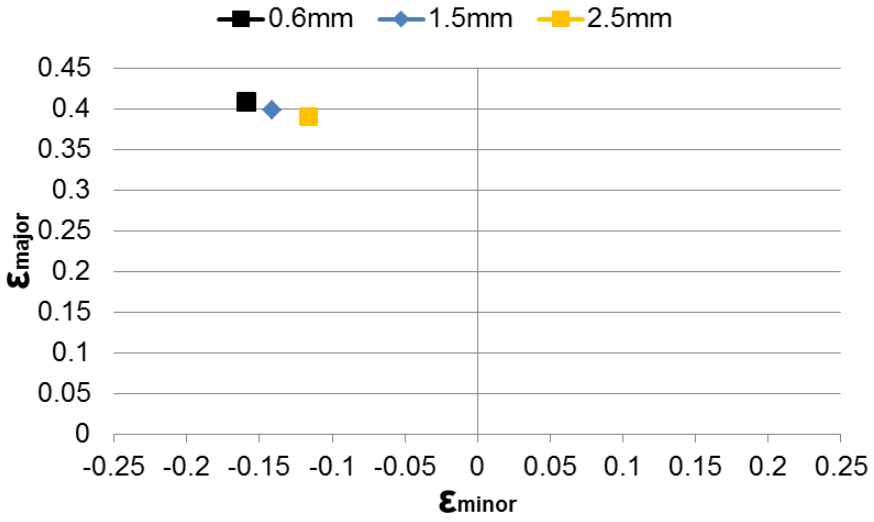

Uni-axial FLD point EN 1.4462:

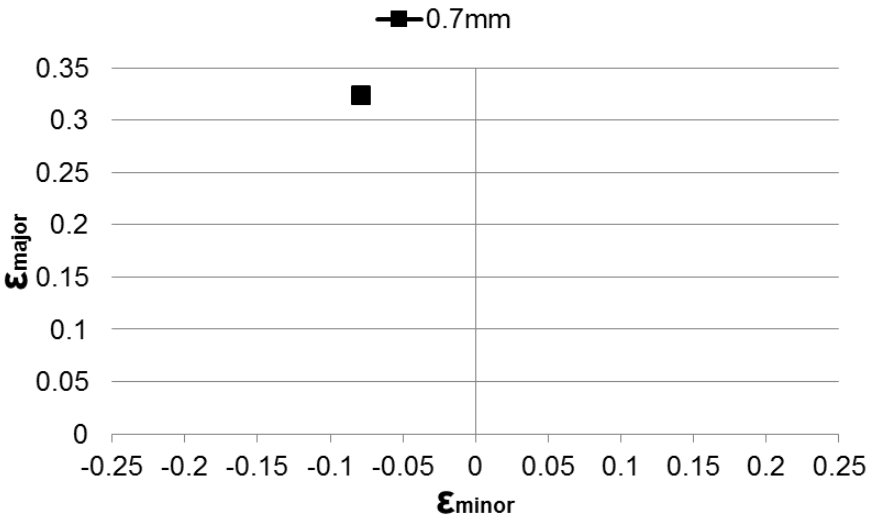

Uni-axial FLD point EN 1.4410: